농학 박사학위 논문

고포도당 처리 인간 제대혈 유래 중간엽 줄기세포의 E-cadherin 발현 변화와 피부 상처 치유 효능

E-cadherin expression changes and skin wound healing efficacy in human umbilical cord blood-derived mesenchymal stem cells treated with high glucose

2018년 8월

서울대학교 대학원

농생명공학부

오 지 영

농학 박사학위 논문

고포도당 처리 인간 제대혈 유래 중간엽 줄기세포의 E-cadherin 발현 변화와 피부 상처 치유 효능

E-cadherin expression changes and skin wound healing efficacy in human umbilical cord blood-derived mesenchymal stem cells treated with high glucose

2018년 8월

지도교수: 이 창 규

서울대학교 대학원

농생명공학부

오 지 영

Doctoral Thesis

E-cadherin expression changes and skin wound healing efficacy in human umbilical cord blood-derived mesenchymal stem cells treated with high glucose

Ji Young Oh

Advisor: Chang-Kyu Lee, Ph.D.

Department of Agricultural Biotechnology

The Graduate School

Seoul National University

August 2018

ABSTRACT

E-cadherin expression changes and skin wound healing efficacy in human umbilical cord blood-derived mesenchymal stem cells treated with high glucose

Ji Young Oh

Department of Agricultural Biotechnology

The Graduate School

Seoul National University

Glucose plays an important role in stem cell fate determination and its behavior. Stem cell fate is regulated by genes involved in differentiation, proliferation, and migration. Previous investigators have suggested that oxidative stress, especially reactive oxygen species (ROS), increases stem cell migration and the increase of ROS may destroy the homeostasis of the cells, and subsequently serious damage in the cells. High glucose is the cause of excess ROS that leads to diabetic complications. 17β-estradiol (E2) is an important regulator of energy homeostasis and glucose metabolism, so that it should be considered a suitable target of E2 for preventing or treating metabolic disorders. Diabetes is closely related to oxidative stress and the risk of diabetes is high in patients who are deficient in E2. Thus, E2 has protective roles against oxidative stress exposure which leads to mitochondrial dysfunction and damage. However, it remains unclear how glucose contributes to the precise molecular mechanism for producing ROS in the stem cell and E2 evokes protective antioxidant mechanisms. Therefore, present study aimed to investigate 1) the effect of high glucose on stem cell migration and its related signaling pathways, 2) the role of E2 in glucose-mediated mitochondrial ROS (mtROS) level in human umbilical cord blood-derived mesenchymal stem cells (hUCB-MSCs), and 3) the effect of hUCB-MSC transplantation on mouse skin wound healing by E2 in ovariectomized (OVX) diabetic mice *in*

vivo.

First, I investigated the effect of high glucose on regulation of hUCB-MSC migration. High glucose treatment (D-glucose) induced hUCB-MSC migration, expression of cleaved Notch, Snail and enhancer of zeste homolog2 (EZH2), but repressed epithelial cadherin (E-cadherin) expression. E-cadherin repression was regulated by high glucose through Snail and EZH2 upregulation, and Snail was modulated in parallel with EZH2 in hUCB-MSCs. Next, I demonstrated that high glucose enhanced ROS, which activates either c-Jun N-terminal kinase (JNK) or phosphatidylinositol-3-kinses (PI3K)/protein kinase B (Akt) signaling. High glucose-induced JNK activation elicit the cleavage of Notch protein through γ-secretase activation, following Notch intracellular domain (NICD) translocation into the nucleus. In the nucleus, Snail interacted with polycomb repressive complex 2 (PRC2) components by high glucose. And then EZH2, one of the major component of PRC2, and Snail bound with E-box of the E-cadherin promoter by high glucose, which in turn causes E-cadherin repression. Taken together, these results suggest that high glucose-induced ROS production increases the migration of hUCB-MSCs through E-cadherin repression via EZH2 and Snail upregulation.

Next, I investigated the role of E2 on mtROS-mediated autophagic cell death by high glucose in hUCB-MSCs. High glucose

increased mtROS to upregulate Beclin1 and LC-II expression, leading to decreased cell viability. In contrast, E2 treatment significantly decreased high glucose-induced mtROS levels and subsequently restored cell viability, suggesting that E2 serves as a strong antioxidant. I found that treatment of both E2 and high glucose promoted ERα translocation into the nucleus leading to increased Nrf2 in the nucleus. However, high glucose produced mtROS via downregulating Nrf2 nuclear translocation. This subsequently culminated in Sirtuin3 (Sirt3) downregulation and manganese superoxide dismutase (MnSOD) acetylation. The increased nuclear translocation of Nrf2 triggered upregulation of Sirt3 expression and activated MnSOD; both of which play important roles in decreasing mtROS. The therapeutic effect of hUCB-MSC transplantation on skin wound healing for OVX diabetic mice was enhanced by E2 treatment when compared to the mice without E2 treatment. In addition, the blood vessels that had well-developed branches were observed in OVX diabetic mice that received hUCB-MSC transplantation with E2 when compared to *ERα* siRNA-transfected hUCB-MSC transplantation.

In conclusion, present study presented that 1) high glucose-induced ROS stimulates the hUCB-MSC migration through E-cadherin repression via Snail and EZH signaling pathways, and 2) E2 leads to the protective effect on high glucose-induced mtROS

production and autophagic cell death through ERα-dependent Nrf2, followed by subsequent Sirt3 upregulation and MnSOD activation.

Keywords: High glucose, Reactive oxygen species, E-cadherin, 17β-Estradiol, Sirtuin-3, Manganese superoxide dismutase

Student Number: 2010-21245

CONTENTS

ABSTRACT · i

CONTENTS · vi

LIST OF FIGURES · viii

LIST OF TABLES · xii

ABBREVIATIONS · xiii

CHAPTER I

LITERATURE REVIEW · · · · · · · · · · · · · · · · · · · 1

CHAPTER II

Regulation of migration in hUCB-MSCs by high glucose-induced ROS via Snail/EZH2/E-cadherin pathway 26

1. INTRODUCTION · · · · · · · · · · · · · · · · 27

2. MATERIALS AND METHODS · · · · · · · · · 31

3. RESULTS · 46

4. DISCUSSION · · · · · · · · · · · · · · · · · · 92

CHAPTER III

17β-Estradiol enhances hUCB-MSCs-induced wound healing in the ovariectomized diabetic mouse model through estrogen receptor α-dependent MnSOD activation via Nrf2 and Sirt3 upregulation 101

1. INTRODUCTION · · · · · · · · · · · · · · · 102

2. MATERIALSAMD METHODS · · · · · · · · 106

3. RESULTS · · · · · · · · · · · · · · · · · · 124

4. DISCUSSION · · · · · · · · · · · · · · · · 172

CHAPTER IV

GENERAL CONCLUSION · · · · · · · · · · · · · · · · · 180

REFERENCES · 183

ABSTRACT IN KOREAN · · · · · · · · · · · · · · · · 212

LIST OF FIGURES

Figure 1 Glucose metabolism in stem cells

Figure 2 Production and scavenging of mitochondrial ROS

Figure 3 Four stages of wound healing process

Figure 4 Role of stem cells in wound healing

Figure 5 Effect of high glucose on hUCB-MSC migration

Figure 6 Effect of high glucose on F-actin reorganization of hUCB-MSCs

Figure 7 Effect of high glucose on AD-MSC migration

Figure 8 Effect of high glucose-pretreated hUCB-MSC transplantation in mouse skin wound

Figure 9 Effect of high glucose-pretreated hUCB-MSC transplantation on cell survival and angiogenesis

Figure 10 Effect of high glucose on E-cadherin, Notch, Snail and EZH2 expression

Figure 11 Effect of high glucose on E-cadherin, through Snail and EZH2 signaling in hUCB-MSCs

Figure 12 Role of high glucose on ROS generation

Figure 13 Time-dependent activation of MAPK by high glucose

Figure 14 Role of ROS-dependent JNK signaling pathway

Figure 15 Role of ROS-dependent Notch signaling pathway under high glucose conditions

Figure 16 Role of ROS-dependent PI3K/Akt/GSK-3β signaling pathway

Figure 17 Effect of high glucose on nuclear translocation of Snail and EZH2

Figure 18 Effect of high glucose on PRC2 complex formation

Figure 19 Relationship between Snail and PRC2 by high glucose in nucleus

Figure 20 Role of high glucose on E-cadherin repression and hUCB-MSC migration

Figure 21 Role of E-cadherin in high glucose-induced migration of hUCB-MSCs

Figure 22 Role of Snail on enhancing the therapeutic efficacy in repairing skin wound

Figure 23 Role of EZH2 on enhancing the therapeutic efficacy in repairing skin wound

Figure 24 The hypothetical model for the proposed signaling network was involved in high glucose-induced hUCB-MSC migration

Figure 25 Effect of STZ on blood glucose in female mice with or without ovariectomy

Figure 26 Effect of E2 on uterine weight of OVX diabetic mice

Figure 27 Effect of E2 on serum E2 of OVX diabetic mice

Figure 28 Effect of E2 on uterine myometrium thickness in OVX diabetic mice

Figure 29 Effect of high glucose on autophagy-related proteins in hUCB-MSCs

Figure 30 Effect of high glucose on survival of hUCB-MSCs

Figure 31 Effect of high glucose on autophagic cell death in hUCB-MSCs

Figure 32 Effect of E2 on high glucose-induced autophagy in hUCB-MSCs

Figure 33 Effect of E2 on high glucose-induced cell death in hUCB-MSCs

Figure 34 Effect of E2 on high glucose-induced ROS in hUCB-MSCs

Figure 35 Effect of high glucose on mtROS in hUCB-MSCs

Figure 36 Effect of E2 on high glucose-induced mtROS in hUCB-MSCs

Figure 37 Effect of E2 on high glucose-induced ERα nuclear translocation

Figure 38 Effect of high glucose on ERα-dependent Nrf2 nuclear translocation

Figure 39 Effect of high glucose on ERα-dependent Sirt3 upregulation

Figure 40 Effect of high glucose on SOD activity through ERα signaling

Figure 41 Effect of high glucose on ROS through Nrf2 signaling in hUCB-MSCs

Figure 42 Effect of high glucose on decreased Nrf2 nuclear translocation in hUCB-MSCs

Figure 43 Effect of high glucose on Sirt3 and MnSOD repression through Nrf2 signaling in hUCB-MSCs

Figure 44 Effect of E2 on Nrf2 nuclear translocation in hUCB-MSCs

Figure 45 Effect of high glucose on MnSOD activation and Sirt3 expression in hUCB-MSCs

Figure 46 Effect of high glucose on MnSOD activation through

Sirt3 signaling in hUCB-MSCs

Figure 47 Effect of high glucose on ROS production through MnSOD signaling in hUCB-MSCs

Figure 48 Effect of E2 on high glucose-induced Sirt3 repression in hUCB-MSCs

Figure 49 Effect of E2 on SOD activity under high glucose conditions in hUCB-MSCs

Figure 50 Effect of ERα-silenced hUCB-MSC transplantation with E2 injection in OVX diabetic mouse model

Figure 51 Effect of ERα-silenced hUCB-MSC transplantation in OVX diabetic mouse model

Figure 52 Effect of ERα-silenced hUCB-MSC transplantation on HNA expression in OVX diabetic mouse model

Figure 53 Effect of ERα-silenced hUCB-MSC transplantation with E2 injection on blood vessel formation in OVX diabetic mouse model

Figure 54 The schematic model for mechanism in the protective effect of E2 on high glucose-induced mtROS through ERα-dependent Nrf2 and Sirt3 upregulation in hUCB-MSCs

LIST OF TABLES

Table 1 Sequences of siRNAs used for gene silencing

Table 2 Sequences of siRNAs and its suppliers used for gene silencing

ABBREVIATIONS

Ac-K68 MnSOD	Acetylation of manganese superoxide dismutase at lysine 68
Acetyl-CoA	Acetyl coenzyme A
AD-MSCs	Adipose-derived mesenchymal stem cells
ADP	Adenosine diphosphate
α-MEM	Alpha-minimum essential medium eagle modification
ATP	Adenosine triphosphate
BCA	Bicinchoninic acid
bFGF	Basic fibroblast growth factor
BMP4	Bone morphogenic protein 4
CDH1	Cadherin-1
CHIP	Chromatin immunoprecipitation
Co-IP	Co-Immunoprecipitation
Cyt	Cytochrome
DCF-DA	2',7'-Dichlorodihydrofluorescein diacetate
DM	Diabetic mellitus
E2	17β-Estradiol
E-cadherin	Epithelial cadherin
EDTA	Ethylenediaminetetraacetic acid
EED	Embryonic ectoderm development

EGTA	Ethylene glycol-bis(beta-aminoethyl ether)-N, N, N′, N′-tetraacetic acid
ER	Estrogen receptor
ERK	Extracellular signal-related kinase
ESCs	Embryonic stem cells
ETC	Electron transport chain
EZH2	Enhancer of zeste homolog 2
F1,6P	Fructose 1,6-bisphosphate
F6P	Fructose 6-phosphate
FAD	Flavin adenine dinucleotide
FBS	Fetal bovine serum
FITC	Fluorescein isothiocyanate
FMN	Flavin mononucleotide
G6P	Glucose 6-phosphate
GLUT	Glucose transporter
GSK-3β	Glycogen synthease kinase-3 beta
HCl	Hydrogen chloride
HDAC1	Histone deacetylase 1
H&E	Hematoxylin and eosin
HG	High glucose
HK	Hexokinase
hMSC	Human mesenchymal stem cell
hUCB-MSCs	Human umbilical cord blood-derived MSCs

HNA	Human nuclear antigen
HRP	Horseradish peroxidase
HSCs	Hematopoietic stem cells
IACUC	Institutional animal care and use committee
iPSCs	Induced pluripotent stem cells
JNK	c-Jun N-terminal kinases
Keap1	Kelch-like ECH-associated protein 1
LC3	Microtubule-associated protein light chain 3
LiCl	Lithium chloride
LIF	Leukemia inhibition factor
MAPK	Mitogen activated protein kinase
MnSOD	mitochondrial superoxide dismutase
mtROS	Mitochondrial ROS
NAC	N-acetyl-L-cysteine
NADH	Nicotinamide adenine dinucleotide
NGS	Normal goat serum
NICD	Notch intracellular domain
Nrf2	Nuclear factor (erythroid-derived 2)-like 2
NT	Non targeting
OXPHOS	Oxidative phosphorylations
OVX	Ovariectomy
PBS	Phosphate buffered solution
PFA	Paraformaldehyde

PI	Propidium iodide
PI3K	Phosphoinositide 3-kinase
PFA	Paraformaldehyde
PRC2	Polycomb repressive complex 2
PVDF	Polyvinylidene difluoride
RFU	Relative fluorescence units
ROD	Relative optical density
ROS	Reactive oxygen species
RT-PCR	Real-time reverse transcriptase-polymerase chain reaction
SEM	Standard error of mean
SDS-PAGE	Sodium dodecyl sulfate polyacryl-amide gel electrophoresis
SSTA	Stage-specific embryonic antigen
STZ	Streptozotocin
siRNA	Small interfering RNA
Sirt3	Sirtuin-3
SUZ12	Suppressor of zeste 12
TCA	Tricarboxylic acid
TBST	Tris-buffered saline containing 0.1% Tween-20

CHAPTER I.

LITERATURE REVIEW

1. Stem cells

A. Definition of stem cells

Stem cells are undifferentiated cells with self-renewal ability. They have the capacity to produce functionally several differentiated cells (Weissman et al., 2001; Smith, 2001). Stem cells are classified based on their differentiation potential; totipotent, pluripotent and multipotent stem cells. Totipotent stem cells have unlimited capability to form all lineages of an organism. Pluripotent stem cells are capability of differentiating into almost all cell types, which are derived from ectoderm, mesoderm and endoderm. Multipotent stem cells have potential to form cells that are restricted to organ sources. In mammals, there are two types of stem cells: embryonic stem cells (ESCs) and adult stem cells. ESCs are derived from inner cell mass of blastocysts. Whereas, adult stem cells are derived from adult tissues such as adipose, bone, and umbilical cord blood (UCB), which offer easy source for use in research and therapy *in vivo*. Taken together, stem cells can be described as having replication ability, which is the capacity of proliferation, and their differentiation potency.

B. Embryonic stem cells

ESCs are derived from the inner cell mass of the blastocyst of the preimplantation embryo at the early stage and has the potential to differentiate into all cell types. The basic characteristics of ESC are self-renewal, multilineage differentiation, clonality, and normal karyotype. ESCs have potential to differentiate into three germ layers (ectoderm, mesoderm, and endoderm). Pluripotency of ESCs distinguishes themselves from adult stem cells that can differentiate into restricted cell types. In order to maintain the ESCs undifferentiated, the cells should be cultured on the feeder layer or in the presence of leukemia inhibitory factor (LIF). LIF may affect cell proliferation or cell cycle progression rate. In addition, LIF can also act on the stem cell phenotype by activating signaling cascade by regulating genes expressed only in pluripotent and differentiated cells. Basic fibroblast growth factor (bFGF) is required for self-renewal of human ESCs through Activin/Nodal signaling-regulated OCT4 expression (Honda et al., 2009), and feeder layer, conditioned medium and cytokines are essential under human ESC culture system. Moreover, bone morphogenetic protein 4 (BMP4), along with LIF, has been shown to be a growth factor that maintains self-renewal of ESCs and blocks neural differentiation (Ying et al, 2003). Human ESCs have similar markers and expression patterns, but some of them exhibit the same pattern as mouse ESCs. In

mouse ESCs, Stage-specific embryonic antigen (SSEA) 1 is considered as undifferentiated marker, whereas in human ESCs, the increase in SSEA1 is closely related to differentiation. Because of the unlimited self-renewal capacity of ESCs, it has been suggested as an alternative source for regenerative medicine and tissue replacement. Furthermore, ESCs also play a role as tools for genetic studies and toxicity testing (Thomson et al., 1998). However, safety issues including teratoma formation must be addressed first in order for ESCs to be used extensively in clinical environments. Therefore, further studies are needed to establish strategies to improve ESCs therapy safety.

C. Mesenchymal stem cells

Adult stem cells (also known as somatic stem cells) are undifferentiated cells that are found in the body after development. The basic characteristics of adult stem cells are their ability to differentiate and self-renew. Adult stem cells can be isolated from most tissues of the body, including bone marrow, fat, human umbilical cord and placenta tissue. There are various types of adult stem cells including hematopoietic, mammary, intestinal, mesenchymal, endothelial, and neural stem cells.

Mesenchymal stem cells (MSCs) are multipotent stem cells that

possess self-renewal ability and exist in almost all tissues. They also have the potential to differentiate into distinct mesenchymal cells, including osteoblasts, adipocytes, chondrocytes, myoblasts, and neural cells (Pittenger et al., 1999; Barry and Merphy, 2004), but are not capable of reconstituting the entire organ. Due to various limitations in ESCs and induced pluripotent stem cells (iPSCs) research such as teratoma formation, immune rejection, political and ethical restrictions, MSCs are a very attractive candidate for tissue repair and gene therapy because of their ability to migrate to places where they are needed. Among other MSCs, MSCs derived from umbilical cord blood are known to regulate the immune system, reduce inflammation, and secrete factors necessary to improve regeneration of various tissues of the body. In particular, hUCB-MSCs accelerate wound healing through angiogenesis and differentiation, which can improve therapeutic potential in the treatment of clinical diseases (Chang et al., 2016; Lee et al., 2016; Ryu and Han, 2015). Thus, the use of hUCB-MSCs in stem cell-based therapies has been regarded as a future medicine that can provide new potential for regenerative medicine, but further studies of hUCB-MSCs are needed to develop more advanced stem cell therapies.

2. Glucose as a stem cell regulator

A. Glucose metabolism

Glucose represents important regulatory elements that modulate cell fate determination in both physiological and pathological states. Glucose also plays a role in maintaining the function of stem cells, and glucose metabolism regulates the balance between the quiescence and proliferation of stem cells. Proliferation of the cells depends on the significant ATP production, which is normally maintained through oxidative phosphorylations (OXPHOS). Glucose molecules metabolized by OXPHOS can provide the energy necessary for maintaining protein synthesis, proliferation, and migration. However, stem cells do not depend solely on OXPHOS. Previous studies have shown that oxygen consumption in stem cells decreases and the acidity of the medium is independent of glucose uptake (Zhang et al., 2011). Stem cells depend on glycolysis rather than OXPHOS to produce the energy needed for homeostasis (Simsek et al., 2010). In addition, the pluripotency of stem cells is closely correlated with glucose metabolism (Figure 1). Excessive exposure to glucose can produce more ATP than OXPHOS via glycolysis (Guppy et al., 1993) that results in metabolic changes in stem cells. Many researchers reported that high glucose induces

the variety of responses in stem cells, such as proliferation, senescence, migration, and apoptosis (Li et al., 2007; Cramer et al., 2010). Changes in glucose homeostasis can have serious consequences on the ability of stem cells to self-renew and differentiate themselves, as changes in cellular metabolism occur earlier than stemness changes (Folmes et al., 2011; Ochocki and Simon, 2013). Thus, these findings suggest that the regulation of intracellular glucose signaling has an ability to control the metabolism and behavior of stem cells.

B. Glucose transporters

Glucose is the major substrate for energy source, which is transported in the blood of animal. Blood glucose is maintained at a constant level by two substances, insulin and glucagon, produced in the pancreas. Increased glucose concentration in the blood causes glucose metabolism syndrome including diabetes mellitus, diabetic ketoacidosis, and hyperosmolar coma. Diabetes is a metabolic disorder characterized by decreased glucose tolerance due to insulin secretion or dysfunction for glycemic control. As the blood glucose level rises abnormally, glucose flows into the urine which is also called glucosuria. Type 1 diabetes is caused by an absolute deficiency of insulin and type 2 diabetes is caused by impaired

insulin function. Glucose tolerance is also reduced in type 2 diabetes due to impaired tissue sensitivity to insulin action. Recent studies have shown that microvascular damage by diabetes is directly related to the degree of hyperglycemia and duration of diabetes. The concentration of blood glucose in people with non-diabetes is maintained between 4.5-5.5 mmol/L, which fluctuates throughout the day. However, according to the American Diabetes Association, the target range for blood glucose in diabetic patients should not exceed 5-7.2 mmol/L before meal and up to 10 mmol/L after meal. Diabetes mellitus is considered to be diabetes if the blood glucose level is higher than 11.1 mmol/L 2 hours after food intake. If the blood glucose level is above 25 mmol/L, the risk of diabetic complications increases. If it is higher than 33.3 mmol/L, it may cause hyperosmolar syndrome and lead to dehydration and diabetic coma. Thus, blood glucose control is essential to prevent diabetes and its complications.

Maintaining a stable level of glucose in the blood is one of the important mechanisms to maintain cell homeostasis. Glucose transporters have two main types: glucose transporter (GLUT) and sodium-dependent glucose cotransporters (SGLTs). GLUTs are facilitative transport proteins involved in glucose translocation across the cell membrane. It undergoes structural changes transported into the cells of glucose when they bind together.

Among all GLUTs, GLUT1−4 are the major glucose receptors and most widely studied. GLUT2 has a low affinity for glucose because it has a high Km value (15−25 mmol/L), and the rate of glucose uptake is proportional to the amount of glucose. GLUT4 is activated when insulin binds to the insulin receptor, and is primarily found in adipose and muscle tissues. The Km values of GLUT1 and GLUT3 are similar or lower than the basic blood glucose in humans (4.5−5.5 mmol/L), so they have high affinity for glucose and are constantly absorbed from the bloodstream. When blastomere is differentiated into trophectoderm and pluripotent inner cell mass, metabolic activity increases steeply. ESCs that are derived from inner cell mass of blastocyst upregulate the expression of GLUT1 and GLUT3 to increase glucose uptake. Thus, glycolytic flux increases rapidly and lactate synthesis increases. However, when stem cells differentiate, the glycolytic flux decreases sharply and the expression of GLUT1 and GLUT3 decreases. Decreased expression of GLUT1 and GLUT3 under stress circumstances reduces glucose uptake in MSCs, meaning glucose metabolic profile is regulated through GLUT1 and GLUT3 in MSCs (Peppicelli et al., 2015).

C. ROS and stem cell fate

ROS are mainly produced by mitochondria, endoplasmic reticulum, and plasma membranes. Mitochondrial ROS is mainly present in three forms: superoxide anion (O_2^-), hydrogen peroxide (H_2O_2), and hydroxyl radical (OH^-). O_2^- includes non-covalent electrons that confer high reactivity and require rapid reduction to H_2O_2 by antioxidant enzyme superoxide dismutase (SOD) (Figure 2). H_2O_2 can be reduced by various cellular antioxidants including SOD and catalase that eliminate ROS production.

For both development and tissue homeostasis, proper balance between self-renewal and differentiation is important for stem cell function. Recent studies of pluripotent stem cells and adult stem cells demonstrate that this balance is partially regulated by ROS that mediates the cellular redox state (Wang et al, 2013). ROS directly interacts with various proteins such as kinase, phosphatase, or transcription factor to alter the process of regulating cell cycle progression, apoptosis and differentiation. In particular, high ROS levels can promote stem cell motility after acute stress situations, meaning that the production of ROS results in stem cell migration and invasion. High glucose is especially crucial for stem cell function through ROS-mediated PI3K/Akt activation (Kim et al., 2006). Elevated ROS production mediates self-renewal and

neurogenesis by PI3K/Akt signaling in neural stem cells (Le Belle et al., 2011). Thus, these findings suggest that ROS can be considered to be a signaling molecule that participates in cross talk between metabolism and stem cell fate determinations.

D. Autophagy and ROS

Mitochondria are the principal source of ROS for inducing autophagy (Murphy, 2009; Scherz-Shouval et al., 2007). Autophagy allows the degradation and recycling of cellular components under various stressful conditions such as excess of ROS to maintain intracellular homeostasis during protein and organelle turnover (Rosa et al., 2016). In addition, ROS by oxidative stress induces cell death, but antioxidants contribute to autophagic clearance of oxidized biomolecules (Giordano et al., 2013). However, impaired autophagy can be caused by hyperglycemia, which can lead to the accumulation of unfolded proteins and dysfunctional organelles in the cells. This implies that autophagy plays a role in the pathology and physiology of diabetic complications (Volpe et al., 2018). Exposure to high glucose affects cell death by autophagy dysfunction (Wang et al., 2015). In addition, it has been reported that high glucose-induced oxidative stress regulates autophagy through mitochondrial damage (Park and Park,

2013). Thus, reduced autophagy dysfunction may prevent oxidative stress-induced, diabetes-associated diseases. However, it remains unknown that which modulator by oxidative stress contributes to high glucose-evoked autophagy in stem cells. Therefore, further investigation into the role of ROS in stem cell physiology and metabolism under high glucose conditions is needed for the establishment of an efficient metabolic regulation in stem cells.

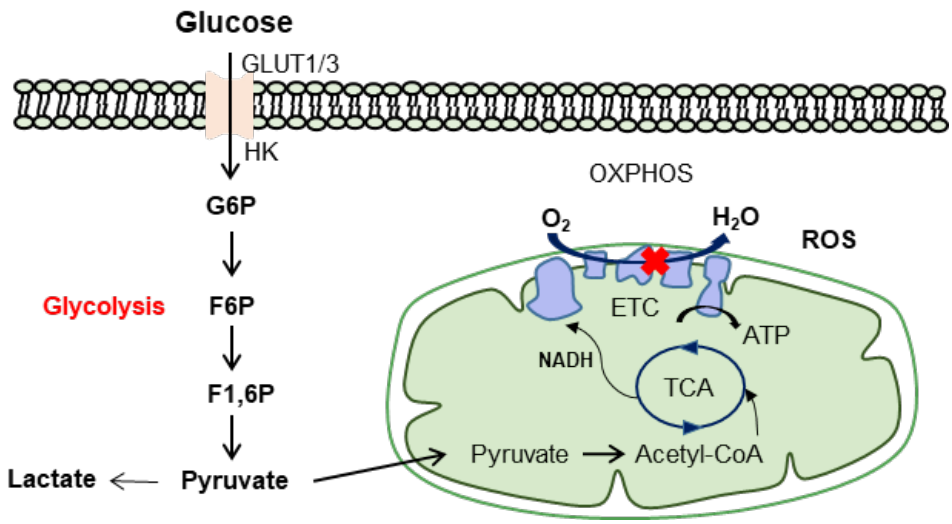

Figure 1. Glucose metabolism in stem cells. The schematic model shows the glucose metabolic in stem cells. Stem cells rely on glycolysis rather than OXPHOS to produce the energy needed for homeostasis. GLUT, glucose transporter; G6P, glucose 6-phosphate; F6P, fructose 1,6-bisphosphate; ETC, electron transport chain; TCA, tricarboxylic acid; NADH, nicotinamide adenine dinucleotide; ATP, adenosine triphosphate; HK, hexokinase; Acetyl-CoA, acetyl coenzyme A

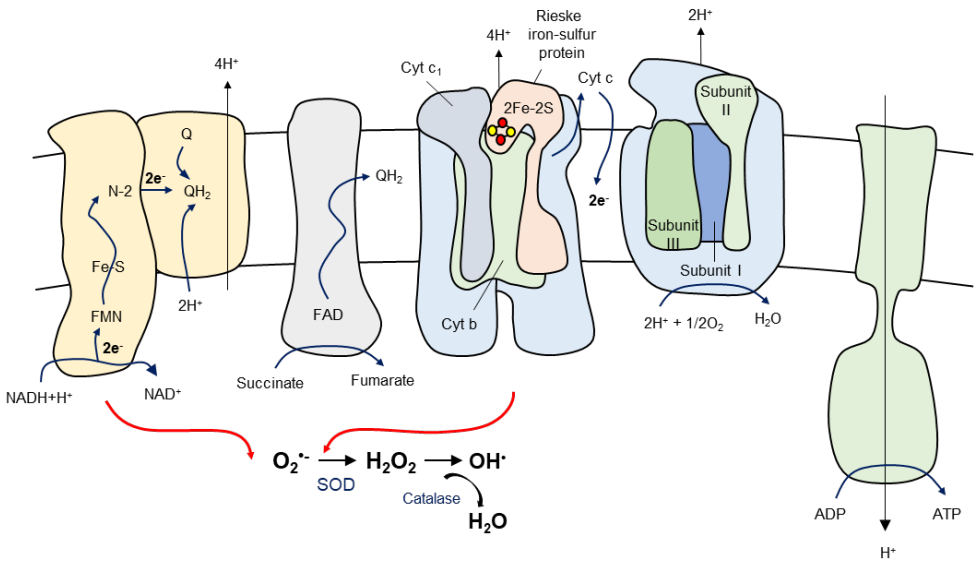

Figure 2. Production and scavenging of mitochondrial ROS. The schematic model indicates that superoxide ($O2^{\bullet -}$) is produced from the O_2 molecule, that can be also produced from complexes I and III in mitochondria. H_2O_2 is catalyzed by SOD enzyme, which can be further reduced to H_2O molecule by catalase enzyme. FMN, Flavin mononucleotide; FAD, Flavin adenine dinucleotide; Cyt, cytochrome; ADP, adenosine diphosphate; ATP, adenosine triphosphate.

3. Wound healing

A. Stem cells in wound healing mechanism

Wound healing is a natural recovery process for tissue damage, which involves restructuring and restoring the injured skin through complex cellular cascade events. Wound healing is divided into four phases: hemostasis, inflammatory, proliferation, and remodeling (Figure 3). The initial wound shrinks and blood coagulates in the blood vessels showing characteristic signs of inflammation. In the proliferation phase, wound sites are filled with new granulation tissues and angiogenesis is followed. In the maturation phase of wound healing, the wound is observed to be closed. Cell activity is reduced and the number of blood vessels at the wound site is decreased. During wound healing process, cells often migrate through cell-cell junction (Li et al., 2013). In addition, epithelial cells proliferate and migrate to the center of wound sites while the wound heals. Migration plays an essential role when cells are in stable connections. Epithelial cells are tightly connected by cell-cell adhesion molecules, including E-cadherin. Stem cells are an attractive candidate to enhance the therapeutic potential for cutaneous wound healing and tissue regeneration due to secretion of various cytokines, including vascular endothelial growth factor

(VEGF), epidermal growth factor (EGF), and keratinocyte growth factor. In wound proliferation stages, fibroblasts show phenotypic switch toward myofibroblasts as a typical characteristic of wound healing process (Siebert et al., 2011; Hinz, 2007). Stem cells secrete various cytokines and paracrine factors as well as migration and proliferation to the wound, which can affect the microenvironment and increase tissue repair and angiogenesis. Stem cells differentiate into keratinocytes which are activated by pro-inflammatory cytokines and growth factors, and then migrate to wound sites. Activated keratinocytes communicate with other cells and cause reepithelization (Figure 4). The effect of MSC transplantation on tissue regeneration was induced by the paracrine effect rather than cell replacement, and the migration of the transplanted cells to the wound site was reported to be related to wound healing process initiation and immune regulatory processes (Granero-Molto et al., 2009; Kwon et al., 2013). However, many researchers revealed that MSCs are a key factor of regenerative wound healing because MSCs contribute to the secretion of growth factors that promotes neovascularization and reepithelization (Balaji et al.,2012; Lee et al., 2016). Furthermore, MSCs enhance wound healing by structural repair through cellular differentiation (Kanji and Das, 2017). Based on these findings, further studies for successful stem cell therapy will be needed to improve the

therapeutic effect of MSCs in wound healing and tissue regenerative medicine.

B. Role of E-cadherin in stem cell migration

E-cadherin is a crucial component of cell adhesion molecules that perform the formation of cell-cell adherens junctions to bind cell via a hemophilic mechanism (Takeichi, 1991). In particular, the role of E-cadherin is critical in maintaining the adhesion of cells and in the formation of specialized cell-cell junctions (Shirayoshi et al., 1983; Boller et al., 1985). The cadherin-based adherens junctions interact with α-catenin and β-catenin, which are involved in the cytoskeleton network, to form a stable adherens junctions (Drees et al., 2005). In addition, the interaction between E-cadherin and β-catenin modulates actin-filament assembly (Drees et al., 2005). However, during dissolution of adherens junctions, E-cadherin can no longer interact with β-catenin, resulting in the reduction of adhesion and increase in cell motility (Christofori and Semb, 1999).

The processes of cell migration involve four major parts including extension, adhesion, translocation and detachment. Cells are tightly attached to other cells or to the extracellular matrix and need to detach by disrupting the cell-cell interaction in order to migrate. Therefore, cell-cell detachment-related events are much

emphasized while cell migration processes occur through the down-regulation of adhesion molecules. Many researchers have studied that detachment is important during cell migration by which adhesions disassemble (Palecek et al., 1998; Webb et al., 2002; Kirfel et al., 2004).

The metabolic function and migration capacity of stem cells are essential in maximizing their therapeutic benefits. Several studies have mentioned that stem cells enhance the efficacy of migration to the target tissue for stem cell-based therapies (Horwitz et al., 1999; Sohni and Verfaillie, 2013). E-cadherin is the most studied molecule for adhesion of stem cells. E-cadherin accumulates between stem cells and niche cells (Song and Xie, 2002). When E-cadherin is removed from stem cells, the stem cells rapidly detach from the niche cells (Song et al., 2002; Song and Xie, 2002). Moreover, E-cadherin overexpression inhibited stem cell migration whereas E-cadherin inhibition enhanced stem cell migration (Chen et al, 2015). Combined with the results, E-cadherin is the crucial roles in the interaction of stem cells and niche cells as well as stem cell migration. However, the precise mechanisms by which E-cadherin regulates stem cell migration and improves the efficacy of stem cell-based therapies have not been established.

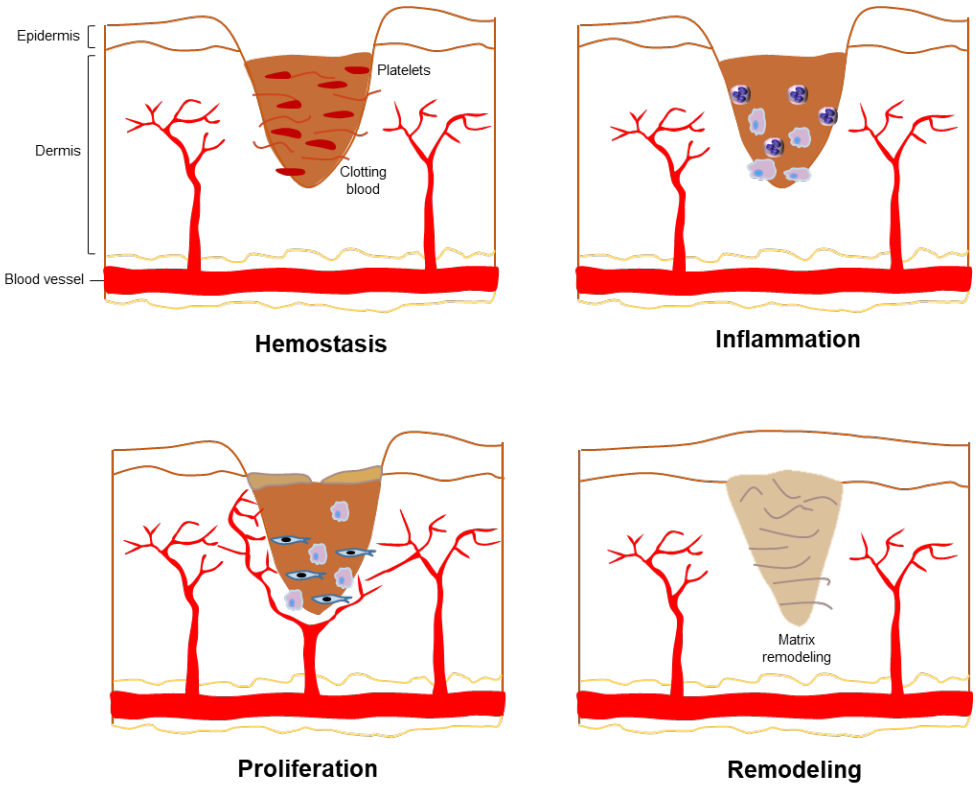

Figure 3. Four stages of wound healing process. The schematic model indicates that wound healing is divided into four stages: hemostasis, inflammation, proliferation, and remodeling.

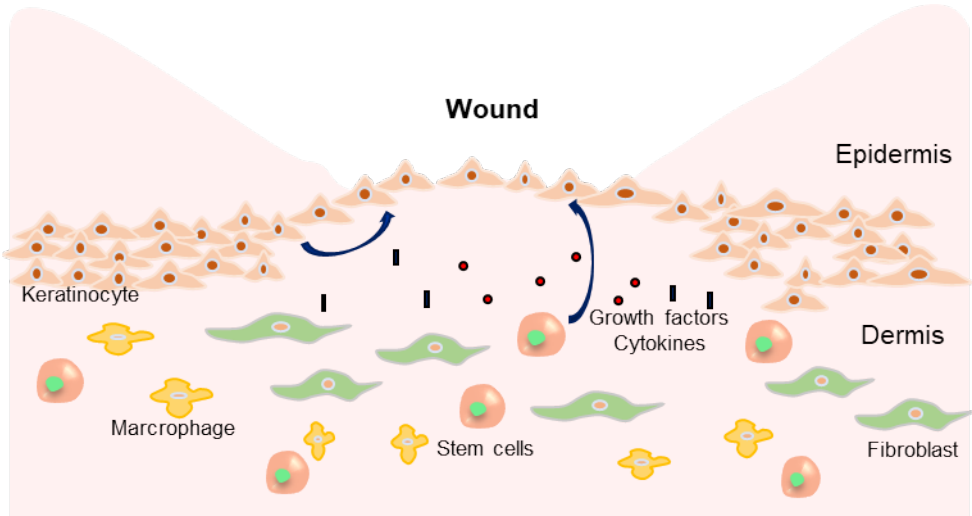

Figure 4. Role of stem cells in wound healing. The schematic model indicates that stem cells differentiate into keratinocytes that are activated by pro-inflammatory cytokines and growth factors. Activated keratinocytes migrate to the wound site and communicate with other cells including fibroblasts and marcrophages, leading to reepithelization.

4. Diabetes and menopause

A. The relationship between E2 and hyperglycemia

E2, a well-known female steroid hormone, plays important roles in regulating the processes of many tissues that participate reproductive physiology, cardiovascular, skeletal and central nerve system (Murphy, 2011; Cersosimo and Benarroch, 2015; Wend et al., 2012). In addition, E2 has recently been shown to play important roles in physiological and pathological aspects in not only women but also in men. However, endogenous sex hormones, insulin resistance, visceral obesity, sleep disorder and depression, all of which contribute to risk factors for diabetes have been shown to change in postmenopausal women with E2 deficiency. Furthermore, middle-aged women are more at risk for diabetes than younger women. Indeed, early menopausal women are at high risk of incidence of type 2 diabetes because of more prolonged E2 deficiency (Brand et al., 2013). Many studies demonstrated that postmenopausal hormone therapy has been studied to improve glucose homeostasis and body composition in clinical trials conducted primarily in women without diabetes (Mauvais-Jarvis et al., 2013; Cagnacci et al., 1992; Davidson et al., 2000; Margolis et al., 2004). In particular, the use of E2 has been reported to

decrease fasting blood glucose and total cholesterol in diabetic postmenopausal women (Crespo et al., 2002).

Female mitochondria produce less peroxidase than male and have higher antioxidant enzymes. So males are more vulnerable to mitochondrial damage by oxidative stress (Vina et al., 2003). Since estrogen receptors (ER) and its signaling are involved in the regulation of antioxidant enzyme expression, female mitochondria have a lower ROS and a higher antioxidant defense effect than males. For this reason, premenopausal women have less metabolic disorders than men with lower E2. ER belongs to the nuclear receptor superfamily, which regulates gene expression involved in glucose uptake and insulin sensitivity. However, due to the reduction in the level of endogenous estrogens, ERα reduction is observed in postmenopausal women. Indeed. glucose and energy metabolism are dysregulated in female ER$\alpha^{-/-}$ mice (Park et al., 2011). In addition, ERα knockout mice have found to be susceptible to oxidative stress result in induction of induce insulin-deficient diabetes (Le May et al., 2006). Even if the regulation of ERα may play an important role in preventing various complications caused by diabetes, it is unclear how E2-induced ER regulation in diabetic postmenopausal women controls the deleterious consequence of diabetes.

B. Antioxidant enzymes

Nuclear factor (erythroid-derived 2)-like 2 (Nrf2) is an antioxidant enzyme, which is degraded as Keap1 binds to Nrf2 under normal conditions. Oxidative stress induces that Nrf2 translocation into the nucleus. Subsequent translocated Nrf2 binds to the antioxidant-related elements and expresses antioxidant genes such as MnSOD and catalase, thus cellular protection by ROS suppression. However, Nrf2 is degraded by Keap1 glycosylation under high glucose conditions, resulting in failure of translocation into the nucleus (Rosa et al., 2016). It has been demonstrated that Nrf2 expression is reduced in the diabetic/insulin resistance model (Essick and Sam, 2010). In addition, oxidative stress levels have been reported to increase in Nrf2-deficient diabetic mice (He and Ma, 2012, Yoh et al., 2008). Thus, Nrf2 is considered to be an essential factor to protect against high glucose-evoked oxidative stress and related diseases, but the exact mechanism has not been elucidated.

Sirtuins are a group of seven members of proteins involved in the regulation of various biological processes, particularly in longevity, metabolism and stress response. Sirt1/2 are located in cytoplasm and Sirt3/4/5 are located in mitochondria. Sirt1/6/7 are present in the nucleus. Sirtuins in mitochondria regulate the acetylation levels

and activity of the antioxidant enzymes to protect mitochondria from oxidative stress. In particular, overexpression of Sirt3, a nicotinamide adenine dinucleotide (NAD^+)-dependent mitochondrial deacetylase, has been reported to accumulate mtROS and mitigates damage to mitochondria. Excess of ROS can lead to apoptosis through membrane lipid and protein oxidation. In addition, Sirt3-mediated deacetylation activates enzymes that plays in reducing ROS in protecting oxidative stress-induced diseases such as diabetes and cancer. Indeed, decreased Sirt3 contributes to vascular dysfunction in obesity by increasing mtROS and Sirt3-mediated MnSOD modulates insulin sensitivity (Qiu et al., 2010; Li et al., 2004). MnSOD is a major mitochondrial antioxidant enzymes and Sirt3 improves antioxidant activity by deacetylation of two key lysine residues on MnSOD. In Sirt3 knockout cells, the acetylation of MnSOD was significantly increased and the activation of MnSOD was decreased (Tao et al., 2010). Additionally, Sirt3 mediated high glucose-evoked oxidative stress through MnSOD deacetylation at lysine 68 (Guodong et al., 2015). However, the exact mechanism by which high glucose-induced oxidative stress reduces the antioxidant response elements is not known. Therefore, further studies are needed to see how increasing the antioxidant response element can lead to prevention of oxidative stress-related diseases.

C. Antioxidant effect of E2

In postmenopausal women, decreased ovarian production reduces circulating E2 levels, whereas E2 acts to distant target tissues in healthy premenopausal women. This endocrine changes lead to lack of glycemic control, which is associated with oxidative stress (Monnier and Colette, 2008; Dandona, 2017). E2 is associated with antioxidant enzymes expression, which affects circulating redox state (Bellanti et al. 2013). E2 acts as a regulator of antioxidant gene expression to prevent aging (Hall and Phillips, 2005), diabetes (Naziroglu et al., 2004), neurodegenerative disease (Goodman et al., 1996) and bone loss (Weitzmann and Pacifici, 2006). It has been reported that E2 upregulates the nuclear gene expression of antioxidant enzymes and interacts with ERs to activate antioxidant enzymes through mitogen activated protein kinase (MAPK) and nuclear factor kappa B (Borras et al., 2010). Changes in oxidative damage and antioxidant enzymes after menopause affect physiological changes (Bednarek-Tupikowska et al., 2004; Bednarek-Tupikowska et al., 2001). Thus, a decrease in endogenous E2 in postmenopausal women may increase the incidence of diabetes due to increased oxidative stress (Naziroglu et al., 2004), but the exact mechanisms by which E2 signaling are activated antioxidative enzymes through oxidative stress regulation remain elusive.

CHAPTER II.

Regulation of migration in hUCB-MSCs by high glucose-induced ROS via Snail/EZH2/E-cadherin pathway

The content in Chapter II is published in *Cellular Physiology and Biochemistry*. 2018 46:1749-1767

1. INTRODUCTION

Glucose is an essential nutrient resource for cellular bio-energetics and components synthesis, such as protein and lipid (Saki et al., 2013). Furthermore, glucose is an important regulatory element that controls cell fate determination in both physiological and pathological conditions (Madonna et al., 2013). Glucose metabolism plays a key role in proliferation, self-renewal ability, and senescence of stem cells (Ito and Suda, 2014). Previous reports investigating the effects of high glucose on stem cell functions are controversial as there are differing perspectives. For example, some studies have shown that high glucose induces senescence and apoptosis in stem cells (Saki et al., 2013; Chang et al., 2015; McClelland et al., 2016). Conversely, other studies have shown that high glucose stimulates proliferation and enhances osteogenic differentiation potential in mesenchymal stem cells (MSCs) (Li et al., 2007). These diverse responses to the high glucose condition may be relevant for the different glucose tolerance of stem cells (Dhanasekaran et al., 2013; Sen et al.,

2015). Therefore, further investigation into the underlying mechanism of high glucose on stem cell functions is needed to develop a therapeutic strategy for stem cell therapy.

The migratory ability of stem cell to injury site is a critical factor in determining the therapeutic effect of stem-based therapy. Previous reports suggested that enhancing stem cell migration is a potential strategy for improving the efficacy of tissue regeneration (Horwitz et al., 1999; Sohni and Verfaillie, 2013; De Becker and Riet, 2016). Moreover, there have been previous studies showing the stimulatory effect of glucose on migration in the various types of cells (Takatani-Nakase et al., 2014; Panchatcharam et al., 2010; Huang and Sheibani, 2008). However, the effect of glucose on stem cell migration is not fully determined. Therefore, identification of a key factor regulating migratory mechanism of stem cells under high glucose conditions is required to improve therapeutic efficacy of stem cell transplantation. Disrupting the cell-cell interaction has been considered an essential step for cell migration. Additionally, cell detachment is regulated by reducing cell adhesion molecules (Vogelmann et al., 2005; Han et al., 2016). Many studies have highlighted that detachment is significant during cell migration by

which adhesions disassemble (Palecek et al., 1998; Webb et al., 2002; Kirfel et al., 2004). E-cadherin is a major component of the cell adhesion molecules that are formed at cell-cell adherens junctions to bind cells via a homophilic mechanism (Takeichi, 1991). During dissolution of adherens junctions by the reduced E-cadherin expression level, E-cadherin can no longer interact with β-catenin, which results in increased cell motility (Zhu et al., 2018). E-cadherin expression can influence various processes that occur during development, organogenesis, tissue formation, and tumor progression (Hyafil et al., 1981; Gumbiner, 2005; Takeichi, 1991). In particular, E-cadherin expression has emerged as an important regulator in cellular movement and invasion (Niewiadomska et al., 1999; Theveneau and Mayor, 2012; Cai et al., 2014). Furthermore, E-cadherin reduction and delocalization accelerated cell migration through the Notch signaling which controls the disassembly of cell-cell adherens junction (Marambaud et al., 2002). However, the effect of high glucose on the disruption of E-cadherin-dependent cell-cell adherens junction in enhancing cell migration is still unknown.

MSCs are multipotent stem cells, which have differentiation

potentials for various kinds of somatic cells, such as osteoblasts, adipocytes, chondrocytes, myoblasts, and neural cells (Pittenger et al., 1999; Barry and Murphy, 2004). Due to various limitations in ESCs and induced pluripotent stem cells (iPSCs) research in teratoma formation as well as political and ethical restrictions, hUCB-MSCs are considered promising stem cell resources for stem cell-based therapies. In addition, previous studies demonstrated that the transplantation of hUCB-MSCs accelerates the wound healing process by promoting their migratory activity (Lee et al., 2016; Ryu and Han, 2015). Thus, I investigated the molecular mechanisms underlying the effect of high glucose on hUCB-MSC migration and the wound healing effect of high glucose-pretreated hUCB-MSC transplantation in the mouse skin wound model.

2. MATERIALS AND METHODS

2.1. Materials

Human UCB-MSCs were kindly provided from the MEDIPOST Co., Ltd. (Seoul, Korea) which were isolated and expanded according to previous report (Yang et al., 2004). Fetal bovine serum (FBS) was purchased from BioWhittaker Inc. (Walkersville, MO, USA). Antibodies specific for phospho (p)-JNK (sc-6254), JNK (sc-7345), p-ERK (sc-7383), ERK (sc-94), p38 (sc-7149), p-GSK-3β (sc-11757), GSK-3β (sc-9168), Snail (sc-28199), EZH2 (sc-25383), E-Cadherin (sc-7870), β-actin (sc-47778), and Lamin A/C (sc-20681) were purchased from Santa Cruz Biotechnology, Inc. (Santa Cruz, CA, USA). Anti-cleaved Notch1 (4147), Suz12 (3737), Akt (9272), p-p38 (9211) p-Akt^{Thr308} (13038) and p-Akt^{Ser473} (4060) antibodies were purchased from Cell Signaling Technology, Inc. (Danvers, MA, USA). Antibody specific for EED (09-774) was purchased from Millipore (*Billerica, MA, USA*). Secondary antibodies (anti-rabbit; sc-2004, anti-mouse; sc-2005, anti-goat; sc-2768) were obtained from

Santa Cruz Biotechnology, Inc. (Santa Cruz, CA, USA). D-, L-Glucose, N-Acetyl-L-cystein (NAC), L-685,458, LY294002, and lithium chloride (LiCl) were obtained from Sigma Chemical Company (St. Louis, MO, USA). Human Nuclear Antigen (HNA; Alexa Fluor 488 antibody) was purchased from Novus Biologicals (Littleton, CO, USA). 5-(and-6)-carboxy-2', 7'-dichloro-fluorescein diacetate (DCF-DA) was purchased from Molecular Probes (Eugene, OR, USA). Akt specific inhibitor was purchased from CalBiochem (La Jolla, CA, USA).

2.2. hUCB-MSC culture

hUCB-MSCs were cultured according to previous report (Jung et al., 2015). In this study, passage of hUCB-MSCs from five to eight was used and there is no discernible difference between passages (Chang et al., 2013). hUCB-MSCs without feeder layer were cultured in the α-MEM supplemented with 0.1 mM β-mercaptoethanol, 1% penicillin and streptomycin, and 10% FBS. Cells were grown on gelatinized 100-mm diameter culture dishes at 37° C with 5% CO_2 in the incubator. Cells were transferred to fresh

serum-containing α-MEM at least once every two days. Cells, cultured at 70-80% confluence, were washed twice with phosphate-buffered saline (PBS), and were transferred to serum-free α-MEM prior to experiments.

2.3. AD-MSC culture

AD-MSCs without feeder layer were cultured in the α-MEM supplemented with 0.1 mM β-mercaptoethanol, 1% penicillin and streptomycin, and 10% FBS. Cells were grown on gelatinized 100-mm diameter culture dishes at 37° C with 5 % CO_2 in the incubator. Cells were transferred to fresh serum-containing α-MEM at least once every two days. Cells were washed twice with PBS, and were transferred to serum-free α-MEM prior to experiments.

2.4. Mouse Excisional Wound Splinting Model

Mouse excisional wound splinting model and hUCB-MSC transplantation were performed, as described in the previous reports (Wang et al., 2013) and were approved by the Institutional

Animal Care and Use Committee (IACUC) at Seoul National University (SNU-161128-6). Male ICR mice aged 8 weeks were purchased from Han Lim Experimental Animal (Suwon, Korea). Mice were acclimated and stabilized in new surroundings for 4 days prior to the start of research and collecting data. To investigate the functional effects of high glucose-pretreated hUCB-MSC, mice were randomly divided into four groups (n = 6 each group): Vehicle, high glucose, hUCB-MSCs, and high glucose-pretreated hUCB-MSCs. To investigate the role of Snail and EZH2 in the migration of hUCB-MSC toward wound site, mice were randomly divided into six groups (n = 6 each group): non-targeting (NT) siRNA + hUCB-MSC, NT siRNA + high glucose-pretreated hUCB-MSC, *Snail* siRNA + hUCB-MSC, *Snail* siRNA + high glucose-pretreated hUCB-MSC, *EZH2* siRNA + hUCB-MSC, and *EZH2* siRNA + high glucose-pretreated hUCB-MSC. Cells were transfected with either *Snail* or *EZH2* siRNA for 24 h prior to the high glucose treatment for 24 h. Mice were anesthetized with 3% isoflurane in a mixture of N_2O/O_2 gas. Wounds were created by a 6 mm diameter biopsy punch (Kai Medical, Seki, Japan) on the back of a mouse, and a silicone splinting ring was attached around the wound using medical

adhesive with several stitches. 1 × 10^6 hUCB-MSCs in 100 μL saline were transplanted into the dermis at four sites around the wounds. Wound dressings were applied using Tegaderm™ (3M, St. Paul, MN, USA) to keep out water, dirt and germs. Mice were placed in individual cages in controlled rooms (24 ± 2° C, 12/12 h light/dark cycle with lights on at 7 AM). All wounds were monitored and photographed at different times (days 0, 3, 6, 9, and 11) by using a digital camera system (Canon, Tokyo, Japan). Percentages of wound size were calculated and analyzed by using Image J program. Mice were euthanized for the collection of wound tissue samples at day 11. The samples were fixed with 4% paraformaldehyde (PFA) in PBS for 4 h. Subsequently, for dehydration, the samples were incubated in 20% sucrose in PBS at room temperature for 2 h, and then were incubated in 30% sucrose at 4° C overnight. The next day, the tissues were embedded in O.C.T. compound (Sakura Finetek, Torrance, CA, USA) and were frozen immediately at − 70° C.

2.5. Haematoxylin and Eosin (H&E) staining

Wound tissues were cut at thickness of 6 ㎛ using a cryostat (Leica Biosystems, Nussloch, Germany) and mounted on SuperFrost Plus slides (Thermo Fisher Scientific, Waltham, MA, USA). The frozen tissue sections were fixed with 4% PFA for 5 min and were washed with running tap water for 5 min. Next, the tissues were stained with haematoxylin for 3 min and washed with running tap water for 5 min. The slides were placed in acid alcohol solution (1% HCl in 70% alcohol) and were stained with eosin solution for 30 sec. The slides were repeatedly dehydrated with 95% and 100% alcohol 3 times, each for 3 sec. Next, the slides were placed in xylene for 3 sec and then were mounted on clear glass slides. The slides were photographed using Eclipse Ts2-FL microscope (Nikon Corporation, Tokyo, Japan).

2.6. Intracellular ROS detection

Intracellular ROS detection was described in previous reports (Song et al., 2016). ROS was detected using DCF-DA, which is a fluorescence-based probe for ROS detection. Cells were treated

with 10 μM DCF-DA and were wrapped it in foil, due to light sensitivity, then placed on shaking incubator for 30 min at room temperature. Cells were observed using FluoView™ 300 confocal microscope (Olympus, Tokyo, Japan). To measure the intracellular hydrogen peroxide (H_2O_2) levels, the cells were treated with DCF-DA and were washed using ice-cold PBS twice. The cells were measured by using a luminometer (Victor3; PERKin-Elmer, Waltham, MA).

2.7. Oris™ cell migration assay

hUCB-MSCs were placed at a density of 10^4 cells/0.1 mL into a α-MEM containing serum in Oris™ cell seeding stoppers (Platypus Technologies, WI, USA), and were incubated until the cells had achieved 90% confluence of monolayers around the cell exclusion zone. The cells were transferred to serum-free α-MEM prior to experiments, and then silicone stoppers were carefully removed after 24 h. The cells were incubated in both with and without high glucose and each signal pathway-related molecule inhibitors/siRNAs, followed by fixation and staining with 5 μM

calcein AM (Wako, Osaka, Japan) in dark for 30 min. Fluorescence was measured using a luminometer (Victor3; PERKinElmer Inc., Waltham, MA, USA) and a fluorescent plate reader with excitation and emission wavelengths at 485 nm and 535 nm, respectively. The measurements were shown as Relative Fluorescence Units (RFU).

2.8. Wound-healing migration assay

hUCB-MSCs were seeded at density of 10^4 cells/0.1 mL in 35 mm diameter plates (IBIDI™, Martinsried, Germany) in a medium containing serum, and were incubated until the cells had achieved 90% confluence of monolayers into the inner well of the μ-Dish at 37° C and 5% CO_2 as usual. The old medium was aspirated carefully and fresh media was replaced every 2 days. The silicone inserts were carefully removed with sterilized forceps after serum-free treatment for 24 h. The cells were incubated with and without high glucose and indicated agents. Cells were pictured by either an Olympus FluoView™ 300 confocal microscope (Olympus, Tokyo, Japan) or Eclipse Ts2-FL microscope (Nikon Corporation, Tokyo, Japan).

2.9. Transfection of small interfering RNA (siRNA)

hUCB-MSCs that reached 80% confluence were transfected for 24 h with either a siRNA specific for *Snail1*, *EZH2* or a NT siRNA as a negative control (25 nM; Dharmacon, Lafayette, CO, USA) using DharmaFECT transfection reagent according to the manufacturer's instructions. The culture medium was replaced with transfection mixture- and serum-free medium after 6 h of incubation at 37° C and the cells were incubated for 24 h. The sequences of the siRNAs used in this experiment are described in Table 1.

Target gene	Sequence 5'-3'
Snail1	GCGAGCUGCAGGACUCUAA
	AAUCGGAAGCCUAACUACA
	GUGACUAACUAUGCAAUAA
	GAGUAAUGGCUGUCACUUG
EZH2	GAGGACGGCUUCCCAAUAA
	GCUGAAGCCUCAAUGUUUA
	UAACGGUGAUCACAGGAUA
	GCAAAUUCUCGGUGUCAAA
Non-targeting	UUCUCCGAACGUGUCACGUTT
	ACGUGACACGUUCGGAGAATT

Table 1. Sequences of siRNAs used for gene silencing.

2.10. Co-immunoprecipitation (Co-IP)

hUCB-MSCs were lysed with the co-IP buffer (50 mM Tris-HCl [pH 7.4] containing 150 mM NaCl, 5 mM EDTA, 2 mM $Na3VO_4$, 2.5 mM Na_4PO_7, 100 mM NaF, 200 nM microcystin lysine-arginine and protease inhibitors) according to the previous report (Ryu et al., 2015). Cell lysates were added with anti-Snail or EZH2 antibodies and Protein A/G PLUS-agarose IP reagent (Pierce; Rockford, IL, USA), and then the cell lysates were incubated for 4 h in a shaking incubator maintained at 4° C. The beads were washed more than three times with the co-IP buffer, and then the bound proteins with beads were eluted by boiling for 5 min. Samples were analyzed by western blotting with anti-EZH2, EED, Suz12, Snail and histone deacetylase 1 (HDAC1) antibodies.

2.11. Cytosol and nuclear fractionation

hUCB-MSCs were lysed in lysis buffer (20 mM Tris-HCl, 10 mM EGTA, 2 mM EDTA, 2 mM Dithiothreitol, 1% Triton X-100, 1 mM phenylmethylsulfonylfluoride [PMSF], 25 mg/mL aprotinin and 10 mg/mL leupeptin). Lysates were homogenized with lysis buffer

and sonicated using a Branson Sonifier 250 (All-spec, Wilmington, NC, USA) with set to 4 of output power for 10 sec. The lysates were then centrifuged at 8,000 rpm for 5 min at 4° C. The supernatant, containing cytosol and membrane, was centrifuged at 15,000 rpm for 60 min at 4° C, and were divided into cytosol and membrane. The pellet, containing the nucleus, was homogenized with lysis buffer and sonicated for 10 sec. It was centrifuged at 15,000 rpm for 15 min at 4° C and the supernatant was collected as a nuclear lysate fraction.

2.12. SDS-PAGE and Western blot analysis

hUCB-MSCs were washed twice with cold-PBS followed by incubation on ice. Cells were lysed with lysis buffer (20 mM Tris [pH 7.5], 1 mM EDTA, 1 mM EGTA, 1% Triton X-100, 1 mg/mL aprotinin, 1 mM PMSF, and 0.5 mM sodium orthovanadate) and shared with 1 set of 3-second pulses on ice using a Branson Sonifier 250 with set to 3 of output power. Sample protein separations were resolved by SDS-polyacrylamide gel electrophoresis (SDS-PAGE) and transferred to polyvinylidene

difluoride (PVDF) membranes. The membranes were incubated with primary antibody (1:800 or 1:1000 dilutions) at 4° C incubator for overnight after blocked with TBST (10 mM Tris-HCl [pH 7.6], 150 mM NaCl, and 0.01% Tween-20) containing 5% skim milk for 1 h. Next day, the membranes were washed with PBS and then incubated with a HRP secondary antibody. The specific bands were detected by ChemiDoc™ XRS+ System (Bio-Rad, Richmond, CA).

2.13. Chromatin Immunoprecipitation assay

EZ-ChIP-Chromatin Immunoprecipitation Kit (EMD Millipore) was used for Chromatin Immunoprecipitation (CHIP) assay. Cells were cross-linked by incubation at room temperature with 37% formaldehyde for 10 min and added 1 M glycine to quench the unreacted formaldehyde according to the manufacturer's instructions. Fixed cells were harvested in SDS lysis buffer (1% SDS, 10 mM EDTA, 50 mM Tris [pH 8.1] and protease inhibitors). Cell lysates were sonicated, and then were incubated with protein G beads (50% protein G agarose slurry) for IP. IP included positive control (Anti-RNA polymerase II), negative control (IgG), and antibody of interest. The negative control IgG of the same species as the antibody of interest was used. Protein/DNA complexes were

eluted by incubation at room temperature with elution buffer (20% SDS, 1 M $NaHCO_3$ and distilled water) for 15 min. After centrifugation, supernatant was collected into new microfuge tubes. All IPs and inputs with 5 M NaCl were incubated at 65° C for overnight to reverse the protein/DNA cross-links. The purified DNA was subjected to PCR and DNA fragments were run on agarose gel (2.5%) to facilitate quantitation of the PCR products. The sequences of the primers used in the PCR reactions were as follows: E-box human promoter (forward primer) 5' CTCCAGCTTGGGTGAAAGAG 3', E-box human promoter (reverse primer) 5' GGGCTTTTACAC TTGGCTGA 3'.

2.14. Immunofluorescence staining

hUCB-MSCs were cultured in confocal dish. Cells were washed twice with cold-PBS, and then were fixed with 4% PFA for 10 min according to previous report (Jung et al., 2015). 0.1% Triton X-100 diluted in PBS was used for permeabilization for 5 min. 5% Normal Goat Serum (NGS) was used to decrease non-specific binding of antibody for 30 min, followed by incubation with primary antibody with dilution of 1:100 for overnight. Subsequently, cells were incubated with either fluorescein isothiocyanate (FITC)

conjugated anti-rabbit and -mouse IgG antibody or Alexa Fluor® goat anti-rabbit IgG to either propidium iodide (PI) or phalloidin in dark for 1 h. Next, cells were observed using Eclipse Ts2-FL microscope (Nikon Corporation, Tokyo, Japan).

2.15. Phalloidin staining

hUCB-MSCs were cultured in confocal dish. Cells were washed twice with cold-PBS, and then were fixed with 4 % PFA for 10 min. Subsequently, cells were permeabilized with 0.1 % Triton X-100 in PBS for 5 min. After blocking with 1 % FBS or 5 % normal goat serum for 30 min, cells were incubated with Alexa Fluor 488-conjugated to phalloidin (Invitrogen Co., Carlsbad, CA) in dark for 1 h. Cells were washed twice with PBS. Next, cells were observed using Eclipse Ts2-FL microscope (Nikon Corporation, Tokyo, Japan).

2.16. Statistical analysis

Data are represented as mean ± standard error mean (SEM).

Statistical analyses were performed using the analysis of variance (ANOVA), and Bonferroni–Dunn test allows for multiple comparisons in some cases. A p value of < 0.05 was accepted as statistical significance.

3. RESULTS

3.1. Effect of high glucose on migration and effect of hUCB-MSCs on mouse skin wound healing

To confirm the effect of high glucose on hUCB-MSC migration, cells were incubated under high glucose conditions for various concentrations of D-glucose or L-glucose from 5 to 50 mM and for times ranging from 0 to 24 h. D-glucose increased the number of migrating cells after cell incubation for 24 h, while L-glucose did not have an effect on the cells (Figure 5A), suggesting that the osmotic effect did not influence high glucose on hUCB-MSC migration. I also quantified the percent migration by using the Oris™ cell migration assay and observed a maximum increase of up to 151% after incubating cells with 25 mM D-glucose for 24 h (Figure 5B). High glucose also facilitated hUCB-MSC migration to the detection zone (Figure 5C). In order to distinguish cell migration from proliferation, cells were pretreated with Mitomycin C to inhibit cell proliferation. As a result, I observed no significant

differences between the groups treated with or without Mitomycin C under high glucose conditions. This means that high glucose-induced hUCB-MSC proliferation did not affect hUCB-MSC migration (Figure 5D). As shown in Figure 6, high glucose induced F-actin cytoskeleton reorganization, and formed cell-motility structures at the leading edges of the cells. The cytoskeleton changes occurred at various time periods by high glucose in hUCB-MSCs. In addition, other sources of MSCs, Adipose-derived mesenchymal stem cells (AD-MSCs), significantly stimulated the migration after incubating cells with 25 mM glucose for 24 h (Figure 7). In order to investigate the wound healing effect of high glucose-pretreated hUCB-MSCs, I used a mouse skin excisional wound splinting model and performed wound size measurements, histological examinations, and blood vessel density measurements. The wound area of the high glucose-pretreated hUCB-MSC group compared to that of the hUCB-MSC alone was significantly reduced at 11 days after wounding as well as the wound area of hUCB-MSC transplanted groups compared to basal conditions (Figure 8A and 8B). Histological examination of wound tissues on day 11 showed that the wound site was completely filled with granulation tissues

by high glucose pretreated hUCB-MSCs transplantation compared to the wounds of vehicle, high glucose, or hUCB-MSC group (Figure 8C). To track transplanted hUCB-MSCs in vivo on day 11, wound tissues were stained with anti-human nuclear antigen (HNA) antibody. Immunohistochemistry revealed many HNA-positive cells in high glucose-pretreated hUCB-MSC group, whereas in vehicle or high glucose group, no HNA-positive cells were found (Figure 9A). Blood vessels that developed many branches were observed in hUCB-MSC transplanted groups compared to the vehicle or high glucose treated group (Figure 9B). Collectively, the data suggest that hUCB-MSCs cultured with high glucose significantly increased migratory activity compared to those cultured at a normal physiological glucose level. Moreover, high glucose-pretreated hUCB-MSC transplantation significantly accelerated skin wound healing.

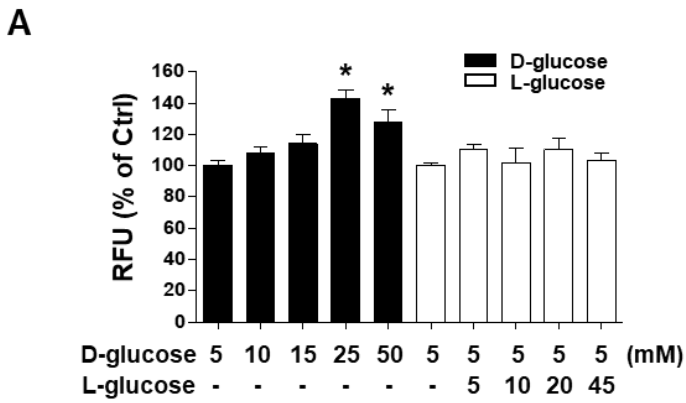
A
D-glucose
L-glucose
RFU (% of Ctrl)
160
140
120
100
80
60
40
20
0
*
*
D-glucose 5 10 15 25 50 5 5 5 5 5 (mM)
L-glucose - - - - - - 5 10 20 45

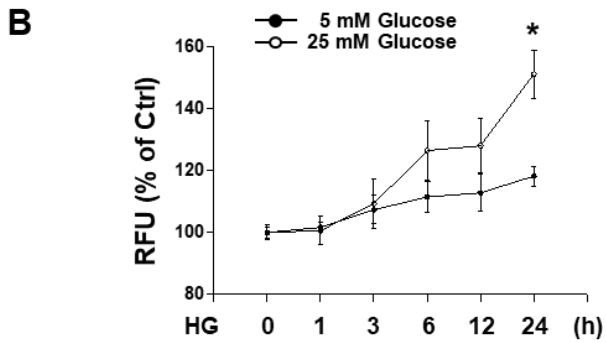
B
5 mM Glucose
25 mM Glucose
RFU (% of Ctrl)
160
140
120
100
80
*
HG 0 1 3 6 12 24 (h)

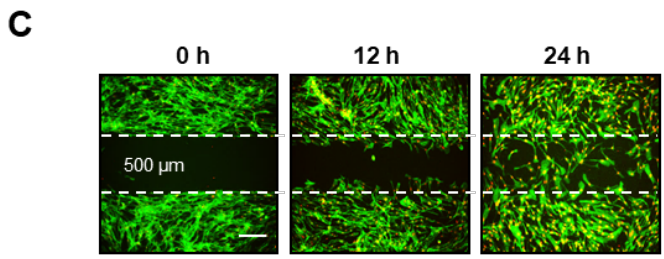
C
0 h
12 h
24 h
500 μm

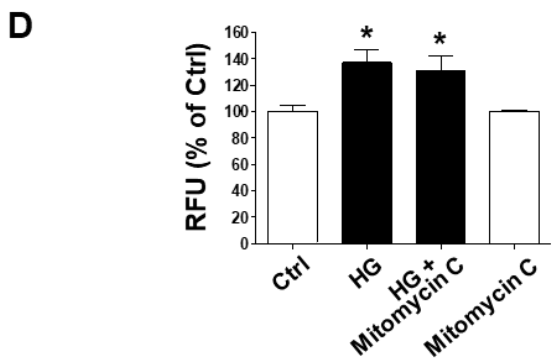
D
RFU (% of Ctrl)
160
140
120
100
80
60
40
20
0
*
*
Ctrl
HG
HG + Mitomycin C
Mitomycin C

Figure 5. Effect of high glucose on hUCB-MSC migration. Dose response effects of D-glucose (5-50 mM) or L-glucose (5-50 mM) for 24 h, and (B) time (0-24 h) response effects of high glucose (D-glucose, 25 mM) or normal physiological conditions of glucose (5 mM) on hUCB-MSC migration were measured with Oris™ cell migration assay. hUCB-MSCs cultured with normal medium were regarded as the control. n = 3. $*p < 0.05$ versus 5 mM D-glucose. (C) Wound healing migration assay was performed in the presence of high glucose (25 mM) and with the IBIDI™ cell culture inserts. Cells were treated with 25 mM glucose for various time periods (0-24 h). Wound width = 500 μm. Scale bars = 100 μm. (D) Cells were pretreated with 1 μg/mL mitomycin C for 90 min prior to 25 mM glucose treatment for 24 h. Fluorescence in the analytical zone was quantified with a plate reader. n = 3. $*p < 0.05$ versus ctrl.

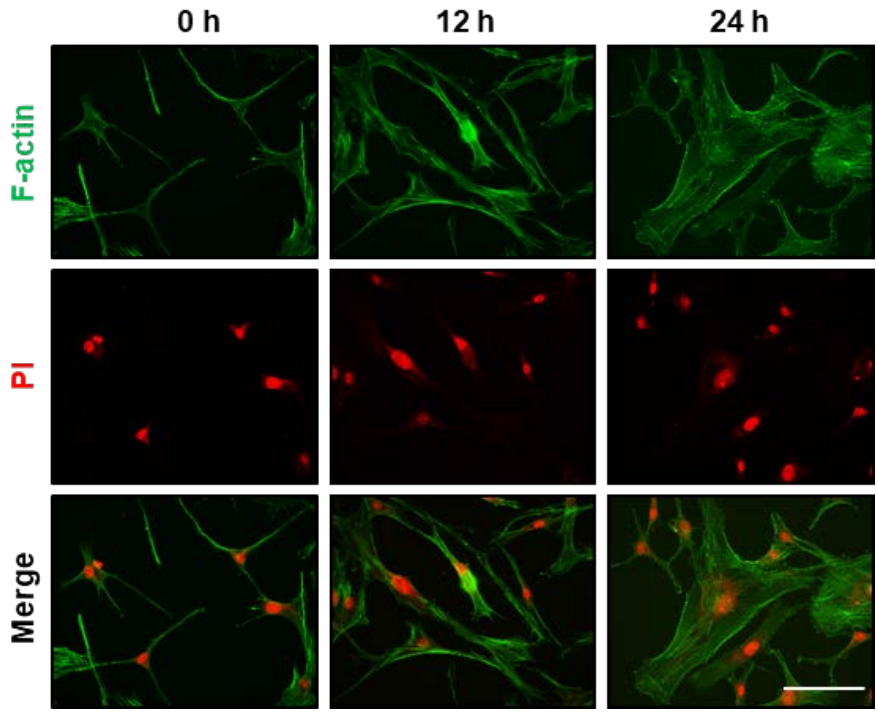

Figure 6. Effect of high glucose on F-actin reorganization of hUCB-MSCs. hUCB-MSCs were treated with 25 mM glucose for various periods (0-24 h). F-actin was stained with phalloidin staining (green) and counterstained with PI (red). Cells were observed with confocal fluorescence microscopy. Scale bar = 100 μm.

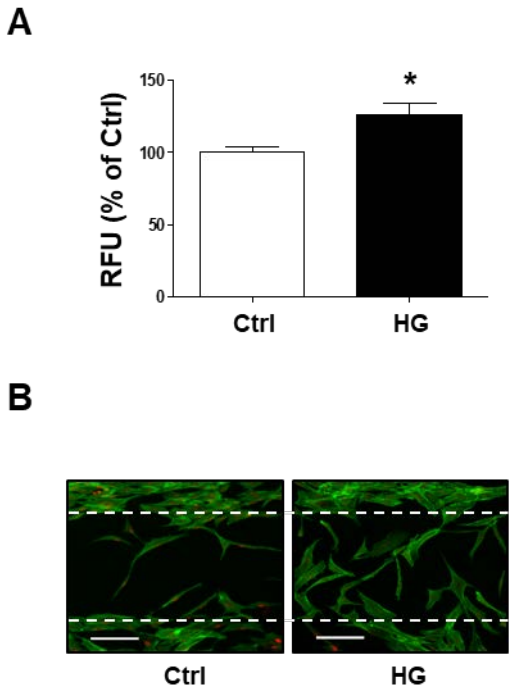

Figure 7. Effect of high glucose on AD-MSC migration. (A) AD-MSCs were incubated with 25 mM glucose for 24 h and migration were measured by Oris™ migration assay. Fluorescence in the analytical zone was quantified with a multiplate reader. n=3. $*p < 0.05$ versus ctrl. (B) Wound healing migration assay was performed. Cells were stained with Alexa Fluor 488-phalloidin and PI and the dishes were photographed using Eclipse Ts2-FL microscopy (Nikon Corporation, Tokyo, Japan). Scale bar = 100 μm.

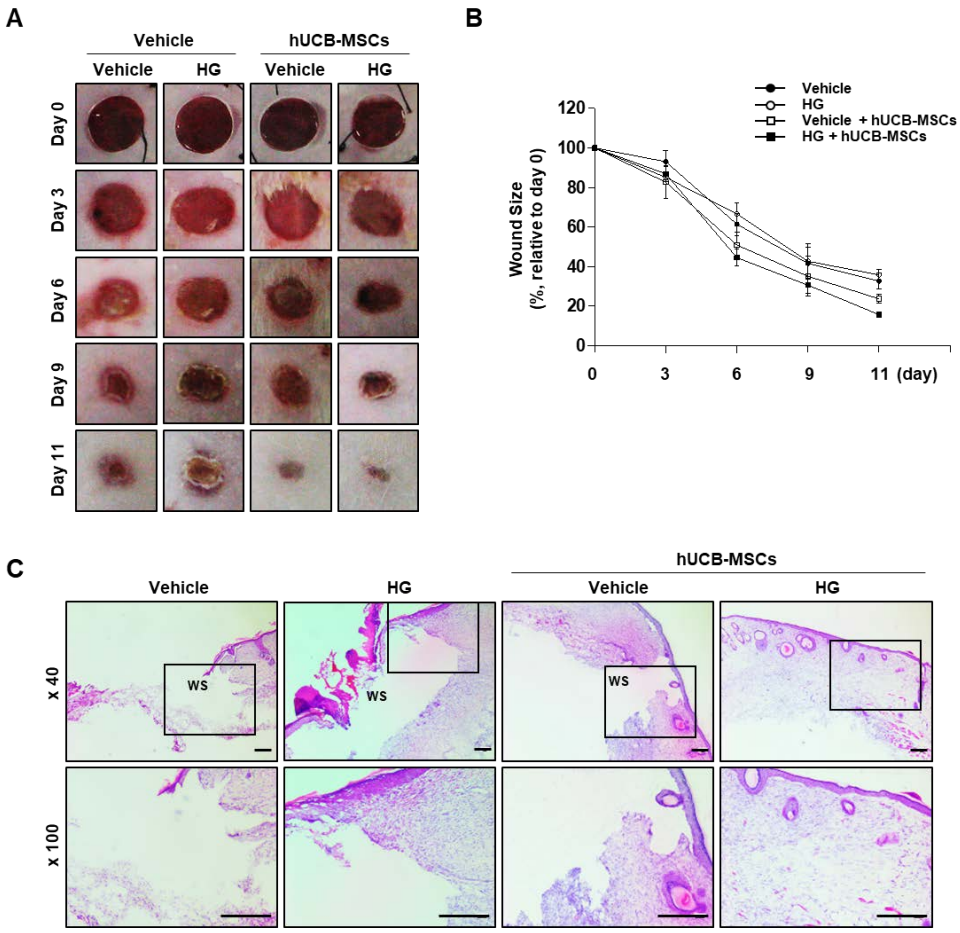
A
Vehicle
hUCB-MSCs
Vehicle
HG
Vehicle
HG
Day 0
Day 3
Day 6
Day 9
Day 11
B
Vehicle
HG
Vehicle + hUCB-MSCs
HG + hUCB-MSCs
Wound Size
(%, relative to day 0)
120
100
80
60
40
20
0
0
3
6
9
11 (day)
C
hUCB-MSCs
Vehicle
HG
Vehicle
HG
x 40
x 100
WS
WS
WS

Figure 8. Effect of high glucose-pretreated hUCB-MSC transplantation in mouse skin wound healing. (A) Representative gross images of wounds at days 0, 3, 6, 9, and 11 are shown. (B) Wound sizes were measured using ImageJ software. n=6 each group. $*p < 0.05$ versus vehicle + hUCB-MSC group. $\#p < 0.05$ versus vehicle group. $\$p < 0.05$ versus high glucose group. (C) Wound tissues were stained by using H&E staining at day 11 after wounding. Scale bar = 200 μm or 100 μm.

A

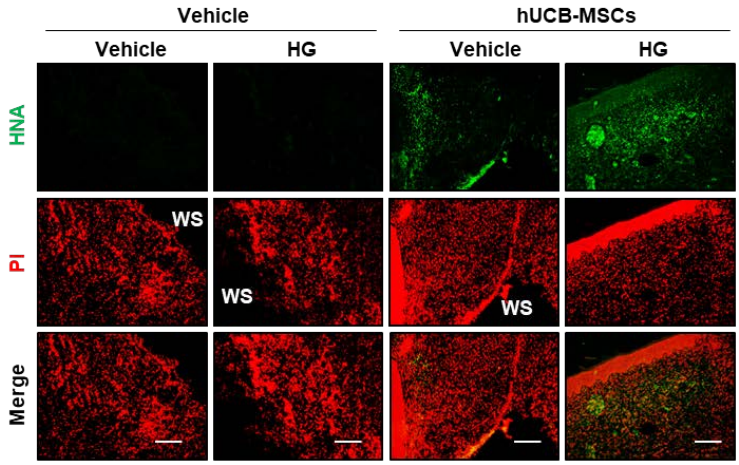
Vehicle
hUCB-MSCs
Vehicle
HG
Vehicle
HG
HNA
PI
Merge
WS
WS
WS

B

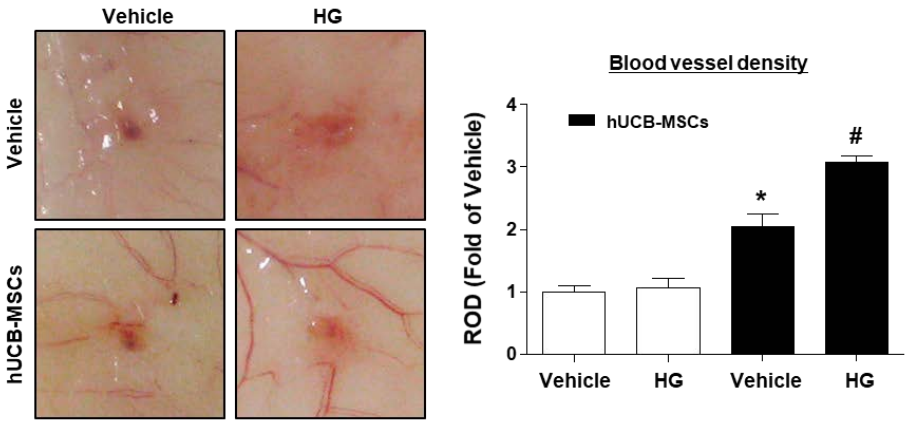
Vehicle
HG
Vehicle
hUCB-MSCs
Blood vessel density
hUCB-MSCs
ROD (Fold of Vehicle)
0
1
2
3
4
*
#
Vehicle
HG
Vehicle
HG

Figure 9. Effect of high glucose-pretreated hUCB-MSC transplantation on cell survival and angiogenesis. (A) Wound tissues were immunostained with human nuclear antigen (HNA; green) and PI (red). Scale bar = 50 μm. (B) Representative gross images of blood vessels in wound site at day 11 are shown (*left panel*). Blood vessel density was analyzed by optical density using ImageJ software (*right panel*). $*p < 0.05$ versus vehicle group, $\#p < 0.05$ versus vehicle + hUCB-MSCs group.

3.2. Effect of high glucose on E-cadherin, cleaved Notch, Snail and EZH2 expression

Because regulation of E-cadherin expression plays an important role in cell migration, I investigated the effect of high glucose-induced E-cadherin repression in hUCB-MSCs. Human UCB-MSCs were incubated at high glucose conditions for up to 48 h to verify E-cadherin expression and to examine whether high glucose affected E-cadherin, which is related with hUCB-MSC migration. E-cadherin expression decreased gradually after 12 h incubation under high glucose conditions (Figure 10A). In addition, cleaved-Notch, Snail and EZH2 expressions were increased in a time-dependent manner under high glucose conditions (Figure 10B). To confirm the role of high glucose-induced E-cadherin by regulating Snail and EZH2 expressions, NT, *Snail,* and *EZH2* siRNA transfections were carried out. The levels of E-cadherin were reduced by NT siRNA while *Snail* and *EZH2* siRNA restored the E-cadherin level under high glucose conditions (Figure 11A). To confirm the signaling relationship between Snail and EZH2, *Snail* and *EZH2* siRNA transfections were carried out. Interestingly, the

protein levels of Snail were not reduced by *EZH2* siRNA, and the levels of EZH2 were not reduced by *Snail* siRNA (Figure 11B). Hence, these results indicate that high glucose-induced E-cadherin repression is regulated by Snail and EZH2, and Snail is regulated in parallel with EZH2 by high glucose.

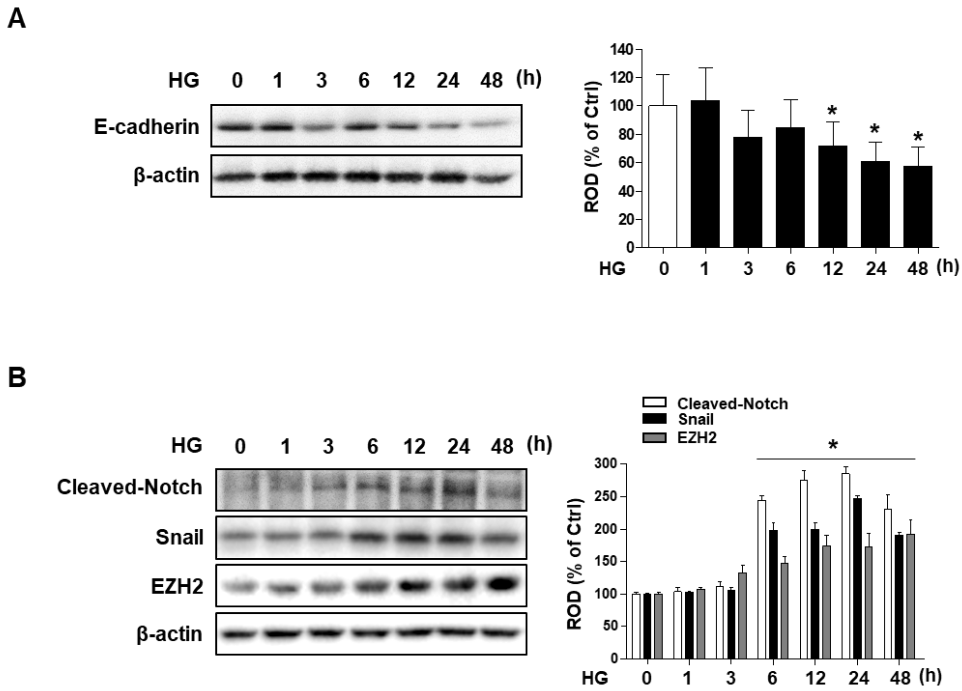

Figure 10. Effect of high glucose on E-cadherin, Notch, Snail and EZH2 expression. (A) Expression of E-cadherin was analyzed by western blot with a specific antibody. Cells were exposed to high glucose for 0 to 48 h, and the total lysates were analyzed by western blot with anti-E-cadherin antibody. β-actin was used as a loading control. n=3. $*p < 0.05$ versus 0 h. (B) hUCB-MSCs were incubated under high glucose conditions for 0 to 48 h, and the total cell lysates were analyzed by western blot with antibodies that recognize cleaved-Notch, Snail and EZH2. β-actin was used as a loading control. n=3. $*p < 0.05$ versus 0 h.

A

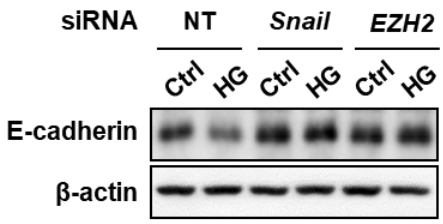
siRNA
NT
Snail
EZH2
Ctrl
HG
Ctrl
HG
Ctrl
HG
E-cadherin
β-actin

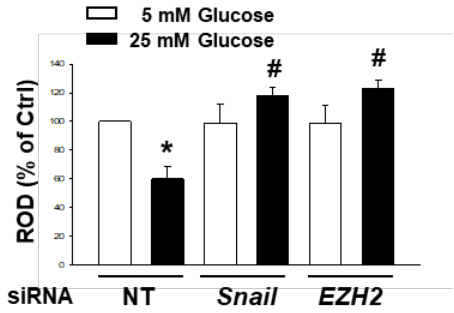
5 mM Glucose
25 mM Glucose
ROD (% of Ctrl)
*
#
#
siRNA
NT
Snail
EZH2

B

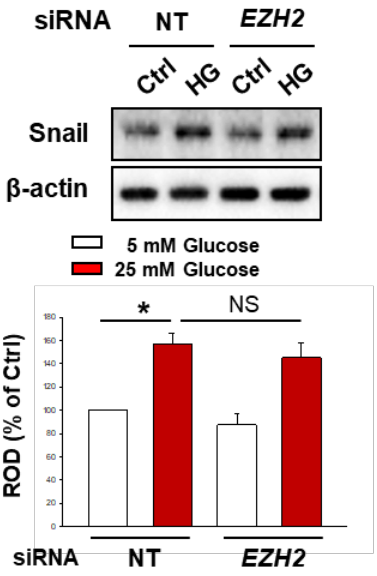
siRNA
NT
EZH2
Ctrl
HG
Ctrl
HG
Snail
β-actin
5 mM Glucose
25 mM Glucose
ROD (% of Ctrl)
*
NS
siRNA
NT
EZH2

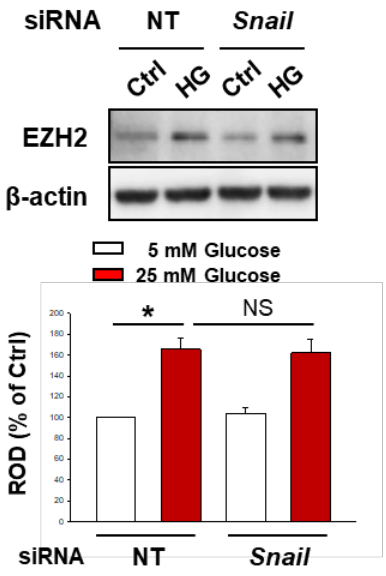
siRNA
NT
Snail
Ctrl
HG
Ctrl
HG
EZH2
β-actin
5 mM Glucose
25 mM Glucose
ROD (% of Ctrl)
*
NS
siRNA
NT
Snail

Figure 11. Effect of high glucose on E-cadherin, through Snail and EZH2 signaling in hUCB-MSCs. (A) Cells were treated with NT-, *Snail*- or *EZH2* siRNA in presence or absence of 25 mM glucose. E-cadherin was analyzed by western blot. n=3. $*p < 0.05$ versus NT siRNA only and $\#p < 0.05$ versus high glucose with NT siRNA transfection. (B) hUCB-MSCs were left untransfected or transfected with NT siRNA or specific siRNA that silences *EZH2* or *Snail* expression and then treated for a further 24 h with 25 mM glucose. n=3. $*p < 0.05$ versus NT siRNA only. NS = non-significant ($p > 0.05$).

3.3. Role of ROS-stimulated JNK/Notch and PI3K/Akt/GSK-3β pathways in high glucose-induced EZH2 and Snail expressions

High glucose stimulation is well known to increase the ROS production. To examine the effect of high glucose on ROS generation in hUCB-MSCs, high glucose-induced ROS generation was examined using DCF-DA, to gradually increase ROS generation (Figure 12). The activation of MAPK and Akt pathways play important roles in migration induction under high glucose conditions (Huang and Sheibani, 2008; Lee and Han, 2010). Thus, I further investigated whether high glucose-induced ROS can modulate the MAPK regulation. High glucose significantly enhanced the JNK activation at 180 min while phosphorylation levels of ERK and p38 MAPK had no time-related changes (Figure 13). Blockage of ROS in hUCB-MSCs under high glucose conditions led to decreased JNK activation compared to high glucose alone. However, ROS inhibition with NAC treatment did not lead to the inhibition of phosphorylation of ERK and p38 MAPK (Figure 14A). Furthermore, high glucose-induced hUCB-MSC migration was blocked by NAC or SP600125

(Figure 14B). In order to investigate whether ROS-induced p-JNK in high glucose conditions regulates γ-secretase in hUCB-MSCs, I performed western blotting after isolating the nuclear fraction. In the nucleus, cleaved-Notch was down-regulated after treating hUCB-MSCs with SP600125. However, pretreatment with PD98059 and SB203580 did not impact the cleaved-Notch as well as the degradation of cleaved-Notch after SP600126 treatment in high glucose conditions in the nucleus (Figure 15A). Furthermore, high glucose elevated the expression of EZH2, which was suppressed by the L-685,458 (Figure 15B). These results show that ROS-mediated JNK activation regulated γ-secretase-induced Notch cleavage for Notch intracellular domain (NICD) under high glucose conditions.

To assess whether high glucose-induced ROS production can regulate PI3K/Akt and GSK-3β signaling pathways, I measured the total expression and activation of Akt and GSK-3β. Akt^{thr308} and Akt^{ser473} phosphorylation were gradually increased by incubation in high glucose conditions (Figure 16A). In addition, NAC blocked high glucose-induced Akt^{thr308} and Akt^{ser473} phosphorylation, which suggest that high glucose-induced activation of Akt at thr308

and ser473 was regulated by ROS (Figure 16B). I next investigated whether PI3K/Akt signaling induced phosphorylation of GSK-3β. In high glucose conditions, the inhibitions of PI3K/Akt with LY294002 or the Akt inhibitor blocked GSK-3β phosphorylation (Figure 16C), resulting in subsequent Snail stabilization. As shown in the details of Figure 16D, although the total expression levels of GSK-3β were unmodified by high glucose, the level of GSK-3β phosphorylation increased in a time-dependent manner. In order to determine whether high glucose increased Snail expression through GSK-3β phosphorylation, the cells were pretreated with LiCl, a well-known GSK-3β inhibitor. LiCl increased the inactive phosphorylated form of GSK-3β at ser9 and Snail expression (Figure 16E). These results suggest that high glucose-induced ROS regulates the activation of PI3K/Akt signaling to inhibit GSK-3β. The GSK-3β inhibition induces an increase in Snail stabilization.

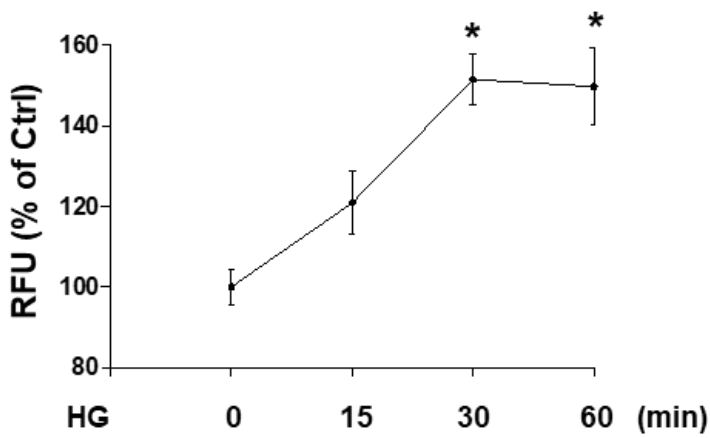

Figure 12. Role of high glucose on ROS generation. The cells were incubated in high glucose conditions for 0–60 min. Dichlorofluorescein-sensitive cellular ROS was detected by luminometer. n=3. $*p < 0.05$ versus 0 min.

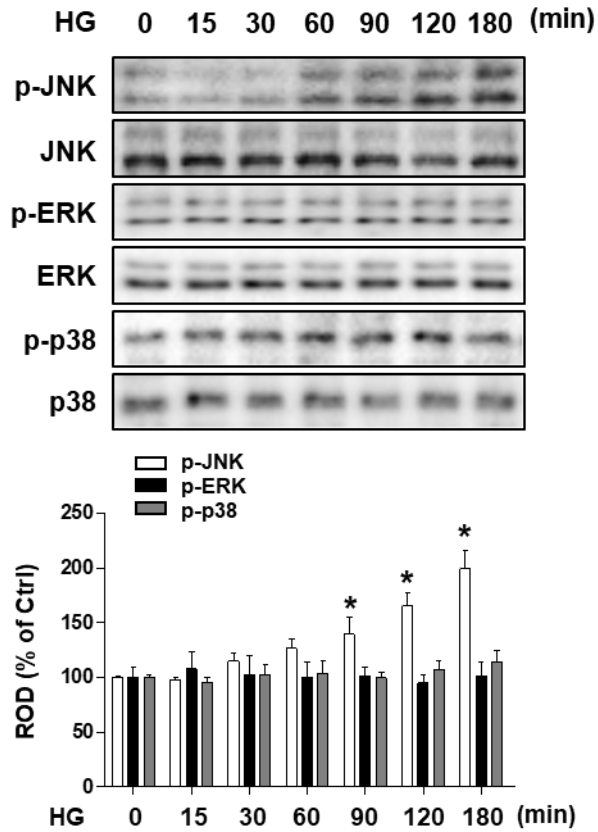

Figure 13. Time-dependent activation of MAPK by high glucose. Cells were incubated under high glucose for 0-180 min, and the total lysates were analyzed by western blot with antibodies that recognize MAPK proteins. n=3. $*p < 0.05$ versus 0 min.

A

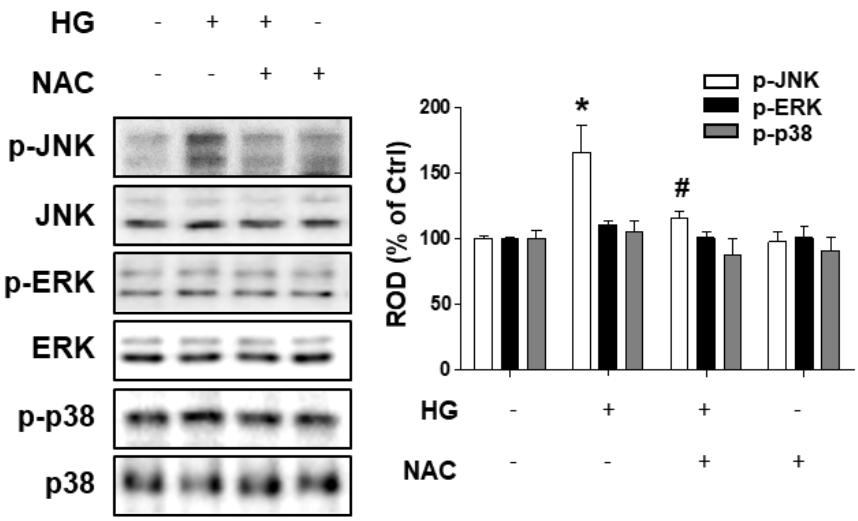
HG - + + -
NAC - - + +
p-JNK
JNK
p-ERK
ERK
p-p38
p38
p-JNK
p-ERK
p-p38
ROD (% of Ctrl)
200
150
100
50
0
*
#
HG - + + -
NAC - - + +

B

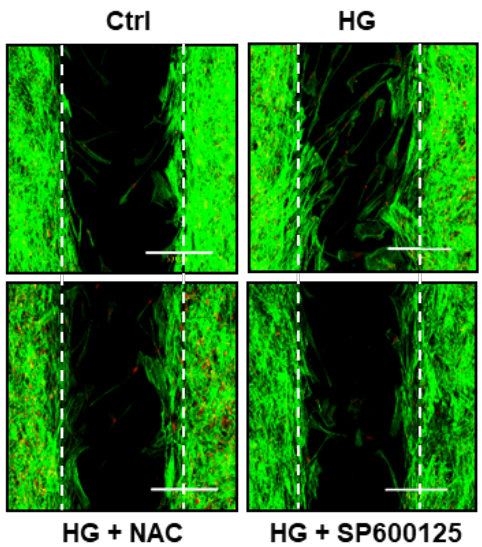
Ctrl
HG
HG + NAC
HG + SP600125

Figure 14. Role of ROS-dependent JNK signaling pathway. (A) NAC (ROS inhibitor; 10 μM) was used for pretreatment prior to incubation in the high glucose conditions. p-JNK, p-ERK or p-p38 was analyzed by western blot. n=3. $*p < 0.05$ versus ctrl of p-JNK. $\#p < 0.05$ versus high glucose alone of p-JNK. (B) Wound healing migration assay was performed in the pretreatment of NAC or SP600125 in the presence of high glucose. Scale bar = 200 μm.

A

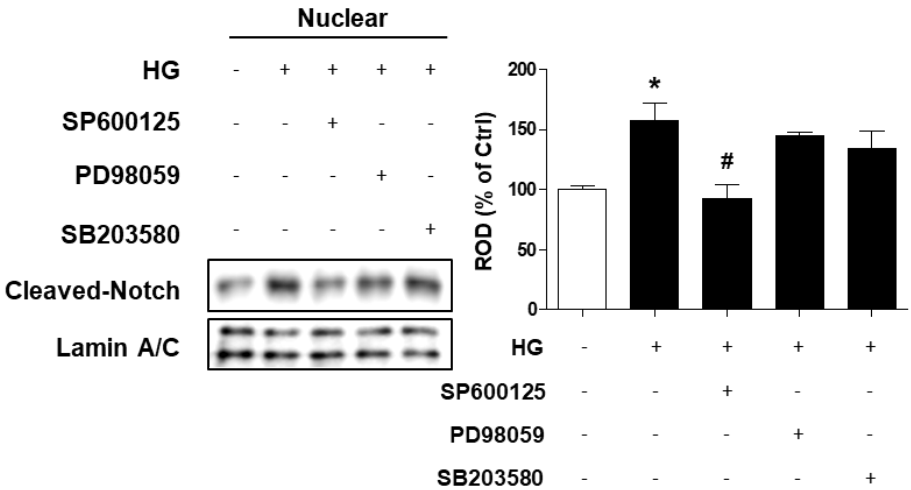
Nuclear
HG - + + + +
SP600125 - - + - -
PD98059 - - - + -
SB203580 - - - - +
Cleaved-Notch
Lamin A/C
ROD (% of Ctrl)
200
150
100
50
0
*
#
HG - + + + +
SP600125 - - + - -
PD98059 - - - + -
SB203580 - - - - +

B

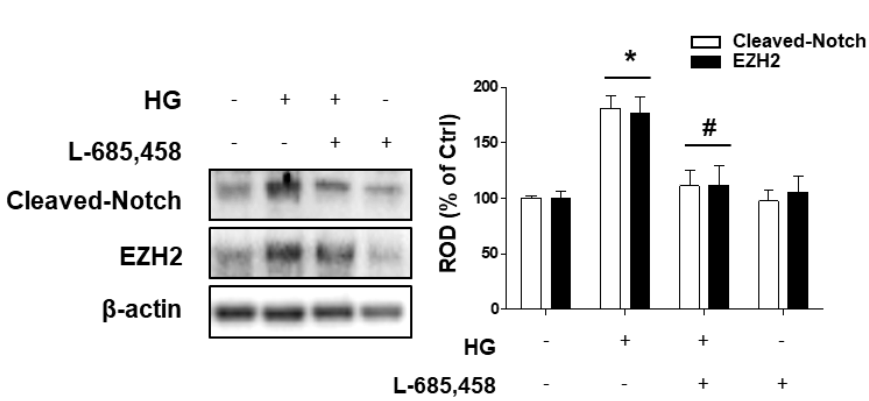
HG - + + -
L-685,458 - - + +
Cleaved-Notch
EZH2
β-actin
Cleaved-Notch
EZH2
ROD (% of Ctrl)
200
150
100
50
0
*
#
HG - + + -
L-685,458 - - + +

Figure 15. Role of ROS-dependent Notch signaling pathway under high glucose conditions. (A) hUCB-MSCs were pretreated with SP600125 (JNK inhibitor; 1 μM), PD98059 (ERK inhibitor, 10 μM), or SB203580 (p38 MAPK inhibitor, 1 μM) for 30 min before incubation under high glucose conditions, and then, the nuclear fractions were isolated from cells as describe in the "*Materials and Methods*". Lamin A/C was used as a nuclear marker. n=3. $*p < 0.05$ versus ctrl. $\#p < 0.05$ versus high glucose alone. (B) L-685,458 (γ-secretase inhibitor; 10 μM) was used for pretreatment prior to incubation under high glucose conditions for 24 h. Cleaved-Notch and EZH2 were detected by western blot. n=3. $*p < 0.05$ versus ctrl. $\#p < 0.05$ versus high glucose alone.

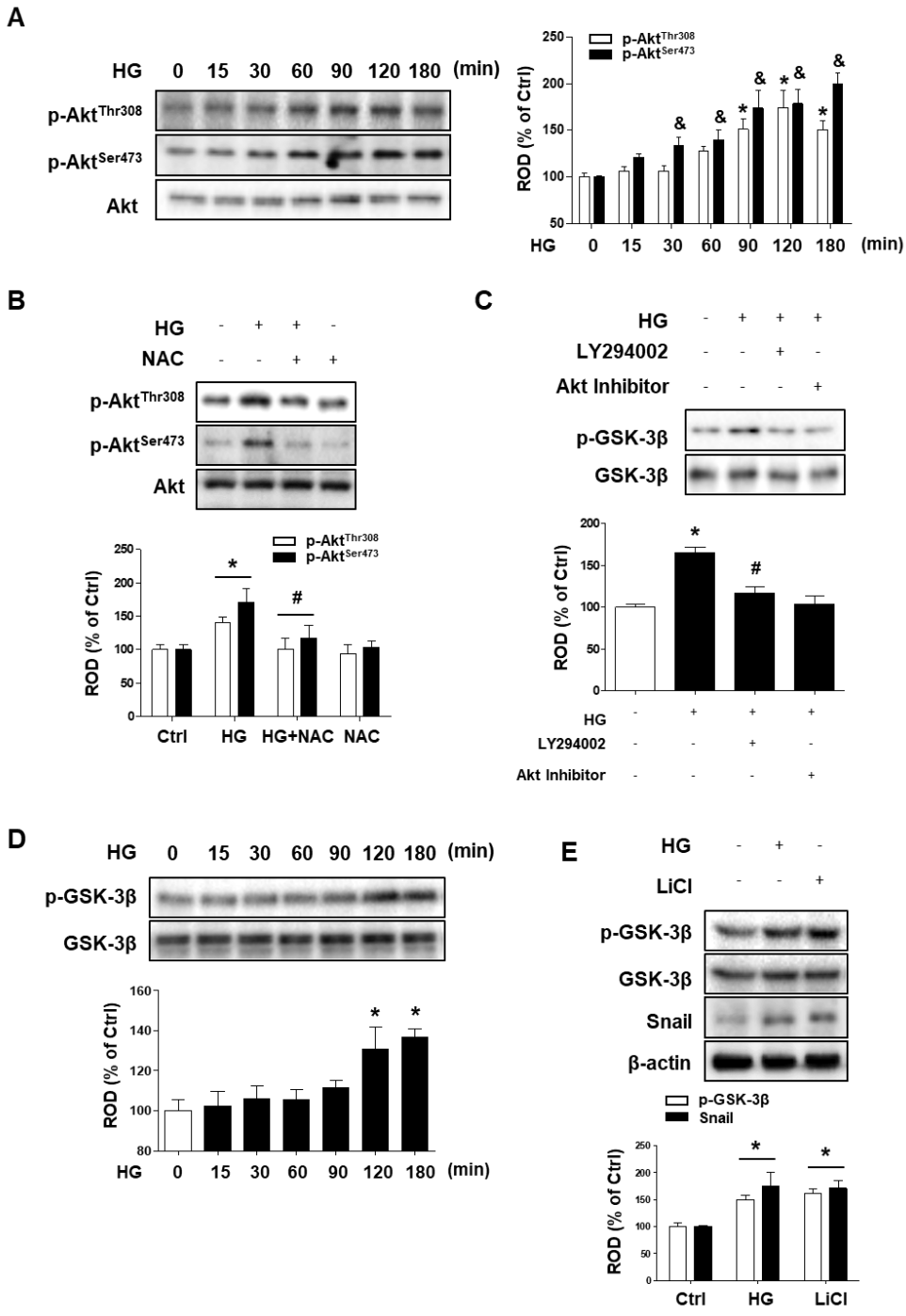
A
HG 0 15 30 60 90 120 180 (min)
p-Akt^Thr308
p-Akt^Ser473
Akt
ROD (% of Ctrl)
p-Akt^Thr308
p-Akt^Ser473
HG 0 15 30 60 90 120 180 (min)
B
HG
NAC
p-Akt^Thr308
p-Akt^Ser473
Akt
ROD (% of Ctrl)
Ctrl HG HG+NAC NAC
C
HG
LY294002
Akt Inhibitor
p-GSK-3β
GSK-3β
ROD (% of Ctrl)
D
HG 0 15 30 60 90 120 180 (min)
p-GSK-3β
GSK-3β
ROD (% of Ctrl)
E
HG
LiCl
p-GSK-3β
GSK-3β
Snail
β-actin
p-GSK-3β
Snail
ROD (% of Ctrl)
Ctrl HG LiCl

Figure 16. Role of ROS-dependent PI3K/Akt/GSK-3β signaling pathway. (A) hUCB-MSCs were incubated under high glucose conditions for 0-180 min, and the total cell lysates were analyzed by western blot with antibodies the recognize p-Akt^{The308}, p-Akt^{Ser473}, or Akt. n=3. $*p < 0.05$ versus 0 min. (B) The cells were pretreated with NAC prior to incubation under high glucose conditions for 180 min. p-Akt^{The308}, p-Akt^{Ser473}, or Akt was analyzed by western blotting. n=3. $*p < 0.05$ versus ctrl, $\#p < 0.05$ versus high glucose alone. (C) The cells were pretreated with LY294002 (PI3K inhibitor; 1 μM), or Akt inhibitor (10 μM) prior to incubation under high glucose conditions, and p-GSK-3β and GSK-3β were detected. n=3. $*p < 0.05$ versus ctrl, $\#p < 0.05$ versus high glucose alone. (D) Cells were incubated under high glucose conditions for 0-180 min, and p-GSK-3β or GSK-3β was detected. n=3. $*p < 0.05$ versus 0 min. (E) Cells were treated with LiCl (10 mM) for 30 min. The total cell lysates were analyzed by western blot using antibodies that recognized p-GSK-3β, GSK-3β and Snail. n=3. $*p < 0.05$ versus ctrl.

3.4. Effect of high glucose on the formation of EZH2/Snail /HDAC1 complex in the nucleus

Next, I examined the role of high glucose-induced Snail and EZH2 accumulation in the nucleus. To determine the cellular fraction where cleaved-Notch, Snail, and EZH2 accumulated, I tested the nuclear and cytosolic fraction before performing a western blot analysis. High glucose enriched cleaved-Notch, Snail, and EZH2 in the nuclear fraction. While the cytoplasmic levels of cleaved-Notch did not change, the cytoplasmic levels of Snail and EZH2 increased (Figure 17A). Immunofluorescence staining indicated that Snail or EZH2 present in the cytoplasm accumulated around the nucleus and translocated to the nucleus under high glucose conditions (Figure 17B and 17C). To examine whether Snail and EZH2 are required for binding to the E-box of the E-cadherin promoter under high glucose conditions, I performed CHIP to analyze whether Snail and EZH2 were recruited to the E-cadherin promoter. The CHIP assays revealed that high glucose enhanced the interaction between Snail and the E-cadherin promoter. In addition, the interaction between EZH2 and the E-

cadherin promoter was also enhanced by high glucose (Figure 18A). To determine the effect of high glucose on PRC2 complex formation, I evaluated the effect of high glucose on co-IP of EZH2 and Suz12, or EZH2 and EED. Suz12 or EED were co-immunoprecipitated with EZH2 by high glucose in the nucleus (Figure 18B). In addition, Snail was also able to associate with the PRC2 complex by high glucose (Figure 18C). Subsequently, to examine the relationship between Snail and PRC2 by high glucose, hUCB-MSCs were transfected with *Snail* siRNA prior to incubation for 24 h in high glucose conditions. In the nucleus, high glucose enhanced the EZH2 and Suz12, or EZH2 and EED complex. However, *Snail* siRNA disrupted the interaction between EZH2 and Suz12, or EZH2 and EED (Figure 19A), suggesting that Snail is required to bind the complexes and has important functions in hUCB-MSC migration. Interestingly, it has been reported that Snail is associated with the PRC2 complex for the repression of E-cadherin by the recruitment of HDAC, so the Snail was checked to see if it controlled the action of HDAC. As shown in Figure 19B, binding HDAC1 with the major component of PRC2, EZH2, was increased under high glucose conditions, whereas Snail-knockdown hUCB-MSCs maintained the interaction between

EZH2 and HDAC1. This suggests that the presence of HDAC1 is necessary to associate the Snail and PRC2 complex. These results demonstrate that Snail interacts with PRC2 by high glucose in the nucleus, and the complex binds with E-box of the E-cadherin promoter, which in turn causes the E-cadherin repression.

A

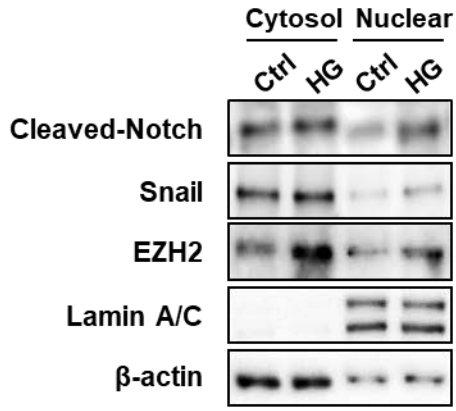
Cytosol
Nuclear
Ctrl
HG
Ctrl
HG
Cleaved-Notch
Snail
EZH2
Lamin A/C
β-actin

B

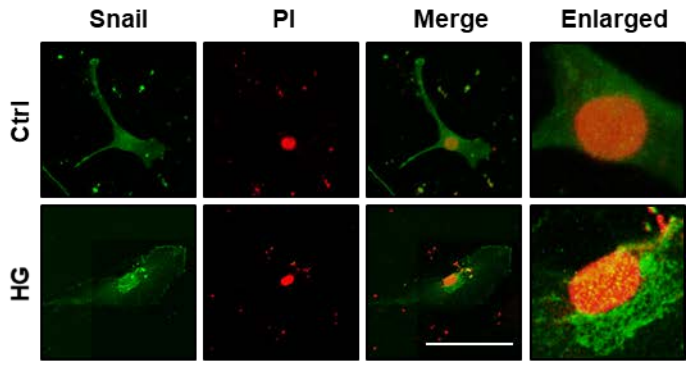
Snail
PI
Merge
Enlarged
Ctrl
HG

C

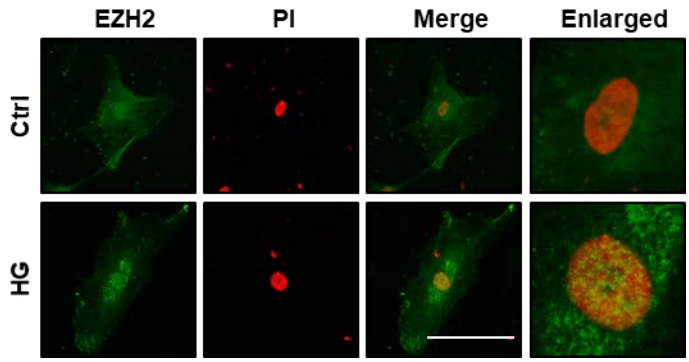
EZH2
PI
Merge
Enlarged
Ctrl
HG

Figure 17. Effect of high glucose on nuclear translocation of Snail and EZH2. (A) Cells were incubated under high glucose conditions for 24 h, and the lysate were fractionized into the cytosol and nuclear parts. The fractions were subjected to SDS-PAGE, and expression levels of cleaved-Notch, Snail and EZH2 were detected. Lamin A/C was used as a nuclear marker and β-actin was used as a cytosolic marker, respectively. n=3. (B, C) Cells were stained with Snail and EZH2 antibody and counterstained with PI. Fluorescence density of Snail and EZH2 in the cellular region was confirmed by fluorescence microscopy. Scale bars = 50 μm.

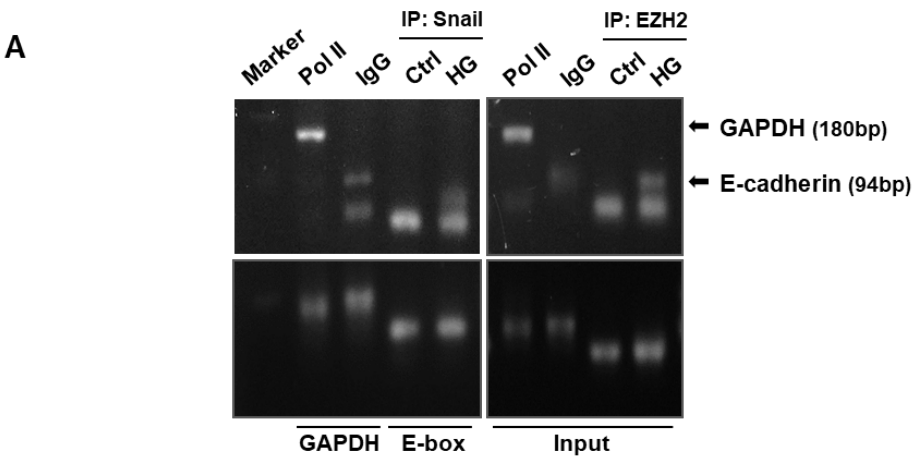
A
IP: Snail
IP: EZH2
Marker
Pol II
IgG
Ctrl
HG
Pol II
IgG
Ctrl
HG
GAPDH (180bp)
E-cadherin (94bp)
GAPDH
E-box
Input

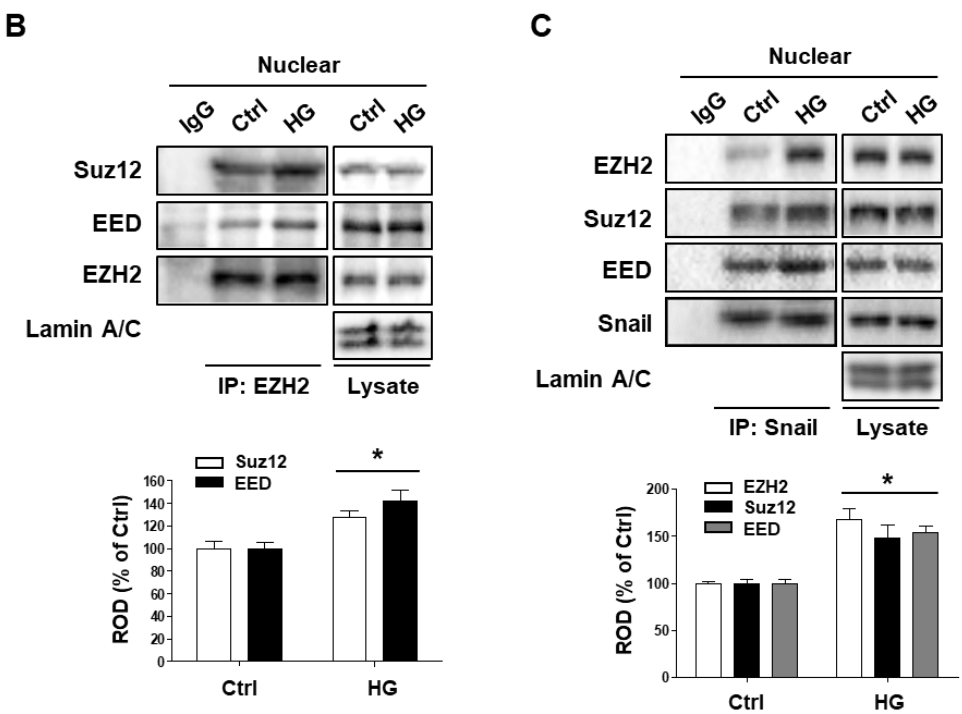
B
Nuclear
IgG
Ctrl
HG
Ctrl
HG
Suz12
EED
EZH2
Lamin A/C
IP: EZH2
Lysate
Suz12
EED
*
ROD (% of Ctrl)
160
140
120
100
80
60
40
20
0
Ctrl
HG
C
Nuclear
IgG
Ctrl
HG
Ctrl
HG
EZH2
Suz12
EED
Snail
Lamin A/C
IP: Snail
Lysate
EZH2
Suz12
EED
*
ROD (% of Ctrl)
200
150
100
50
0
Ctrl
HG

Figure 18. Effect of high glucose on PRC2 complex formation. (A) hUCB-MSCs were cross-linked with formaldehyde directly in the culture medium after treatment with high glucose for 24 h. DNA was sheared and immunoprecipitated with an anti-Snail and anti-EZH2 antibody. After reversing the cross-linking, the DNA was amplified using the E-cadherin primer, CDH-1. (B) Immunoassay of nuclear extracts of hUCB-MSCs was left untreated or incubated with high glucose, assessed by IP with anti-EZH2 (IP: EZH2) or without IP (lysate), followed by IB analysis (IB: Suz12 and EED). Lamin A/C was used as a nuclear marker. n=3. $*p < 0.05$ versus ctrl. (C) Immunoassay of nuclear extracts of hUCB-MSCs was left untreated or incubated with high glucose, assessed by IP with anti-Snail (IP: Snail) or without IP (lysate), followed by IB analysis (IB: PRC2 components). Lamin A/C was used as a nuclear marker. n=3. $*p < 0.05$ versus ctrl.

A

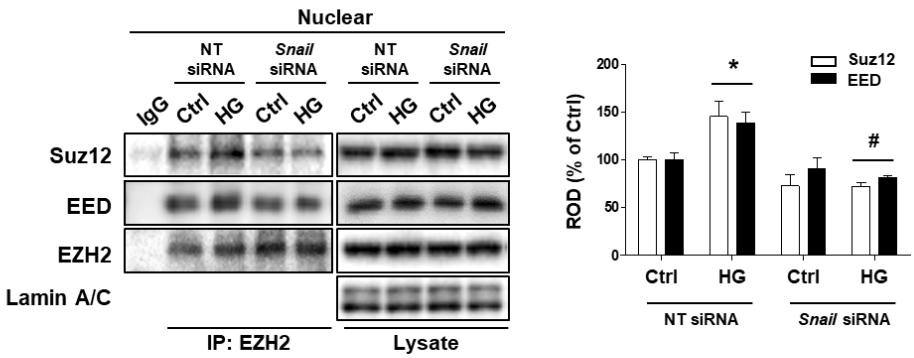
Nuclear
NT siRNA
Snail siRNA
NT siRNA
Snail siRNA
IgG
Ctrl
HG
Ctrl
HG
Ctrl
HG
Ctrl
HG
Suz12
EED
EZH2
Lamin A/C
IP: EZH2
Lysate
ROD (% of Ctrl)
200
150
100
50
0
*
#
Suz12
EED
Ctrl
HG
Ctrl
HG
NT siRNA
Snail siRNA

B

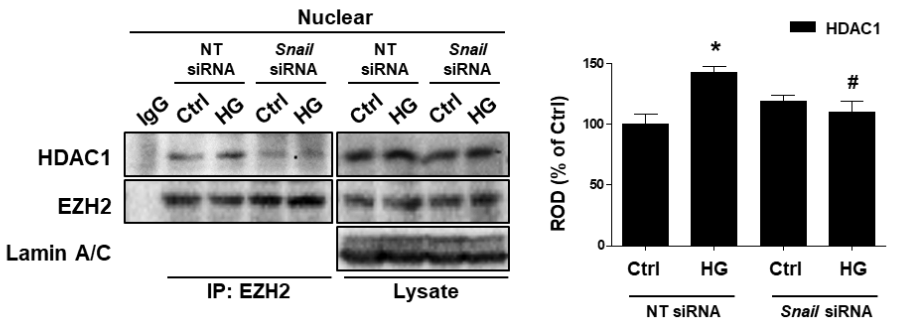
Nuclear
NT siRNA
Snail siRNA
NT siRNA
Snail siRNA
IgG
Ctrl
HG
Ctrl
HG
Ctrl
HG
Ctrl
HG
HDAC1
EZH2
Lamin A/C
IP: EZH2
Lysate
HDAC1
ROD (% of Ctrl)
150
100
50
0
*
#
Ctrl
HG
Ctrl
HG
NT siRNA
Snail siRNA

Figure 19. Relationship between Snail and PRC2 by high glucose in nucleus. (A) Immunoassay of nuclear extracts of hUCB-MSCs was left transfected with *NT* siRNA or specific siRNA that silence Snail expression and then was treated for 24 h with 25 mM glucose, assessed by IP with anti-EZH2 or without IP (lysate), followed by IB (PRC2 components). n=3. $*p < 0.05$ versus *NT* siRNA only. $\#p < 0.05$ versus high glucose with *NT* siRNA transfection. (B) Immunoassay of nuclear extracts of hUCB-MSCs was left transfected with *NT* siRNA or specific siRNA that silence *Snail* expression and then treated for a further 24 h with 25 mM glucose, assessed by IP with anti-EZH2 or without IP (lysate), followed by IB (HDAC1). n=3. $*p < 0.05$ versus *NT* siRNA only. $\#p < 0.05$ versus high glucose with *NT* siRNA transfection.

3.5. Role of high glucose-induced Snail and EZH2 in E-cadherin expression, migration and mouse skin wound healing efficacy

To examine the role of high glucose and its related signal molecules on hUCB-MSC migration, I pretreated the cells with NAC, SP600125, L-685,458, and LY294002 prior to high glucose treatment in normal hUCB-MSC culture conditions. Pretreatment with NAC, SP600125, L-685,458, or LY294002 restored the E-cadherin expression level that has been reduced by high glucose (Figure 20A). The Oris™ cell migration assay was used to quantify the amount of migration. Consequently, high glucose-induced cell migration was inhibited by each signal pathway-related molecule inhibitor or siRNAs (Figure 20B). The effects of high glucose were confirmed with the IBIDI™ culture insert dish assays (Figure 20C). Furthermore, to evaluate the function of E-cadherin, transfection of *E-cadherin* siRNA was performed. Silencing E-cadherin enhanced hUCB-MSC migration, so E-cadherin affects the migration ability in hUCB-MSCs (Figure 21A and 21B). To examine the relationship between Snail/EZH2 expression and skin wound healing effect of

high glucose-pretreated hUCB-MSCs, I performed hUCB-MSC transplantation transfected with *Snail* or *EZH2* siRNA into the wound sites in mice. The wounds of high glucose-pretreated *EZH2* siRNA + hUCB-MSC group remained unrepaired as well as the structures of the epidermis and dermis, compared to the wounds of high glucose-pretreated NT siRNA + hUCB-MSC group (Figure 22A and 22B). HNA-positive cells in the high glucose-pretreated *EZH2* siRNA + hUCB-MSC group were not found much when compared to the high glucose-pretreated NT siRNA + hUCB-MSCs group (Figure 22C). In addition, the wound area of *Snail* siRNA-treated hUCB-MSC group compared to the wounds of high glucose-pretreated NT siRNA + hUCB-MSC group did not heal 11 days after wounding (Figure 23A). The histological examination of wound tissues observed that the wound site was completely filled with granulation tissues in high glucose-pretreated NT siRNA + hUCB-MSCs group as opposed to the wounds of NT siRNA treated hUCB-MSC, *Snail* siRNA-treated hUCB-MSC, or the high glucose-pretreated *Snail* siRNA + hUCB-MSC group (Figure 23B). Immunohistochemistry revealed that there were many HNA-positive cells in the high glucose-pretreated NT siRNA + hUCB-

MSC group, whereas the wound tissues in NT siRNA treated hUCB-MSC, *Snail* siRNA-treated hUCB-MSC, or high glucose-pretreated *Snail* siRNA + UCB-MSC group contained much less HNA-positive cells (Figure 23C). Thus, these results indicate that high glucose-preactivated hUCB-MSC transplantation accelerates skin wound closure.

A

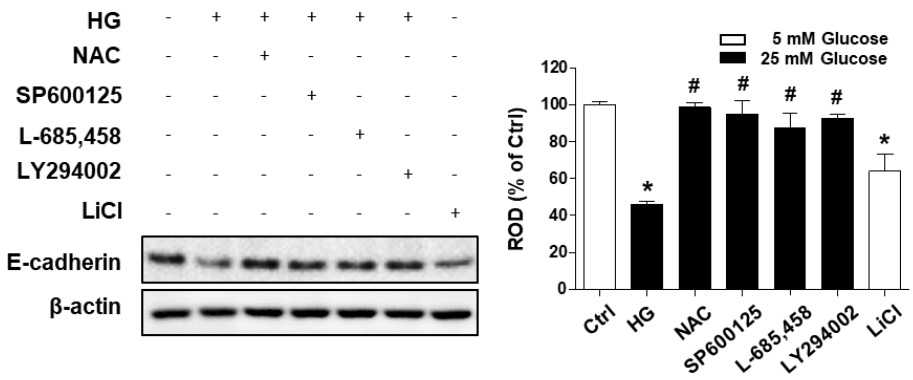
HG
NAC
SP600125
L-685,458
LY294002
LiCl
E-cadherin
β-actin
5 mM Glucose
25 mM Glucose
ROD (% of Ctrl)
Ctrl
HG
NAC
SP600125
L-685,458
LY294002
LiCl

B

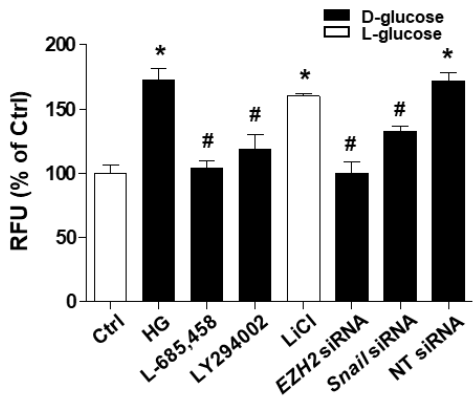
D-glucose
L-glucose
RFU (% of Ctrl)
Ctrl
HG
L-685,458
LY294002
LiCl
EZH2 siRNA
Snail siRNA
NT siRNA

C

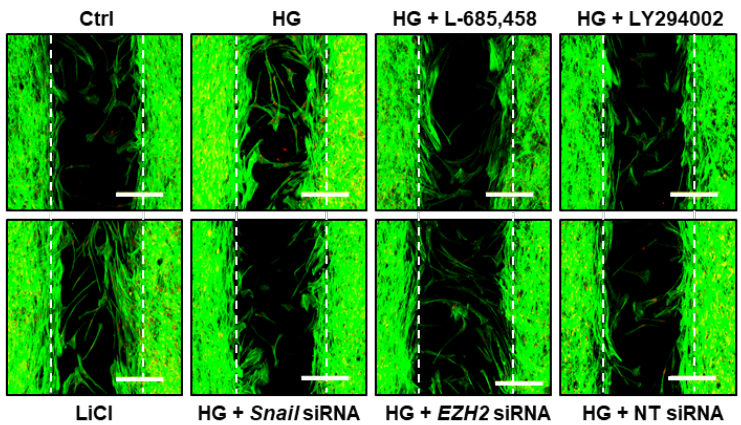
Ctrl
HG
HG + L-685,458
HG + LY294002
LiCl
HG + Snail siRNA
HG + EZH2 siRNA
HG + NT siRNA

Figure 20. Role of high glucose on E-cadherin repression and hUCB-MSC migration. (A) Cells were incubated in 5 mM glucose (ctrl), 25 mM glucose (HG) and 25 mM glucose with either NAC, SP600125, L-685,458, LY294002 or LiCl for 24 h, and E-cadherin was analyzed by western blot. n=3. $*p < 0.05$ versus ctrl; $\#p < 0.05$ versus high glucose alone. (B) Oris^{TM} migration assay was performed with cells pretreated with L-685,458, LY294002, LiCl, *EZH2*-, and *Snail*-specific siRNA prior to treatment of high glucose for 24 h. Fluorescence in the analytical zone was quantified with a plate reader. n=3. $*p < 0.05$ versus ctrl; $\#p < 0.05$ versus high glucose alone. (C) Wound healing assay was performed with the pretreatment of L-685,458, LY294002, LiCl, EZH2-, *Snail*-, *EZH2*-specific siRNA, and NT siRNA in the presence/absence of high glucose. Scale bars = 200 μm.

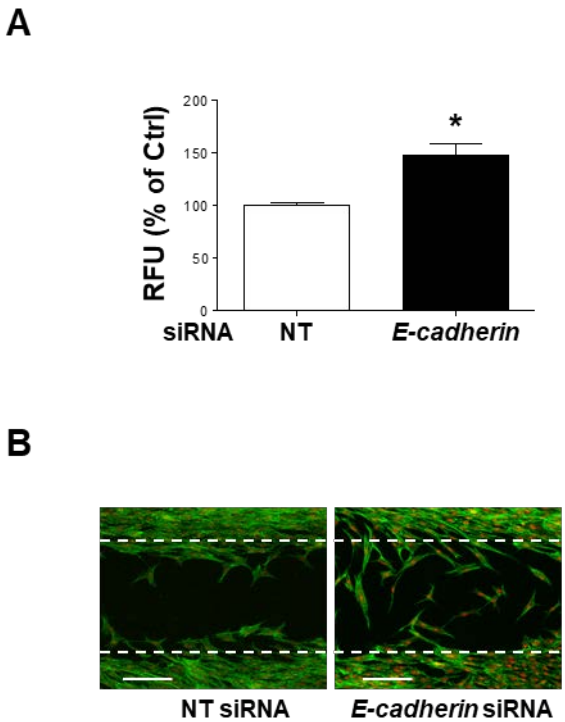

Figure 21. Role of E-cadherin in high glucose-induced migration of hUCB-MSCs. (A) Cells were incubated in 25 mM glucose for 24 h and migration were measured by Oris^{TM} migration assay. Fluorescence in the analytical zone was quantified with a plate reader. n=3. $*p < 0.05$ versus NT siRNA. (B) IBIDI^{TM} wound healing migration assay was performed. Cells were stained with Alexa Fluor 488-phalloidin and PI and the dishes were photographed using Eclipse Ts2-FL microscopy (Nikon Corporation, Tokyo, Japan). Scale bars = 100 μm.

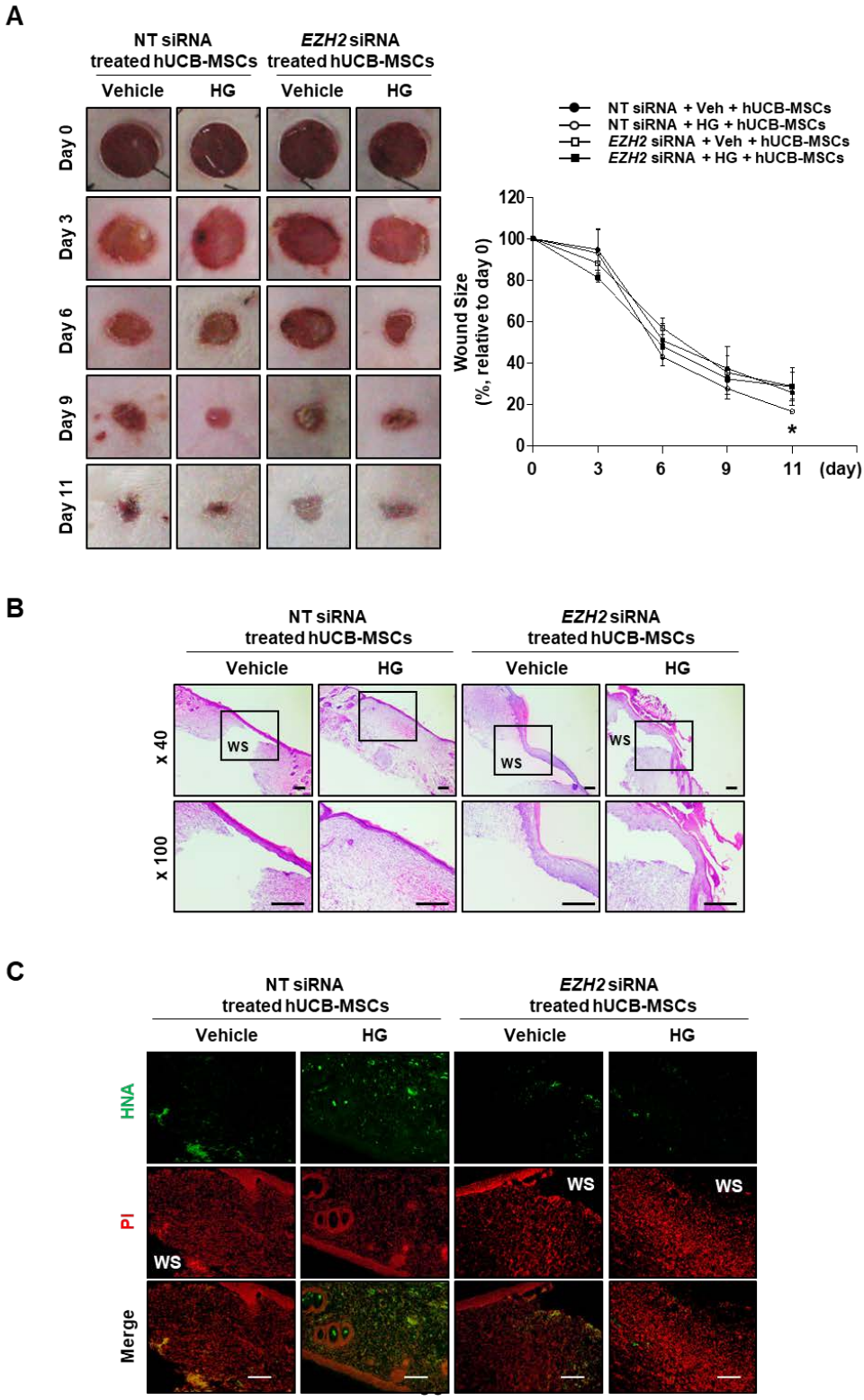
A
NT siRNA treated hUCB-MSCs
EZH2 siRNA treated hUCB-MSCs
Vehicle
HG
Vehicle
HG
Day 0
Day 3
Day 6
Day 9
Day 11
NT siRNA + Veh + hUCB-MSCs
NT siRNA + HG + hUCB-MSCs
EZH2 siRNA + Veh + hUCB-MSCs
EZH2 siRNA + HG + hUCB-MSCs
Wound Size (%, relative to day 0)
120
100
80
60
40
20
0
0
3
6
9
11
(day)
*
B
NT siRNA treated hUCB-MSCs
EZH2 siRNA treated hUCB-MSCs
Vehicle
HG
Vehicle
HG
x 40
x 100
WS
C
NT siRNA treated hUCB-MSCs
EZH2 siRNA treated hUCB-MSCs
Vehicle
HG
Vehicle
HG
HNA
PI
Merge
WS

Figure 22. Role of EZH2 on enhancing the therapeutic efficacy in repairing skin wound. (A) Representative gross images of wounds at days 0, 3, 6, 9, and 11 are shown (*left panel*). Wound sizes were measured using ImageJ software (*right panel*). n=6 each group. $*p < 0.05$ versus NT siRNA + Vehicle + hUCB-MSCs group. (B) Wound tissues were stained by using H&E staining at day 11 after wounding. Scale bar = 200 μm or 100 μm. (C) Wound tissues were immunostained with HNA (green) and PI (red). Scale bar = 50 μm.

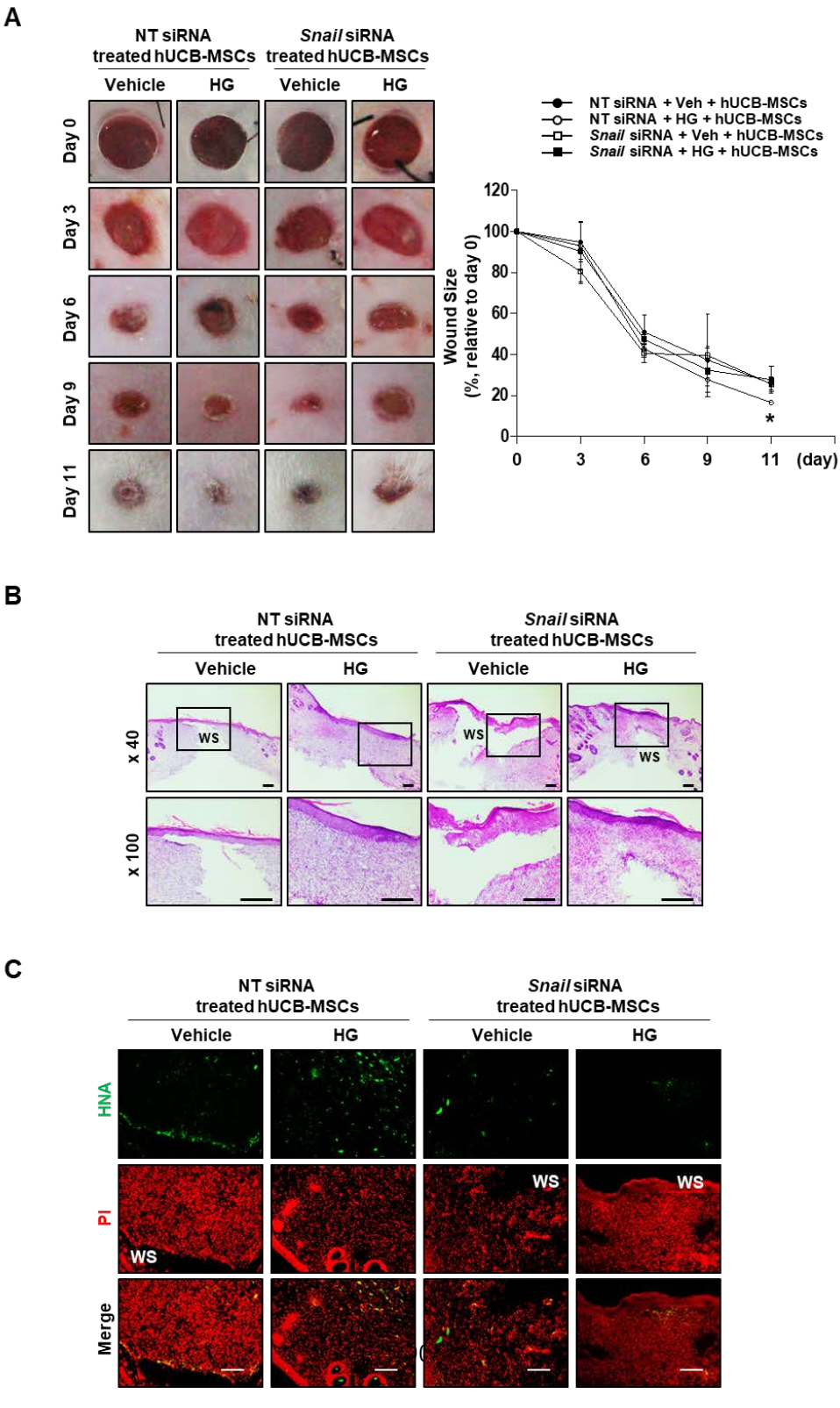
A
NT siRNA treated hUCB-MSCs
Snail siRNA treated hUCB-MSCs
Vehicle
HG
Vehicle
HG
Day 0
Day 3
Day 6
Day 9
Day 11
NT siRNA + Veh + hUCB-MSCs
NT siRNA + HG + hUCB-MSCs
Snail siRNA + Veh + hUCB-MSCs
Snail siRNA + HG + hUCB-MSCs
Wound Size (%, relative to day 0)
120
100
80
60
40
20
0
0
3
6
9
11
(day)
*
B
NT siRNA treated hUCB-MSCs
Snail siRNA treated hUCB-MSCs
Vehicle
HG
Vehicle
HG
x 40
x 100
WS
WS
WS
C
NT siRNA treated hUCB-MSCs
Snail siRNA treated hUCB-MSCs
Vehicle
HG
Vehicle
HG
HNA
PI
Merge
WS
WS
WS

Figure 23. Role of Snail on enhancing the therapeutic efficacy in repairing skin wound. (A) Representative gross images of wounds at days 0, 3, 6, 9, and 11 are shown (*left panel*). Wound sizes were measured using ImageJ software (*right panel*). n=6 each group. $*p < 0.05$ versus NT siRNA + vehicle + hUCB-MSCs group. (B) Wound tissues were stained by using H&E staining at day 11 after wounding. Scale bar = 200 μm or 100 μm. (C) Wound tissues were immunostained with HNA (green) and PI (red). Scale bar = 50 μm.

4. DISCUSSION

In this study, I showed the effect of high glucose on enhancing the migration of hUCB-MSC and the involvement of Notch signaling pathway, which contributes to E-cadherin repression through the interplay between Snail and EZH2. According to previous reports investigating cell migration under high glucose condition, the effect of glucose on cell migration still remains controversial depending on the cell types (Takatani-Nakase et al., 2014; Suzuki et al., 1996; Farnoodian et al., 2016). My data in this study revealed that high glucose stimulates hUCB-MSC migration with suppression of E-cadherin expression (Figure 24). Moreover, I presented *in vivo* proof showing that high glucose-pretreated hUCB-MSCs promoted the migration of transplanted cells into the wound site and accelerated the skin wound closure in a mouse excisional wound splinting model. Previous reports demonstrated that the augmentation of MSC migration to the wound site increases the efficacy of wound healing through beneficial effects (Jung et al., 2015; Rosova et al., 2008; Oh et al., 2015; Chen et al., 2012). Thus,

migration is considered to be an important factor of MSC-induced wound healing. E-cadherin degradation by netrin pretreatment enhances migratory ability of hUCB-MSCs (Lee et al., 2014). The reduction of E-cadherin expression during cell migration can be controlled by epigenetic transcriptional regulation and post-transcriptional modification of transcription for the *CDH1* gene (Serrano-Gomez et al., 2016). My results investigating the effect of high glucose on E-cadherin and its epigenetic regulators showed that high glucose decreased the expression of E-cadherin via increasing the expressions of EZH2 and Snail. Epigenetic factors have key roles in modulating E-cadherin expression, and the epigenetic silencing of E-cadherin is mediated by histone-modifying enzymes including Snail1 and EZH2 (Herranz et al., 2008; Di Croce and Helin, 2013). Based upon these findings, I suggest that epigenetic regulation of E-cadherin is a critical factor for high glucose-stimulated migration in hUCB-MSCs.

Extracellular glucose influences ROS formation as mediators of intracellular signaling cascades (Ha and Lee, 2000; Schroder, 2014). ROS acts as an intracellular messenger inducing a variety of intracellular events such as protein phosphorylation and gene

expression (Chess et al., 2005; Lee et al., 2004, Sauer et al., 2001). Indeed, my results showed high glucose stimulated intracellular ROS production, and JNK phosphorylation was induced by high glucose-induced ROS. Similarly, it was reported that the motility of MSCs was promoted by ROS-induced MAPK phosphorylation under shear stress conditions while high glucose-induced ROS distinctively phosphorylated JNK in renal mesangial cells (Zhang et al., 2012). This observation may indicate that JNK activation is more responsive to high glucose treatment than ERK and p38 MAPK via high glucose-induced ROS dependent manner in hUCB-MSCs. Furthermore, I also showed that JNK phosphorylation stimulates γ-secretase-dependent Notch cleavage, leading to translocation of NICD into the nucleus. Previous reports demonstrated that JNK contributes to γ-secretase activation, but ERK1/2 acts as a negative regulator of γ-secretase activity (Shen et al., 2008; Kim et al., 2006). These findings support my results that high glucose-induced p-JNK could trigger Notch signaling via γ-secretase activation. In addition, it was reported that high EZH2 expression is associated with increased Notch1 activation (Gonzalez et al., 2014). Furthermore, my data showed that pretreatment of

γ-secretase inhibitor suppressed the high glucose-induced cleaved Notch and EZH2 expressions. Therefore, previous and present findings indicate Notch signaling activated by JNK could be involved in high glucose-induced EZH2 expression.

Considering the regulatory mechanism of Snail by high glucose, previous reports demonstrated that the stabilization of Snail was regulated by the Akt/GSK-3β pathway (Guo et al., 2014; Wang et al., 2013). Previous study revealed high glucose-induced ROS/PI3K/Akt pathway involving in functional regulation of stem cells (Kim et al., 2006). Although previous research reported high glucose-activated GSK-3β plays an inhibitory role in proliferation and migration of bone marrow-derived MSCs (Zhang et al., 2016), present data revealed that high glucose-induced ROS phosphorylates Akt, which subsequently induced Snail expression via GSK-3β inhibition in hUCB-MSCs. Consistent with my results, GSK-3β activation can maintain epithelial morphology by proteosomal degradation of Snail, thereby maintaining high E-cadherin expression (Nieto, 2002; Lunyak and Rosenfeld, 2008). Thus, I suggest that the Akt/GSK-3β pathway activated by high glucose is a major pathway upregulating Snail expression in hUCB-

MSCs.

Previous reports have shown that epigenetic regulation is an important factor in the regulation of stem cell fate (Lunyak and Rosenfeld, 2008; Wang et al., 2017). EZH2 has been considered an essential factor for epigenetic regulation of E-cadherin (Herranz et al., 2008). Binding of PRC2 members, such as EZH2, Suz12, and EED, to the promoter of target gene induces epigenetic regulation that is regulated by Snail, which cooperates with PRC2 (Herranz et al., 2008; Di Croce and Helin, 2013; Simon and Kingston, 2013; Tong et al., 2012). Snail is also required for EZH2-mediated E-cadherin repression and the complex of EZH2/HDAC/Snail contributed to E-cadherin silencing in carcinomas (Tong et al., 2012; Peinado et al., 2004). In this study, high glucose stimulated Suz12/EED/EZH2 complex formation for E-cadherin inhibition, which was regulated by the high glucose-stabilized Snail. In addition, several studies reported that Snail interacts with the HDAC to repress E-cadherin (Peinado et al., 2004; von Burstin et al., 2009). HDACs are enzymes that play crucial roles in the deacetylation of chromatin proteins and in the regulation of non-histone proteins for cellular homeostasis (Munshi et al., 2005). As

intermediaries between Snail and PRC2, HDAC promotes PRC2 which links with Snail at the promoter region of E-cadherin (Lin et al., 2014). Additionally, an overexpression of Snail stimulates recruitment of the HDAC1/HDAC2 complex, which leads to deacetylation of histone H3 and H4 at the *CDH1* promoter (Peinado et al., 2004). Indeed, my data showed that Snail induced by high glucose increases the interaction of HDAC1 with EZH2. This finding presents the possibility that high glucose-induced Snail regulates PRC2 activity to repress E-cadherin expression via HDAC1. My data confirmed the regulatory effect of EZH2 and Snail regulated by JNK/Notch and Akt/GSK-3β pathways on high glucose-induced E-cadherin repression and migration of hUCB-MSCs. Furthermore, my skin wound healing results showed that silencing EZH2 or Snail suppressed the wound healing effect of hUCB-MSCs and decreased the migration of transplanted cells into the wound sites. These data indicate that both EZH2 and Snail are critical factors in determining the therapeutic efficacy of high glucose-pretreated hUCB-MSCs. However, further investigations into the role of high glucose-induced epigenetic regulation of E-cadherin in other physiological functions of hUCB-MSC are needed to understand the therapeutic

potential of high glucose for stem cell therapy.

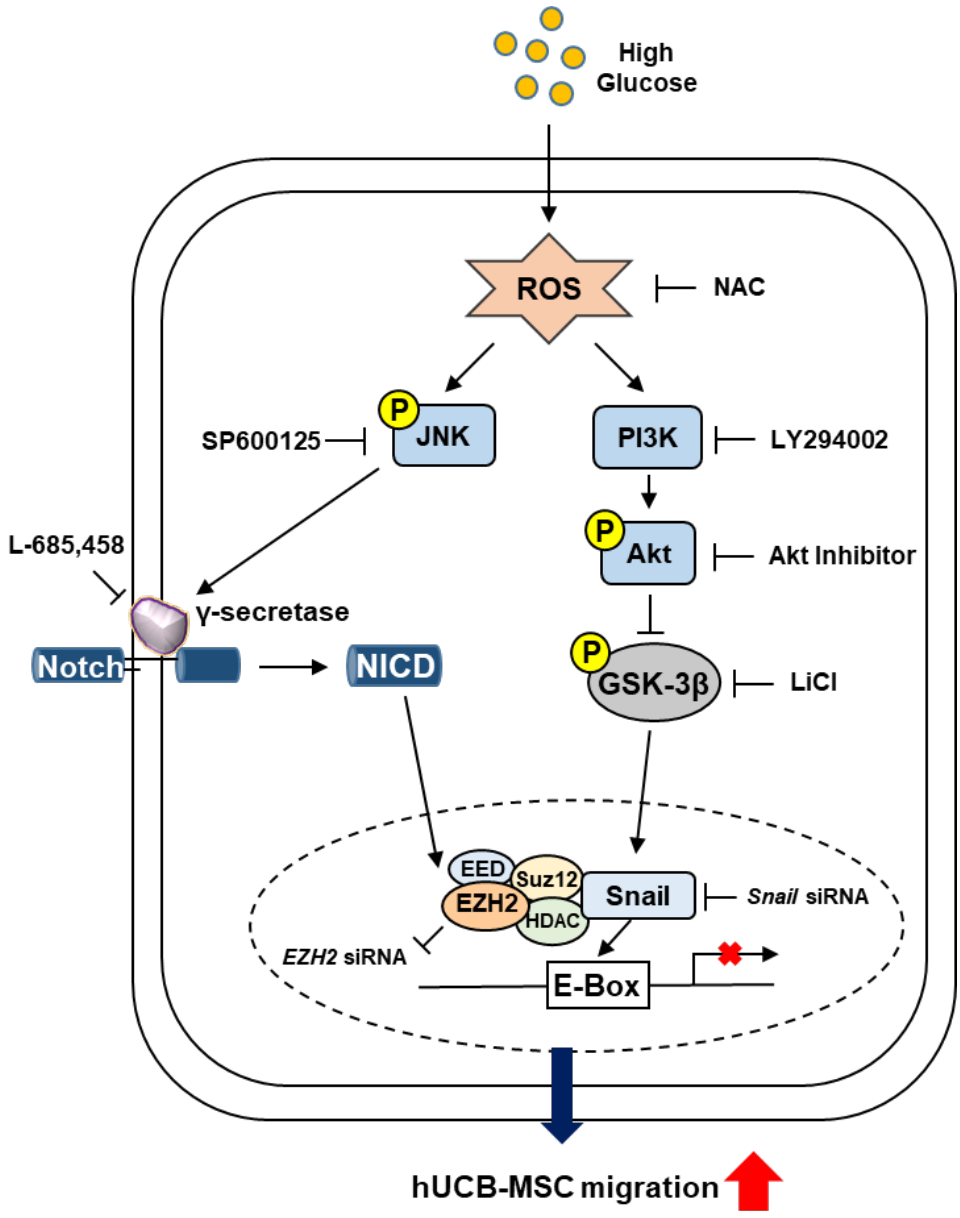
High
Glucose
ROS
NAC
P
JNK
SP600125
PI3K
LY294002
P
Akt
Akt Inhibitor
L-685,458
γ-secretase
Notch
NICD
P
GSK-3β
LiCl
EED
Suz12
EZH2
HDAC
Snail
Snail siRNA
EZH2 siRNA
E-Box
hUCB-MSC migration

Figure 24. The hypothetical model for the proposed signaling network was involving in high glucose-induced hUCB-MSC migration. High glucose enhances ROS, which activates either JNK or PI3K/Akt signaling. High glucose-induced JNK activation stimulated γ-secretase, and elicits the cleavage of the Notch protein. NICD induced the EZH2 expression, and allows them to translocate to the nucleus. Stimulation of high glucose leads to an induction of phosphorylation of GSK-3β via the PI3K/Akt pathway, which leads to Snail stabilization. Once in the nucleus, EZH2 makes a complex with Suz12 and EED, and the complex associates with the E-box of the promoter regions of E-cadherin by Snail. These complexes have an inductive effect on hUCB-MSC migration by the repression of E-cadherin. NAC: ROS inhibitor; SP600125: JNK inhibitor; L-685,458: γ-secretase inhibitor; LY294002: PI3K inhibitor; LiCl: GSK-3β inhibitor. Abbreviations: ROS, reactive oxygen species; JNK, c-Jun N-terminal kinases; PI3K, phosphoinositide 3 kinase; Akt, protein kinase B; NICD, Notch intracellular domains; EZH2, enhancer of zeste homolog 2; GSK-3β, glycogen synthase kinase 3 beta; Suz2, suppressor of zeste 12; EED, embryonic ectoderm development; NAC, N-acetyl-L-cysteine; LiCl, lithium chloride.

CHAPTER III.

17β-Estradiol enhances mesenchymal stem cell-induced wound healing in the ovariectomized diabetic mouse model through estrogen receptor α-dependent MnSOD activation via Nrf2 and Sirt3 upregulation

1. INTRODUCTION

Hyperglycemia plays a role in the pathogenesis of diabetic complications by enhancing oxidative production and impairing the antioxidant defense (Vincent et al., 2004). High glucose enhances NADPH-oxidase activation and subsequently induces ROS production in the mitochondria. Excessive ROS generation by high glucose depletes antioxidant defenses, making cells and tissues more vulnerable to oxidative stress, and eventually changing the cellular functions (Matough et al., 2012). Thus, the loss of efficacy with increased ROS and altered cellular physiology occur in diabetic patients even if many researchers have attempted to use therapeutic applications like stem cell therapy. This unbalanced oxidative mechanism ultimately increases the promoted cell death, including apoptotic and necrotic mechanisms. Interestingly, there have been several recent reports suggesting that high glucose-induced oxidative stress causes cell death that can lead to decreased therapeutic efficacy of stem cells (Gu et al., 2016). However, the mechanisms of how high glucose regulates autophagic cell death through ROS regulation are not fully understood.

Postmenopausal women tend to be in hyperglycemic states and associated with a higher risk of diabetes since E2 is a significant regulator of energy homeostasis and glucose metabolism (Crespo et al., 2002). E2 also plays an important role in regulating antioxidant enzyme expression and redox state (Bellanti et al., 2013). Thus, the protective mechanisms of E2 on preventing excessive ROS production under hyperglycemia must be investigated as they represent the state of diabetic patients. E2 signaling is mediated through the ERs that belongs to the nuclear superfamily: ERα and ERβ. Among ERs, ERα has been reported to have more nuclear transcriptional activity than ERβ (Yi et al., 2002). However, it has not been fully elucidated how E2-induced ERα regulation alleviates complications of diabetic mellitus (DM) in diabetics with E2 deficiency, although extensive studies have been performed on rodent models on the beneficial effects of E2 and ERα activation on glucose homeostasis and diabetes prevention (Bryzgalova et al., 2006; Le et al., 2006). Indeed, reduced E2 may increase the incidence of diabetes by affecting the increased oxidative stress (Naziroglu et al., 2004), but the exact mechanisms of how E2 signaling through ERα activates antioxidative enzymes and

modulates oxidative stress against hyperglycemia remain elusive.

MSCs are widely used to treat cell transplantation, which prevents pathological changes and enhances regeneration in diabetic animals (Volarevic et al., 2011; Jackson et al., 2012). However, due to reduced cell survival in hyperglycemia by various stimuli such as hypoxia, oxidative stress, and inflammation, cell loss may result in decreased efficacy as a stem cell transplantation therapy (Li et al., 2008; Raffaele et al., 2016). Indeed, many molecular and clinical data also support the effects of estrogen on normal skin homeostasis and wound healing. Furthermore, hyperglycemia or estrogen deficiency has harmful effects on the wound healing process. Even though E2 treatments in MSCs could effectively improve cell viability by modulating ROS levels, it is not known how E2 can increase the efficiency of treating injured tissues in diabetes through MSCs transplantation. Therefore, as the effects of E2 on wound healing are complicated, they require further investigation. In this study, in order to understand the effect of E2 and MSCs transplantation on tissue regeneration, the STZ-induced diabetic and ovariectomized (OVX) mice were utilized as a disease model. Although animal models have some limitation, such as in the type 1

DM model, this is not prevalent in the type 2 DM. Thus, the present study investigated the protective role of E2 in high glucose-induced mtROS through ER-dependent signaling and assessed the effect of hUCB-MSC transplantation on mouse skin wound healing by circulating E2 in OVX diabetic mice.

2. MATERIALS AND METHODS

2.1. Materials

hUCB-MSCs were kindly provided from Kangstem Biotech (Seoul, Korea). FBS, PBS and α-MEM culture medium were purchased from GE healthcare life sciences (Pittsburgh, PA, USA). E2, streptozotocin (STZ), sesame oil, haematoxylin, eosin and sucrose were purchased from Sigma-Aldrich (St. Louis, MO, USA). 17β-Estradiol ELISA kit was purchased from Enzo life science (Seoul, Korea). SOD assay kit was obtained from Cayman chemical (Ann Arbor, MI, USA). EzSubcell fractionation kit and EzRIPA lysis kit were purchased from ATTO corporation (Tokyo, Japan). NAC, mitoTempo and Vas 2870 were purchased from Sigma-Aldrich (St. Louis, MO, USA). Primary antibodies against Beclin1 (sc-11427), ERα (sc-544), ERβ, Lamin A/C (sc-20681), and β-actin (sc-47778) were purchased from Santa Cruz Biotechnology (Dallas, TX, USA). Secondary antibodies against HRP-conjugated goat anti-rabbit IgG, goat anti-mouse IgG, and LC3 monoclonal primary antibody (MA5-17115) were purchased from Invitrogen (Thermo

Fisher Scientific, Waltham, MA, USA). Ac-K68-SOD2 (Ab137037) primary antibody were purchased from Abcam (Cambridge, MA, USA). Primary antibodies against LC3 (NB100-2220) and p62 (NBP1-48320) were purchased from Novus (Littleton, CO, USA). Primary antibody against Sirt3 (5490s) was purchased from Cell signaling (Danvers, MA, USA). Primary antibody against Nrf2 (CSB-PA003481) and Keap1 (CSB-PA012147LA01HU) were purchased from CusaBio (Houston, TX, USA) and MnSOD (06-984) primary antibody was purchased from EMD Millipore (Burlington, MA, USA).

2.2. hUCB-MSC culture

The general protocol for hUCB-MSC culture is described in Materials and Method section of CHAPTER II.

2.3. Animal preparation

All animal care and procedures were carried out in accordance with the National Institutes of Health Guidelines for the Humane

Treatment of Animals at Seoul National University and approved by the IACUC at Seoul National University (SNU-180314-2). Seven-week-old female ICR mice weighing 22-25 g were purchased from Han Lim Experimental Animal (Suwon, Korea). Mice were stabilized in the new environment for four days before experimentation to improve animal welfare and experimental results. Animals were housed in groups of 5/cage and had *ad libitum* access to food and purified water. The house was kept under standard environmental conditions (24 ± 2 ° C, 12/12 h light/dark cycle with lights on at 07:00). After surgical procedures, the health status of all animals was checked three times a day. The animal allocation for each experimental group was randomized, which means that all surgical procedures and hUCB-MSC transplantation or drug injection were carried out blindly and the tissue sections were randomly selected from each animal. I was concerned with the "3R principle" (reduction, replacement, refinement) in the context of animal experimentation ethics.

2.4. Experimental design

Mice were randomly divided into two groups: Sham and OVX. All mice were anesthetized with 3% isoflurane in a mixture of N_2O/O_2 gas. The bilateral OVX surgery in mice was performed by veterinarians. 8 days after the OVX surgery, mice were fasted for 6 h before STZ injection. For diabetic induction, OVX mice were randomly selected and received intraperitoneal injection of 180 mg/kg STZ with sodium citrate buffer (0.1 M, pH 4.5). An equal volume of sodium citrate buffer was injected into the mice in the non-diabetic group. Blood glucose levels were measured every 2 days 48 h after STZ injection using Accu-Chek Active glucometer (Roche, Germany). Following STZ injection, mice developed mean blood glucose of 212.2 mg/dL within 4 days. 8 days after the STZ injection, the mean blood glucose was 316 mg/dL in the STZ group (Figure 25). Blood glucose levels that exceeded 250 mg/dL in mice were considered diabetic. The diabetic mice were randomly distributed among six groups (n=6 each group): OVX + STZ, OVX + STZ +E2, OVX + STZ + NT siRNA +hUCB- MSCs, OVX + STZ + NT siRNA + hUCB-MSCs + E2, OVX + STZ + *ERα* siRNA +

hUCB-MSCs + E2, and OVX + STZ + *ERα* siRNA + hUCB-MSCs. NT siRNA or *ERα* siRNA-transfected hUCB-MSC transplantation were performed for four groups: OVX + STZ + NT siRNA + hUCB-MSCs, OVX + STZ + NT siRNA + hUCB-MSCs + E2, OVX + STZ + *ERα* siRNA + hUCB-MSCs + E2, and OVX + STZ + *ERα* siRNA + hUCB-MSCs. To examine the role of E2 and hUCB-MSC transplantation on tissue regeneration, the mouse skin wound splinting and stem cell transplantation were carried out according to the previous report (Wang et al., 2013). The detailed protocol for mouse excisional wound splinting model is described in Materials and Method section of CHAPTER II. All mice were anesthetized with a mixture of 80 mg/kg alfaxaline (Alfaxan™, Jurox Pty Ltd, Rutheford, Australia) and 10 mg/kg xylazine HCl (Rompun™, Bayer, Leverkusen, Germany). In the E2 treated groups, mice received intraperitoneal injection of 40 μg/kg E2, which was dissolved in sesame oil (Sigma-Aldrich, St. Louis, MO, USA) daily. 10 days after wounding, mice were euthanized so that wound tissues, uterus, and blood samples could be collected. To determine the effect of circulating E2, I measured the uterine weight and serum E2 from all mice. Figure 26 shows the uterine changes in sham and OVX mice.

As expected, the uterine weight significantly decreased in OVX with no E2 treatment groups (OVX, OVX + STZ, OVX + STZ + NT siRNA + hUCB-MSCs, and OVX + STZ + ERα siRNA + hUCB-MSCs). In contrast, uterine weight significantly increased in all E2 injection groups. Serum E2 levels were lower in all OVX without E2 treatment groups when compared to the sham or all E2 treatment groups (Figure 27). The histology of uterus cross-sections revealed that uterine myometrium was thicker in all E2 injection groups than all OVX without E2 treatment groups (Figure 28). Skin and uterus tissues samples were fixed with 4% PFA for 4 h at room temperature. The tissues were incubated with 20% sucrose in PBS for dehydration until tissues subsided and were then incubated in 30% sucrose at 4 °C overnight. The tissue samples were embedded with O.C.T. compound (Sakura Finetek, Torrance, CA, USA) and immediately frozen at −70 °C.

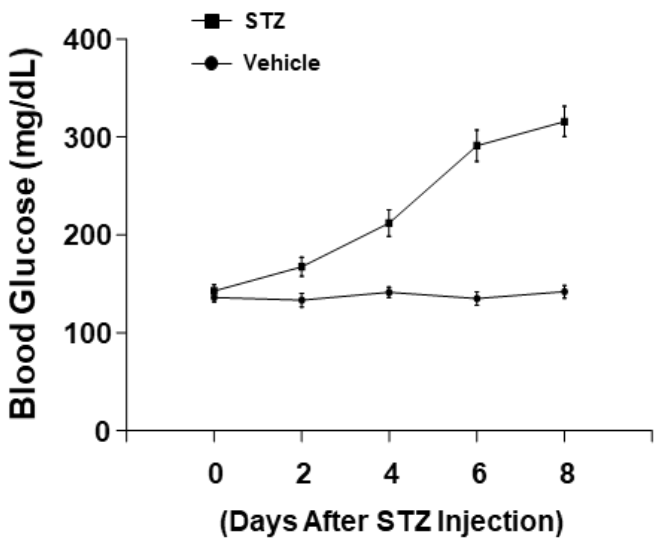

Figure 25. Effect of STZ on blood glucose in female mice with or without ovariectomy. Mice were stimulated with intraperitoneal injection of STZ (180 mg/kg, n = 15) or without STZ (vehicle ctrl, n = 47). Blood glucose concentration were measured every two days. Day 0 measurements were measured immediately before STZ injection.

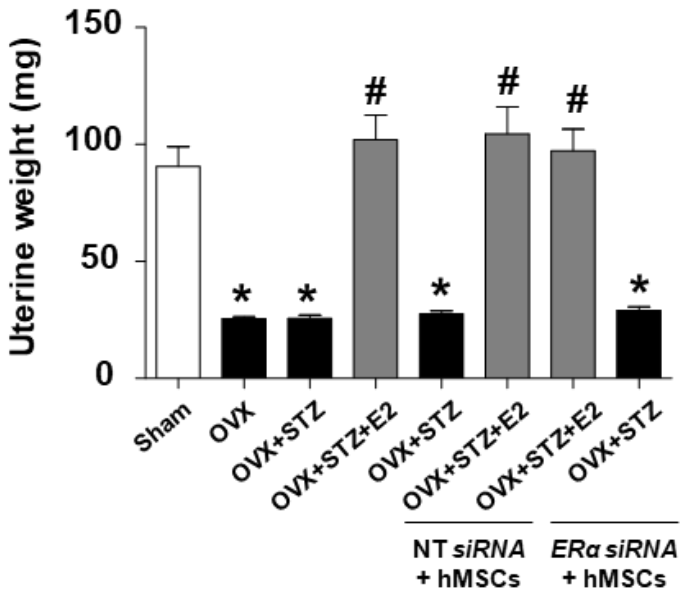

Figure 26. Effect of E2 on uterine weight in female mice. Uterine weighs were measured immediately after tissue collections. Data are presented as mean ± SEM. n=3. $*p < 0.05$ versus sham group and $\#p < 0.05$ versus OVX group.

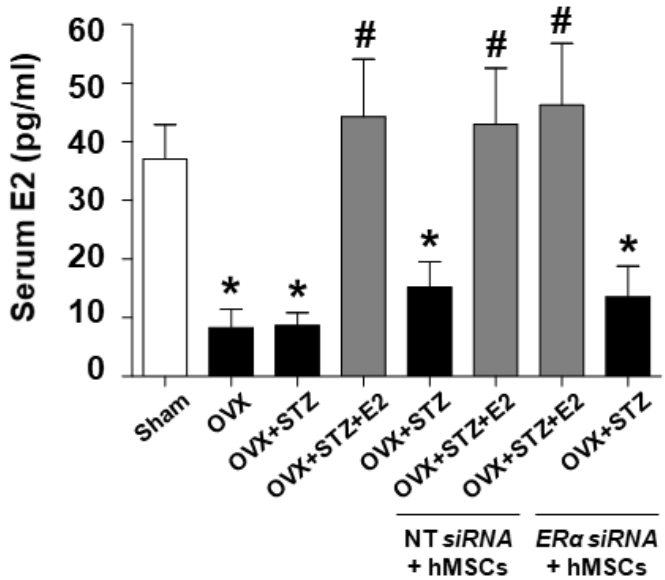

Figure 27. Effect of E2 on serum E2 of OVX diabetic mice. Blood samples were collected and serum E2 were measured by ELISA kit according to the manufacture' s protocol. $*p < 0.05$ versus sham group and $\#p < 0.05$ versus OVX group.

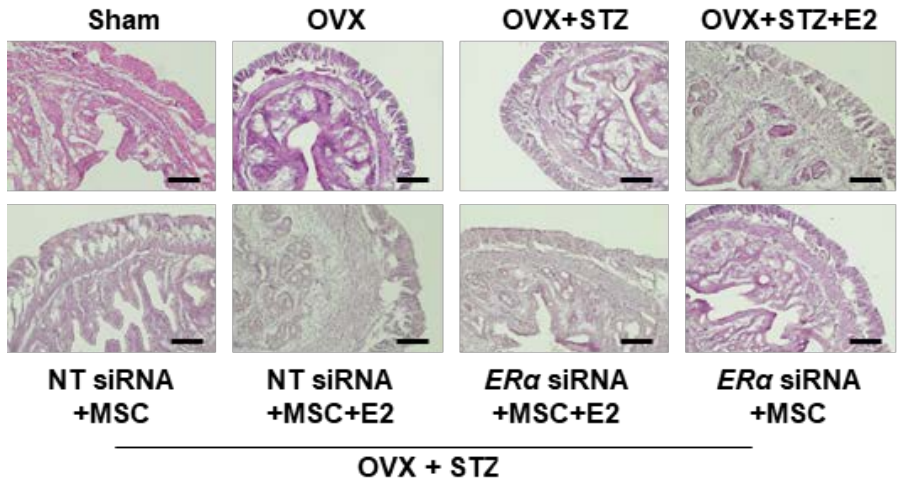
Sham
OVX
OVX+STZ
OVX+STZ+E2
NT siRNA +MSC
NT siRNA +MSC+E2
ERα siRNA +MSC+E2
ERα siRNA +MSC
OVX + STZ

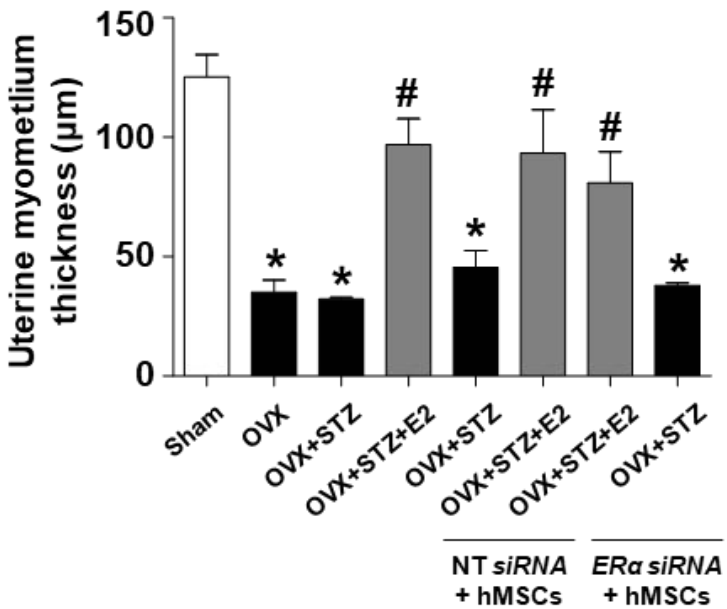
Uterine myometlium thickness (μm)
150
100
50
0
Sham
OVX
OVX+STZ
OVX+STZ+E2
OVX+STZ
OVX+STZ+E2
OVX+STZ+E2
OVX+STZ
NT siRNA + hMSCs
ERα siRNA + hMSCs

Figure 28. Effect of E2 on uterine myometrium thickness in OVX diabetic mice. Representative gross images of uterine cross-section are shown. Uterine tissues were randomized and stained by H&E staining and photographed under brightfield microscope. Uterine myometrium was measured by NIS-elements software (Ver. 4.6). Scale bar was set as 100 μm (Magnification x 100). Data are presented as mean ± SEM. n=3. $*p < 0.05$ versus sham group and $\#p < 0.05$ versus OVX group.

2.5. H&E staining

The detailed protocol for H&E staining is described in Materials and Methods section of CHAPTER II.

2.6. Western blot

The detailed protocol for western blot is described in Materials and Methods section of CHAPTER II.

2.7. Cell viability assay

All procedures of cell viability assay were carried out according to manufacturer's protocol. Cells were seeded in 96-well plates, and the medium was replaced with serum free media for 24 h prior to the experiments. 10 μL of EZ-Cytox reagent (Daeil Lab, Seoul, Korea) was added each wells and the cells were incubated for 2 h in 37 ° C incubator with 5% CO_2 in the dark. The absorbance at 450 nm was determined and analyzed with a multiplate reader (BioTek, Winooski, VT, USA).

2.8. SOD activity assay

All procedures of SOD assay were carried out according to manufacturer's protocol. Cells were harvested and centrifuged at 1,000 x g for 10 min at 4 °C. Cells were lysed with cold 20 mM HEPES buffer (pH 7.2) containing 1 mM EGTA, 210 mM mannitol, and 70 mM sucrose by a Branson Sonifier 250 (Wilmington, NC, USA) with set to 3 of output power and duty cycle of 30% for 10 sec and centrifuged at 1,500 x g for 5 min at 4 °C. The samples were diluted with the sample buffer, and the SOD standard and samples were added in a 96-well plate. Diluted xanthine oxidase was added to all wells. The 96-well plate was shaken gently for a several seconds and incubated on a shaking incubator for 30 min at room temperature. Absorbance at 450 nm was measured using a multiplate reader (BioTek, Winooski, VT, USA).

2.9. 17β-Estradiol ELISA assay

Blood samples were collected from all mice to obtain serum E2 in heparinized tubes and centrifuged for 10 min at 3,000 rpm. The

supernatant was serum. The serum should be stored at −20 ° C until just before analysis. All procedures of 17β−Estradiol ELISA assay were performed according to manufacturer' s protocol. The samples were added with conjugate solution and antibody in appropriate wells and were incubated at room temperature on a shaking incubator for 2 h at 250 rpm. After incubation, every wells were washed with wash buffer for three times. Next, p−Npp substrate solutions were added to every wells and the samples were incubated at room temperature for 45 min without shaking. After incubation, stop solution was added and the absorbance at 570 nm was measured immediately using a multiplate reader (BioTek, Winooski, VT, USA).

2.10. Cytosol and nuclear fractionation

The detailed protocol for subcellular fractionation is described in Materials and Methods section of CHAPTER II.

2.11. Transfection of siRNA

The detailed protocol for siRNA transfection is described in Materials and Methods section of CHAPTER II. Cells were transfected for 24 h with either a siRNA specific for *ATG5*, *ERα*, *SIRT3*, *MnSOD*, *NRF2* or a *NT* siRNA as a negative control (25 pM; Bioneer and 20 nM; Dharmacon) using TurboFECT transfection reagent. The sequences of siRNA used in the study were as described in Table 2.

Target gene	Sequence 5' – 3'	Supplier
ATG5	CAGUAUCAGACACGAUCAU	Bioneer
	AUGAUCGUGUCUGAUACUG	
	AGUAUCCUAAGCAUCUGUA	
	UACAGAUGCUUAGGAUACU	
ERα	CUGUCUUCUGUUGGGAACA	Bioneer
	UGUUCCCAACAGAAGACAG	
	GUCACUACUCAGGCUGACU	
	AGUCAGCCUGAGUAGUGAC	
ERβ	GACACUGAAAAGGAAGGUU	Bioneer
	AACCUUCCUUUUCAGUGUC	
	CGGCUCCAUAUACAUACCU	
	AGGUAUGUAUAUGGAGCCG	
NRF2	GAGACUACCAUGGUUCCAA	Bioneer
	UUGGAACCAUGGUAGUCUC	
	CAGCUAUGGAGACACACUA	
	UAGUGUGUCUCCAUAGCUG	
SIRT3	UCACAUUACCUGCGUGUUU	Dharmacon
	CCUGUGACUUUGCGCCUUA	
	UUGAGAGAGUGUCGGGCAU	
	GGACCAGACAAAUAGGAUG	
Non-targeting	UAGCGACUAAACACAUCAA	Dharmacon
	UUGAUGUGUUUAGUCGCUA	

Table 2. Sequences of the siRNAs and its suppliers used for gene silencing.

2.12. Intracellular ROS detection

The detailed protocol for intracellular ROS detection is described in Materials and Methods section of CHAPTER II.

2.13. Immunofluoresence staining

The detailed protocol for immunofluorescence staining is described in Materials and Methods section of CHAPTER II. Images were visualized by super-resolution radial fluctuations (SRRF) imaging system (Andor Technology, Belfast, UK) or fluorescence microscopy (Nikon Corporation, Tokyo, Japan). The fluorescent intensity was analyzed using Fiji software (NIH, Bethesda, MD, USA).

2.14. Flow cytometry

Cells were seeded in 60 mm diameter culture dish. Media were replaced with serum-free media for 24 h when cells were at 70% confluence. Cells were stained with 5 μM MitoSox for 15 min. Cells

were washed with PBS and treated with trypsin to detach cells from the dish. Cells were centrifuged at 250 x g for 3 min. MitoSox staining was determined with flow cytometry (Beckman Coulter, Atlanta, GA).

2.15. Statistical analysis

All data are represented as mean ± standard error of mean (SEM). Statistical analysis was carried out by using GraphPad Prism Version 5.0 (GraphPad Inc., San Diego, CA, USA) and ANOVA. In some cases, the Bonferroni–Dunn test was used for statistical analysis. All p values less than 0.05 were accepted as statistical significance.

3. RESULTS

3.1. Effect of E2 on high glucose-induced autophagic cell death

To confirm the effect of high glucose on autophagy in hUCB-MSCs, cells were incubated under high glucose conditions (25 mM) at various times ranging from 0 to 72 h. High glucose significantly enhanced Beclin1 at 48 h and LC3-II/LC3-I ratio at 48 h and 72 h while p62 expression decreased gradually after 48 h (Figure 29). In addition, cell viability was decreased in a time-dependent manner under high glucose conditions (Figure 30). To investigate the involvement of high glucose on autophagic cell death, I carried out *ATG5* siRNA transfection to inhibit autophagosome (Chen et al., 2008) and analyzed the cell viability. My results show that high glucose-reduced cell viability was restored following transfection of siRNA against *ATG5* (Figure 31). To determine the effect of E2 on autophagy in hUCB-MSCs, autophagy-related proteins were identified by western blot analysis. High glucose increased Beclin1 expression and the LC3-II/LC3-I ratio while p62 expression

decreased, which were reversed by E2 treatment (10 nM) (Figure 32A). Consistent with these results, immunofluorescence results showed that high glucose-induced LC3 puncta were decreased by E2 treatment. In addition, high glucose-reduced p62 was restored by E2 treatment (Figure 32B). To evaluate the role of E2 on cell viability under high glucose conditions, a cell viability assay was carried out. My results showed that high glucose-reduced cell viability was significantly recovered by E2 treatment under high glucose conditions (Figure 33). Taken together, these data suggest that high glucose induces autophagic cell death and E2 has a protective role on autophagic cell death in hUCB-MSCs.

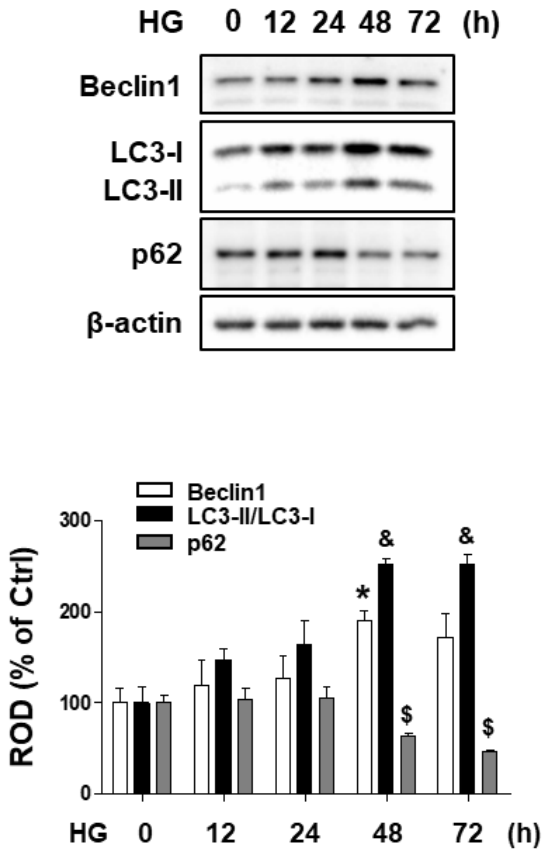

Figure 29. Effect of high glucose on autophagy-related proteins in hUCB-MSCs. Cells were incubated with high glucose (D-glucose, 25 mM) for various times (0-72 h) where the total cell lysates were detected by western blot with antibodies that recognize Beclin1, LC3 and p62. β-actin was used as a loading control. Beclin1, the LC3 ratio and p62 were quantified with ImageJ software. Data are presented as mean ± SEM. n=3. $*p < 0.05$ versus 0 h of Beclin1, $\&p < 0.05$ versus 0 h of the LC3-II/LC3-I ratio, and $\$p < 0.05$ versus 0 h of p62.

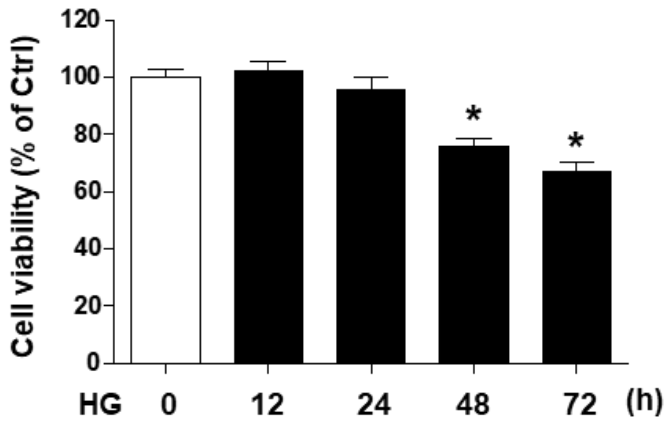

Figure 30. Effect of high glucose on survival of hUCB-MSCs. Cells were incubated with high glucose for various times (0-72 h) where the cell viability was determined by measuring absorbance at 450 nm using a multiplate reader. Data are presented as mean ± SEM. n=3. *$p < 0.05$ versus 0 h.

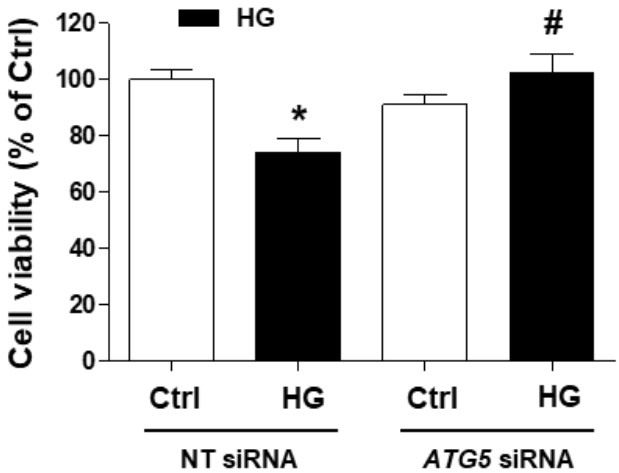

Figure 31. Effect of high glucose on autophagic cell death in hUCB-MSCs. Cells were transfected with *ATG5* siRNA (25 pM) or NT siRNA for 24 h prior to high glucose treatment for 72 h where the cell viability was determined by measuring absorbance at 450 nm using a multiplate reader. Data are presented as mean ± SEM. n=5. *$p < 0.05$ versus ctrl with NT siRNA and #$p < 0.05$ versus high glucose with NT siRNA.

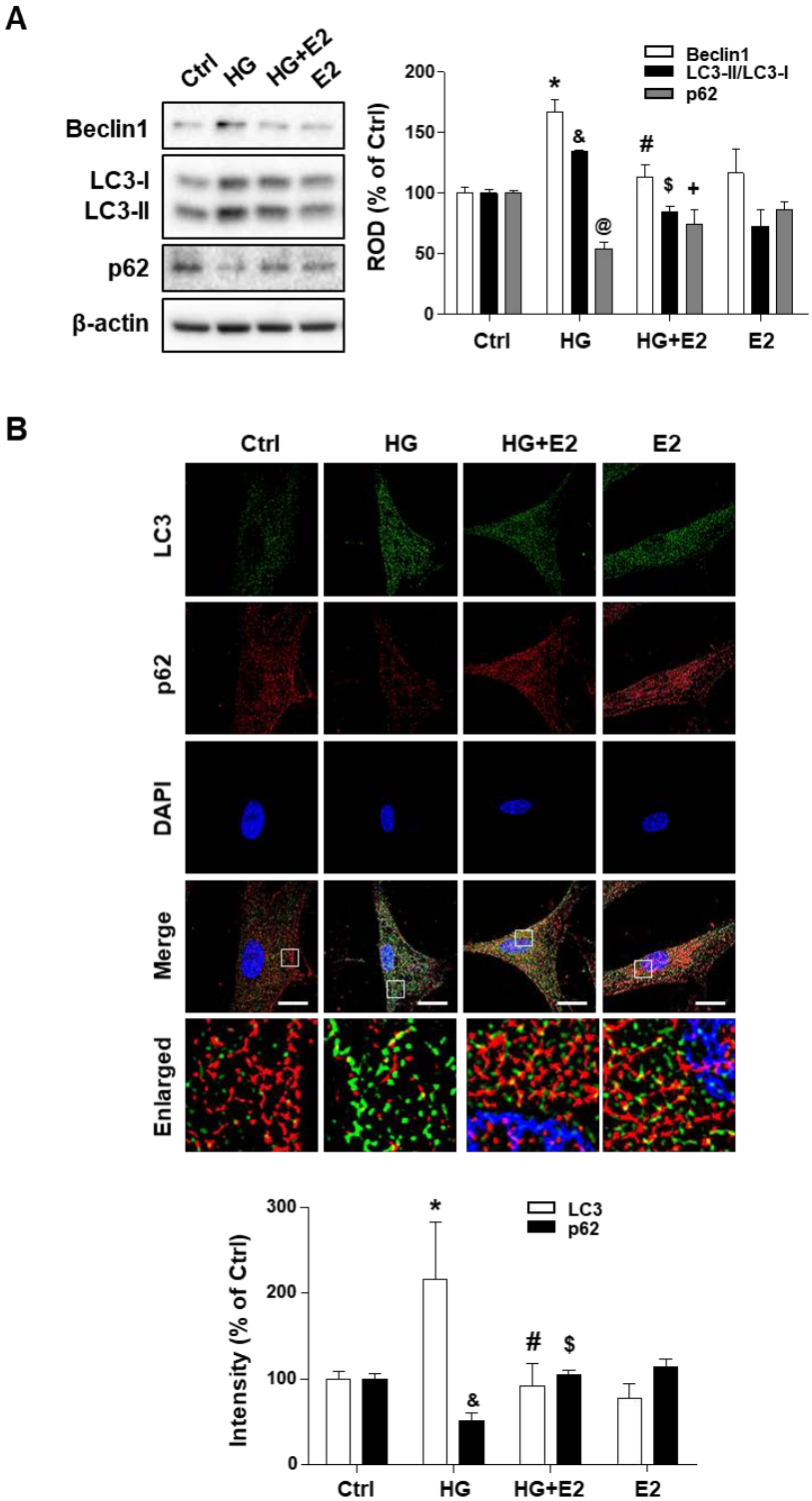
A
Ctrl
HG
HG+E2
E2
Beclin1
LC3-I
LC3-II
p62
β-actin
ROD (% of Ctrl)
Beclin1
LC3-II/LC3-I
p62
200
150
100
50
0
*
&
@
#
$
+
Ctrl
HG
HG+E2
E2
B
Ctrl
HG
HG+E2
E2
LC3
p62
DAPI
Merge
Enlarged
Intensity (% of Ctrl)
LC3
p62
300
200
100
0
*
&
#
$
Ctrl
HG
HG+E2
E2

Figure 32. Effect of E2 on autophagy in hUCB-MSCs. (A) Cells were treated with E2 for 6 h prior to high glucose treatment for 48 h where the expression of Beclin1, LC3 and p62 were detected by western blot. β-actin was used as a loading control. Beclin1, the LC3 ratio and p62 were quantified with ImageJ software. Data are presented as mean ± SEM. n=3. $*p < 0.05$ versus ctrl of Beclin1, $\#p < 0.05$ versus high glucose of Beclin1, $\&p < 0.05$ versus ctrl of LC3-II/LC3-I ratio, $\$p < 0.05$ versus high glucose of LC3-II/LC3-I ratio, $@p < 0.05$ versus ctrl of p62, and $+p < 0.05$ versus high glucose of p62. (B) Cells were treated with E2 for 6 h prior to high glucose treatment for 48 h. The expression of LC3 and p62 were detected by immunofluorescence staining and visualized by SRRF imaging system. Scale bar was set as 20 μm (Magnification x 1,000). Data are presented as mean ± SEM. n=3. Representative gross images of LC3 and p62 were quantified with Fiji software. $*p < 0.05$ versus ctrl of LC3, $\#p < 0.05$ versus high glucose of LC3, $\&p < 0.05$ versus ctrl of p62, and $\$p < 0.05$ versus high glucose of p62.

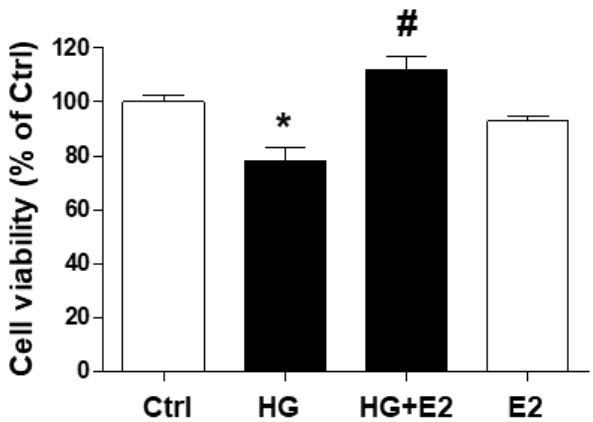

Figure 33. Effect of E2 on survival of hUCB-MSCs. Cells were treated with E2 for 6 h prior to high glucose treatment for 72 h where the cell viability was determined by measuring absorbance at 450 nm using a multiplate reader. Data are presented as mean ± SEM. n=5. $*p < 0.05$ versus ctrl and $\#p < 0.05$ versus high glucose alone.

3.2. Effect of E2 on high glucose-induced mtROS

High glucose is well known to induce excessive production of ROS, and an increase in ROS triggers the dysfunction of mitochondria. To examine the role of high glucose on ROS accumulation in hUCB-MSCs, the ROS level was examined by using DCF-DA (10 μM) where the ROS level was increased in a time-dependent manner (Figure 34A). However, E2 treatment under high glucose conditions decreased ROS levels compared to high glucose alone (Figure 34B). To investigate where ROS occurs within the cells in high glucose conditions, I pretreated NAC (10 μM), mitoTempo (20 μM), and Vas2870 (10 μM) for 30 min prior to high glucose treatments in hUCB-MSCs. High glucose-induced ROS was blocked by NAC and mitoTempo, but Vas2870 did not impact the ROS levels under high glucose conditions (Figure 35A). Mitochondria produce a massive amount of ROS to play an important role in autophagy. To determine the induction of autophagy by mtROS, I analyzed the expression of autophagy-related proteins with mitoTempo pretreatment by western blot. In my results, the protein levels of Beclin1 and the LC3-II/LC3-I ratio were reduced by mitoTempo pretreatment under high glucose conditions. In

contrast, high glucose-reduced p62 was increased by mitoTempo pretreatment (Figure 35B). To determine the effect of E2 on high glucose-induced mtROS, hUCB-MSCs were stained with MitoTracker Green and MitoSox Red. E2 efficiently abolished mtROS generated by high glucose in hUCB-MSCs (Figure 36A). Consequently, high glucose evoked mtROS while E2 efficiently abolished mtROS generated by high glucose in hUCB-MSCs (Figure 36B). These data indicate that high glucose induces autophagy through mtROS, which is reduced by E2 treatment in hUCB-MSCs.

A

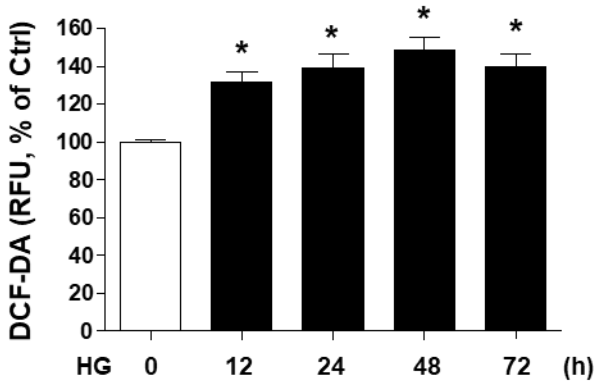
DCF-DA (RFU, % of Ctrl)
160
140
120
100
80
60
40
20
0
*
*
*
*
HG
0
12
24
48
72
(h)

B

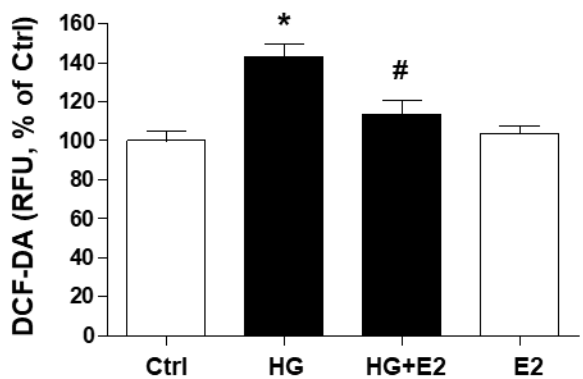
DCF-DA (RFU, % of Ctrl)
160
140
120
100
80
60
40
20
0
*
#
Ctrl
HG
HG+E2
E2

Figure 34. Effect of E2 on high glucose-induced ROS in hUCB-MSCs. (A) Cells were incubated with high glucose for various times (0-72 h) where DCF-DA was detected by luminometer. Data are presented as mean ± SEM. n=3. $*p < 0.05$ versus 0 h. (B) Cells were treated with E2 for 6 h prior to high glucose treatment for 48 h where DCF-DA was detected by luminometer. Data are presented as mean ± SEM. n=5. $*p < 0.05$ versus ctrl and $\#p < 0.05$ versus high glucose alone.

A

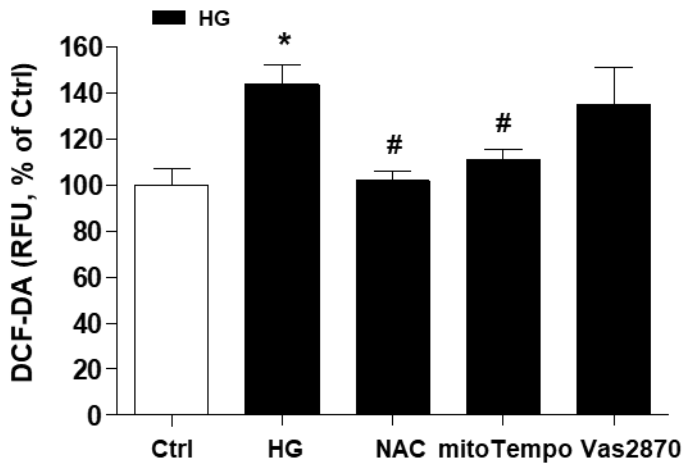
HG
DCF-DA (RFU, % of Ctrl)
160
140
120
100
80
60
40
20
0
*
#
#
Ctrl
HG
NAC
mitoTempo
Vas2870

B

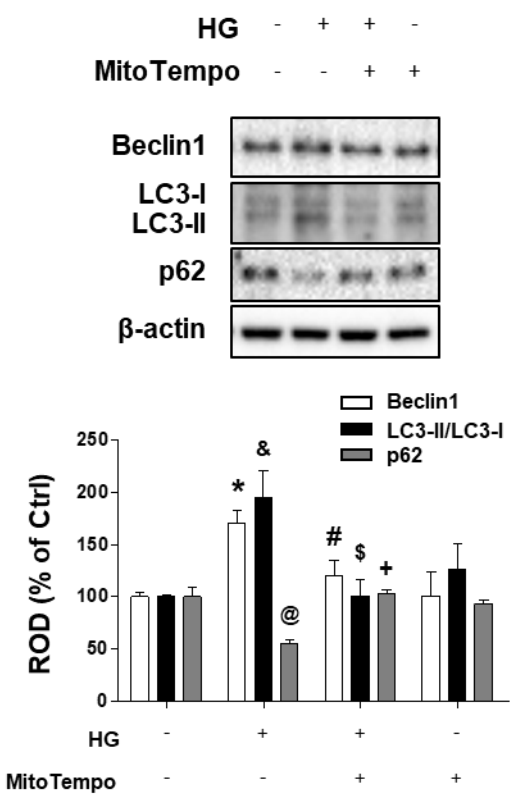
HG - + + -
MitoTempo - - + +
Beclin1
LC3-I
LC3-II
p62
β-actin
Beclin1
LC3-II/LC3-I
p62
ROD (% of Ctrl)
250
200
150
100
50
0
*
&
@
#
$
+
HG - + + -
MitoTempo - - + +

Figure 35. Effect of high glucose on mtROS in hUCB-MSCs. (A) Cells were pretreated with either NAC (10 μM), mitoTempo (20 μM) or Vas2870 (10 μM) for 30 min prior to high glucose treatment for 48 h where DCF-DA was detected by luminometer. Data are presented as mean ± SEM. n=5. $*p < 0.05$ versus ctrl and $\#p < 0.05$ versus high glucose alone. (B) Cells were pretreated with mitoTempo (20 μM) for 30 min prior to high glucose treatment for 48 h where the expression of Beclin1, LC3 and p62 were detected by western blot. β-actin was used as a loading control. Beclin1, the LC3-II/LC3-I ratio and p62 were quantified with ImageJ software. Data are presented as mean ± SEM. n=3. $*p < 0.05$ versus ctrl of Beclin1, $\#p < 0.05$ versus high glucose of Beclin1, $\&p < 0.05$ versus ctrl of LC3-II/LC3-I ratio, $\$p < 0.05$ versus high glucose of LC3-II/LC3-I ratio, $@p < 0.05$ versus ctrl of p62, and $+p < 0.05$ versus high glucose of p62.

A

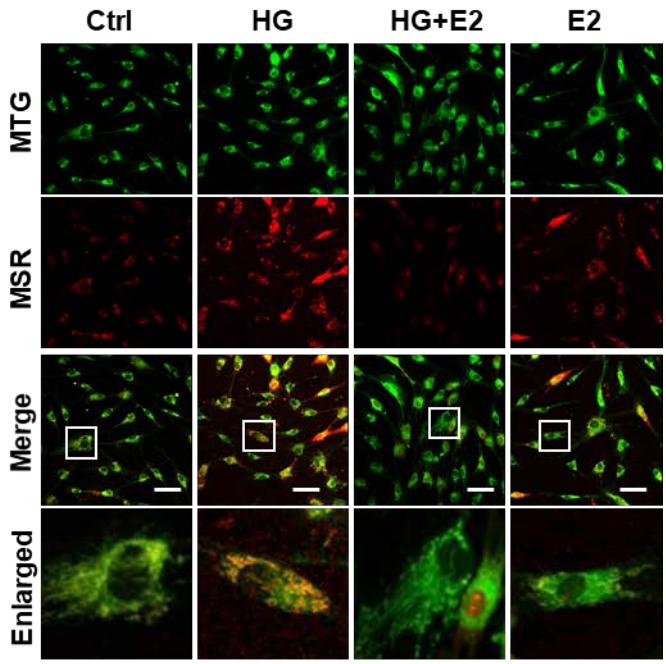
Ctrl
HG
HG+E2
E2
MTG
MSR
Merge
Enlarged

B

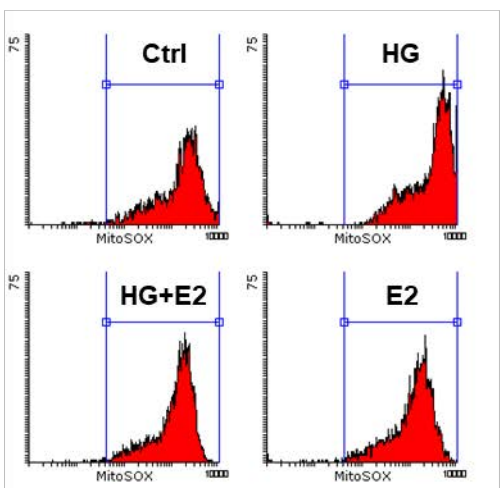
Ctrl
HG
HG+E2
E2
MitoSOX
75

Figure 36. Effect of E2 on high glucose-induced mtROS in hUCB-MSCs. (A) Cells were treated with E2 for 6 h prior to high glucose treatment for 48 h. Mitotracker Green (MTG; 200 nM; green) and Mitosox Red (MSR; 5 μM; red) were detected by immuno-fluorescence staining and visualized by confocal microscopy. Scale bar was set as 100 μm (Magnification x 200). (B) Cells were treated with E2 for 6 h prior to high glucose treatment for 48 h where mtROS with mitoSox was measured using FACS analysis. Total cell counts = 5 x 10^3 cells.

3.3. Involvement of ERα on the upregulation of Nrf2 and Sirt3

To assess the effect of estrogen receptors by E2 under high glucose conditions, I performed western blot after isolating the cytosol and nuclear fractionation. ERα was in high abundance in the nucleus after E2 treatment under high glucose conditions when compared to control or high glucose only. In contrast, E2 treatment did not affect ERβ expression in the nucleus under high glucose conditions (Figure 37). Therefore, to confirm the role of high glucose-reduced Nrf2 in the nucleus by regulating ERα, *ERα* siRNA transfection was carried out. *ERα* siRNA-transfected cells decreased the nuclear Nrf2 level under high glucose conditions (Figure 38A) whereas high glucose did not change the nuclear Nrf2 by *ERβ* siRNA transfection (Figure 38B). To assess the effect of ERα on Sirt3 expression, *ERα* siRNA transfection was carried out. NT siRNA-transfected hUCB-MSCs reduced Sirt3 expression under high glucose conditions compared to NT siRNA-transfected cells. In addition, *ERα* siRNA transfection decreased Sirt3 expression more than NT siRNA-transfected hUCB-MSCs with high glucose (Figure 39). *ERα* siRNA-transfected cells after high

glucose treatment decreased the SOD activity compared to NT siRNA-transfected cells with high glucose (Figure 40). Therefore, ERα is involved in Nrf2 and Sirt3 expression under high glucose conditions.

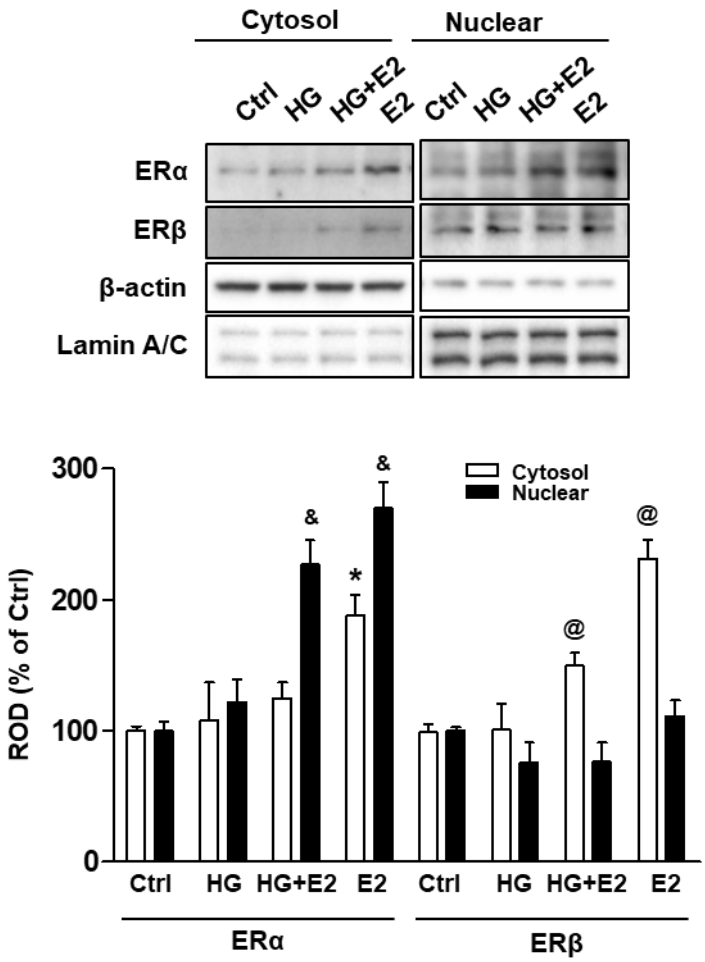
Cytosol
Nuclear
Ctrl
HG
HG+E2
E2
ERα
ERβ
β-actin
Lamin A/C
ROD (% of Ctrl)
300
200
100
0
Cytosol
Nuclear
&
*
@
Ctrl
HG
HG+E2
E2
ERα
ERβ

Figure 37. Effect of E2 on high glucose-induced ERα nuclear translocation. Cells were treated with E2 for 6 h prior to high glucose treatment for 48 h where the subcellular fractionation was carried out according to the manufacturer's protocol. The expression of ERα and ERβ were detected by western blot. β-actin was used as the cytosol marker and Lamin A/C was used as the nuclear marker. ERα and ERβ were quantified with ImageJ software. Data are presented as mean ± SEM. n=3. $*p < 0.05$ versus ctrl of ERα in cytosol, $\&p < 0.05$ versus ctrl of ERα in nuclear, and $@p < 0.05$ versus ctrl of ERβ in cytosol.

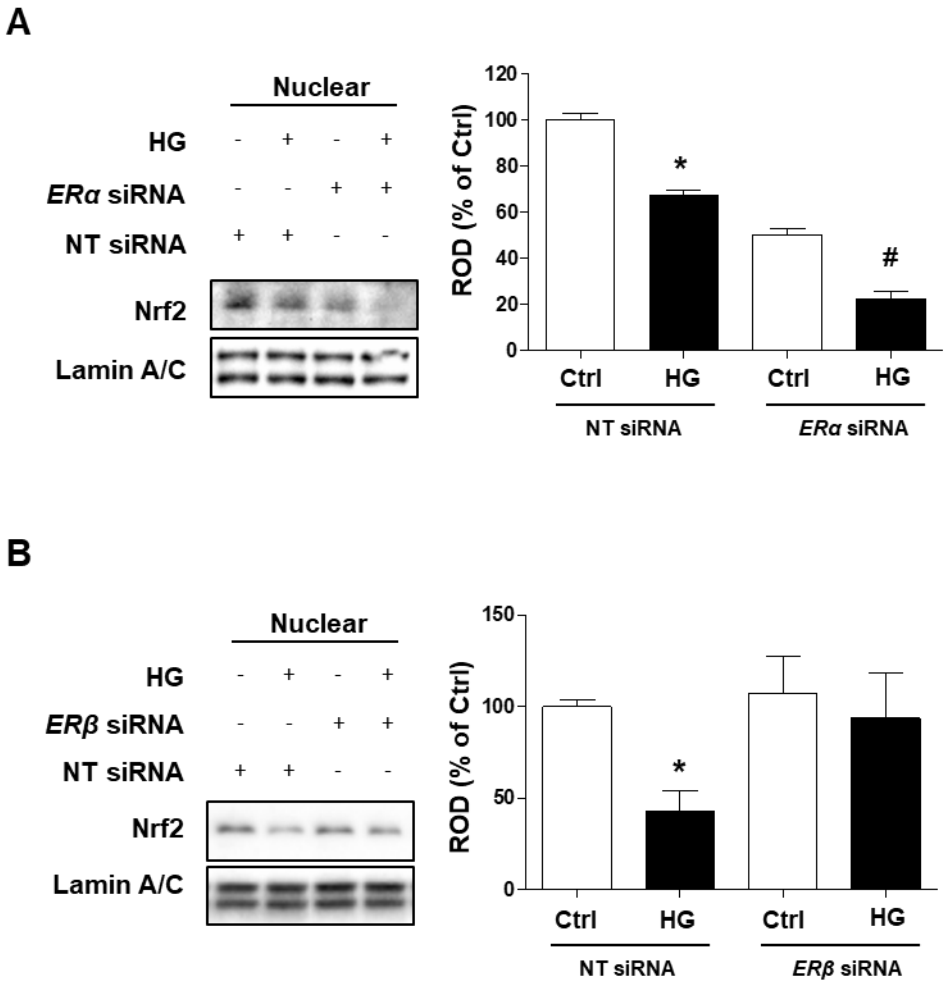
A
Nuclear
HG
ERα siRNA
NT siRNA
Nrf2
Lamin A/C
ROD (% of Ctrl)
120
100
80
60
40
20
0
*
#
Ctrl
HG
Ctrl
HG
NT siRNA
ERα siRNA
B
Nuclear
HG
ERβ siRNA
NT siRNA
Nrf2
Lamin A/C
ROD (% of Ctrl)
150
100
50
0
*
Ctrl
HG
Ctrl
HG
NT siRNA
ERβ siRNA

Figure 38. Effect of high glucose on ERα-dependent Nrf2 nuclear translocation. (A) Cells were transfected with *ERα* siRNA or NT siRNA for 24 h prior to high glucose treatment for 72 h where nuclear fraction was carried out. Nuclear Nrf2 was detected by western blot. Lamin A/C was used as the nuclear marker. Nuclear Nrf2 was quantified with ImageJ software. Data are presented as mean ± SEM. n=3. $*p < 0.05$ versus ctrl with NT siRNA and $\#p < 0.05$ versus high glucose with NT siRNA. (B) Cells were transfected with *ERβ* siRNA or NT siRNA for 24 h prior to high glucose treatment for 72 h where nuclear fraction was carried out. Nuclear Nrf2 was detected by western blot. Lamin A/C was used as the nuclear marker. Nuclear Nrf2 was quantified with ImageJ software. Data are presented as mean ± SEM. n=3. $*p < 0.05$ versus ctrl with NT siRNA.

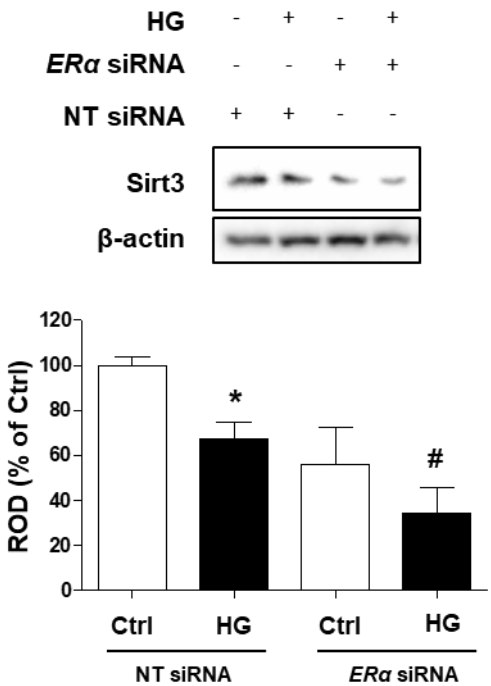

Figure 39. Effect of high glucose on ERα-dependent Sirt3 upregulation. Cells were transfected with *ERα* siRNA or NT siRNA for 24 h prior to high glucose treatment for 72 h where Sirt3 expression was detected by western blot. β-actin was used as a loading control. Sirt3 was quantified with ImageJ software. Data are presented as mean ± SEM. n=3. $*p < 0.05$ versus ctrl with NT siRNA and $\#p < 0.05$ versus high glucose with NT siRNA.

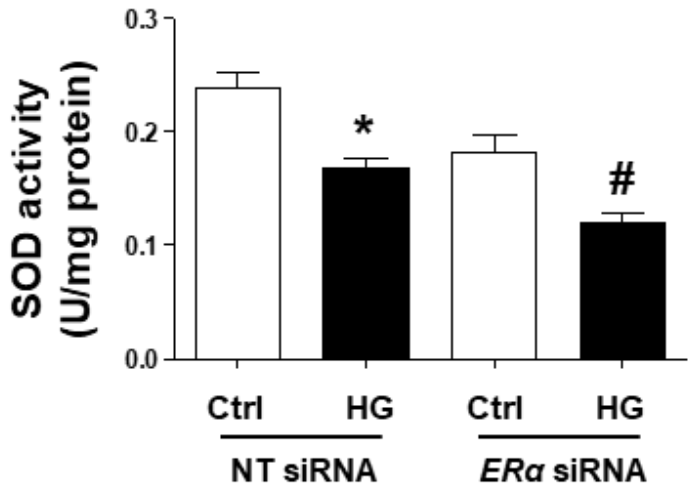

Figure 40. Effect of high glucose on SOD activity through ERα signaling. Cells were transfected with *ERα* siRNA or NT siRNA for 24 h prior to high glucose treatment for 72 h where SOD activity assay was carried out. Absorbance at 450 nm was measured with a multiplate reader. Data are presented as mean ± SEM. n=3. *p < 0.05 versus ctrl with NT siRNA and #p < 0.05 versus high glucose with NT siRNA.

3.4. Role of E2 on Nrf2-dependent mtROS under high glucose conditions

Nrf2/Keap1 signaling causes a protective mechanism against the deleterious effects of oxidative stress. In particular, Nrf2 is a transcription factor that regulates many antioxidant enzyme gene expressions, such as MnSOD and catalase (Li et al., 2004). Therefore, to examined whether ROS levels which were increased by high glucose were affected by Nrf2, I measured ROS levels after performing *NRF2* siRNA transfection with high glucose treatment. In my results, NRF2 silencing enhanced ROS levels under high glucose conditions compared to NT siRNA-transfected cells with high glucose (Figure 41). To confirm the effect of high glucose on Nrf2 nuclear translocation, nuclear fractionation was performed. High glucose treatment for 72 h decreased the levels of nuclear Nrf2, whereas it increased the levels of Keap1 in the total cell lysates (Figure 42A). In addition, the nuclear translocation of Nrf2 was inhibited by high glucose treatment for 72 h (Figure 42B). Furthermore, the knockdown of *NRF2* further decreased Sirt3 and MnSOD expression levels under high glucose conditions (Figure 43). To verify the effect of E2 on Nrf2 nuclear translocation under high

glucose conditions, nuclear fraction was carried out after E2 treatment under high glucose conditions. E2 treatment restored the nuclear Nrf2 levels under high glucose conditions while high glucose decreased nuclear Nrf2 levels (Figure 44A). Consistent with these results, immunofluorescence results showed that Nrf2 present in the cytoplasm accumulated around the nucleus by E2 treatment under high glucose conditions. Nrf2 was upregulated in response to E2 treatment under high glucose conditions, but the loss of Nrf2 was observed in the nucleus by high glucose (Figure 44B). Collectively, these results indicate that high glucose enhances Nrf2-dependent ROS levels, which is reversed by E2 treatment.

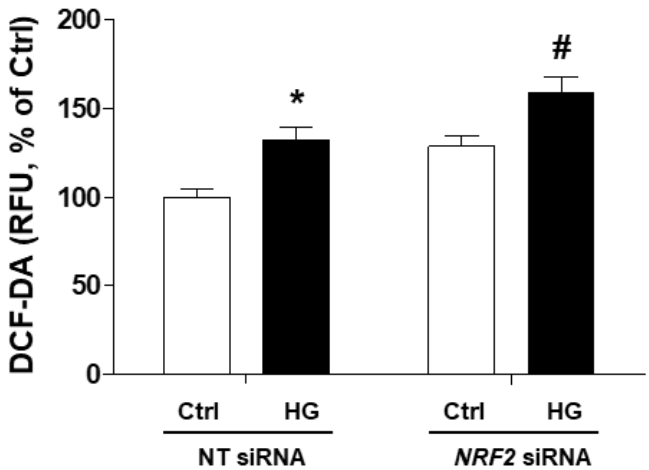

Figure 41. Effect of high glucose on ROS through Nrf2 signaling in hUCB-MSCs. Cells were transplanted with *NRF2* siRNA or NT siRNA for 24 h prior to high glucose treatment for 48 h where DCF-DA was detected by luminometer. Data are presented as mean ± SEM. n=5. *$p < 0.05$ versus ctrl with NT siRNA and #$p < 0.05$ versus high glucose with NT siRNA.

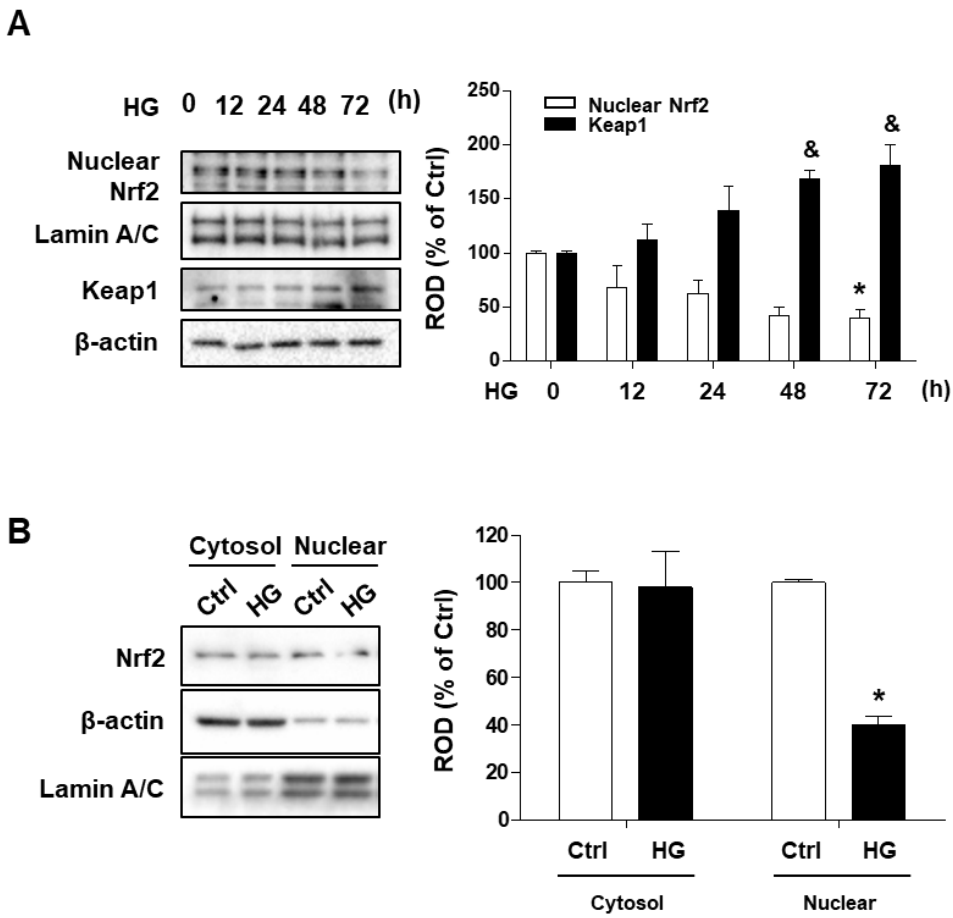
A
HG 0 12 24 48 72 (h)
Nuclear Nrf2
Lamin A/C
Keap1
β-actin
Nuclear Nrf2
Keap1
ROD (% of Ctrl)
250
200
150
100
50
0
&
&
*
HG 0 12 24 48 72 (h)
B
Cytosol Nuclear
Ctrl HG Ctrl HG
Nrf2
β-actin
Lamin A/C
ROD (% of Ctrl)
120
100
80
60
40
20
0
*
Ctrl HG Ctrl HG
Cytosol
Nuclear

Figure 42. Effect of high glucose on decreased Nrf2 nuclear translocation in hUCB-MSCs. (A) Cells were incubated with high glucose for various times (0-72 h) where nuclear fraction was carried out. Nuclear Nrf2 and the total Keap1 were detected by western blot. Lamin A/C was used as the nuclear marker. β-actin was used as a loading control. Nuclear Nrf2 and total Keap1 were quantified with ImageJ software. Data are presented as mean ± SEM. n=3. $*p < 0.05$ versus 0 h of nuclear Nrf2 and $\&p < 0.05$ versus 0 h of Keap1. (B) Cells were treated with high glucose for 72 h where the subcellular fractionation was carried out. Nrf2 was detected by western blot. β-actin was used as the cytosol marker and Lamin A/C was used as the nuclear marker. Nrf2 was quantified with ImageJ software. Data are presented as mean ± SEM. n=3. $*p < 0.05$ versus high glucose in cytosol.

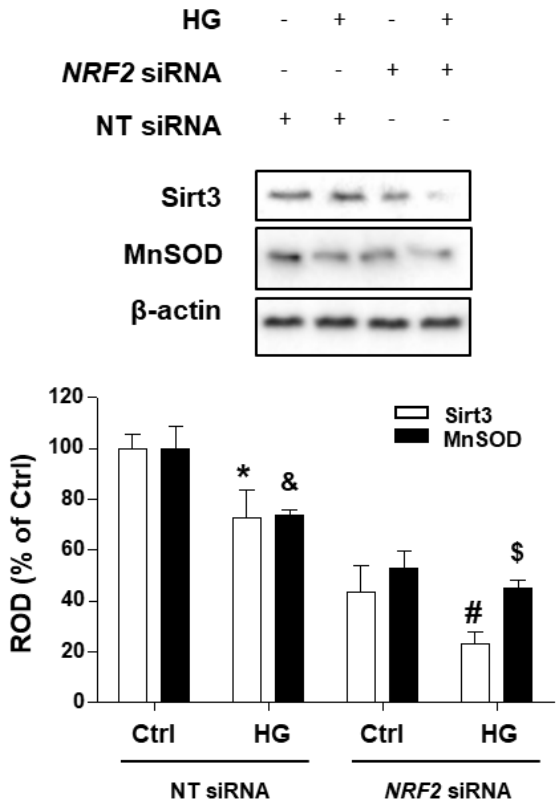

Figure 43. Effect of high glucose on Sirt3 and MnSOD repression through Nrf2 signaling in hUCB-MSCs. Cells were transfected with *NRF2* siRNA or NT siRNA for 24 h prior to high glucose treatment for 72 h where Sirt3 and MnSOD were detected by western blot. β-actin was used as a loading control. Sirt3 and MnSOD were quantified with ImageJ software. Data are presented as mean ± SEM. n=3. $*p < 0.05$ versus ctrl of Sirt3 with NT siRNA, $\#p < 0.05$ versus high glucose of Sirt3 with NT siRNA, $\&p < 0.05$ versus ctrl of MnSOD with NT siRNA, and $\$p < 0.05$ versus high glucose of MnSOD with NT siRNA.

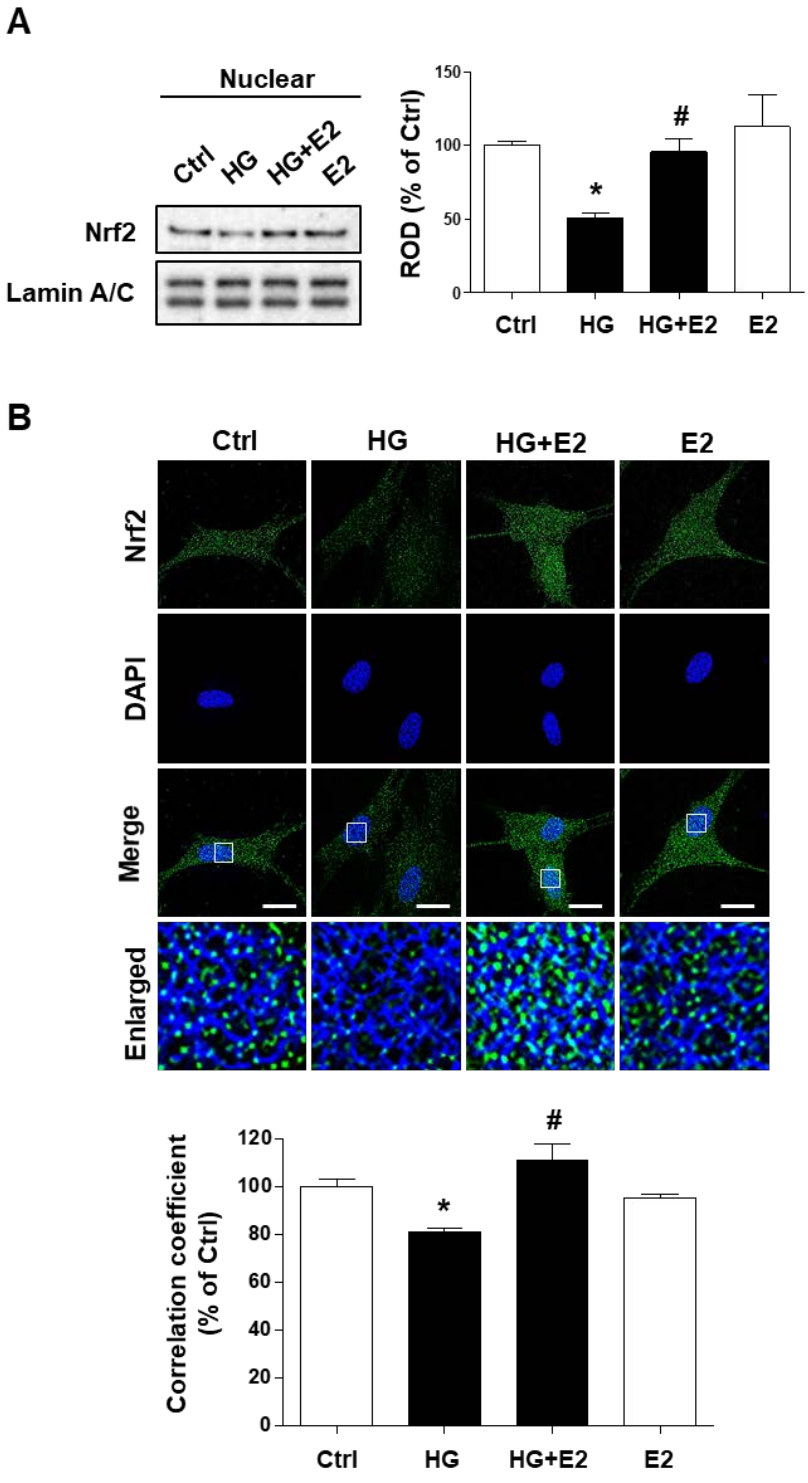
A
Nuclear
Ctrl
HG
HG+E2
E2
Nrf2
Lamin A/C
ROD (% of Ctrl)
150
100
50
0
*
#
Ctrl
HG
HG+E2
E2
B
Ctrl
HG
HG+E2
E2
Nrf2
DAPI
Merge
Enlarged
Correlation coefficient (% of Ctrl)
120
100
80
60
40
20
0
*
#
Ctrl
HG
HG+E2
E2

Figure 44. Effect of E2 on Nrf2 nuclear translocation in hUCB-MSCs. (A) Cells were treated with E2 for 6 h prior to high glucose treatment for 72 h where nuclear fraction was carried out. Nuclear Nrf2 was detected by western blot. Lamin A/C was used as the nuclear marker. Nuclear Nrf2 was quantified with ImageJ software. Data are presented as mean ± SEM. n=3. $*p < 0.05$ versus ctrl and $\#p < 0.05$ versus high glucose alone. (B) Cells were treated with E2 for 6 h prior to high glucose treatment for 72 h, and the expression of Nrf2 was detected by immunofluorescence staining and visualized by SRRF imaging system. Scale bar was set as 20 μm (Magnification x 1,000). Data are presented as mean ± SEM. n=3. Representative gross images of Nrf2 was quantified with Fiji software. $*p < 0.05$ versus ctrl and $\#p < 0.05$ versus high glucose alone.

3.5. Role of E2 on Sirt3-dependent MnSOD in the mtROS production under high glucose conditions

To verify that MnSOD regulates ROS in high glucose conditions, I investigate the change in the MnSOD acetylation at lysine 68 (Ac-K68-MnSOD), because the lysine site of MnSOD is known to be the most important acetylation site for activating MnSOD. My results reveal that high glucose increased the Ac-K68-MnSOD level in a time-dependent manner whereas the MnSOD expression level was decreased under high glucose conditions (Figure 45A). Sirt3, a nicotinamide adenine dinucleotide (NAD^+)-dependent mitochondrial deacetylase, plays an essential role in regulating high glucose/diabetes-induced ROS generation (Jing et al., 2011; Zhang et al., 2013). In time-course experiments, the expression level of Sirt3 was decreased by high glucose treatment (Figure 45B). Sirt3 directly deacetylases MnSOD, indicating the promotion of its antioxidative activity (Qiu et al., 2010). Thus, to verify the effects of Sirt3 on MnSOD activation, *SIRT3* siRNA transfection was carried out. SIRT3 knockdown induced MnSOD acetylation under high glucose conditions (Figure 46), indicating the activation of MnSOD by Sirt3. Next, I tested that MnSOD present in the mitochondria matrix regulates ROS. MnSOD silencing under high glucose conditions significantly increased ROS levels compared to NT siRNA-transfected hUCB-MSC with high glucose (Figure 47).

To verify the effects of E2 on Sirt3 expression under high glucose conditions, western blot was carried out. My results show that high glucose induced Sirt3 repression while E2-treated high glucose increased Sirt3 expression when compared to high glucose alone in hUCB-MSCs (Figure 48A). Consequently, immunofluorescence staining indicated that Sirt3 was decreased by high glucose treatment, which was reversed by treatment with E2 under high glucose conditions (Figure 48B). To verify the protective role of E2 on SOD activity, a SOD activity assay was performed. The level of SOD activity decreased significantly in high glucose-treated hUCB-MSCs compared to control. Furthermore, E2 treatment under high glucose conditions recovered the SOD activity compared to high glucose only (Figure 49). Hence, these findings suggest that E2 treatment enhanced Sirt3-dependent MnSOD activation under high glucose conditions.

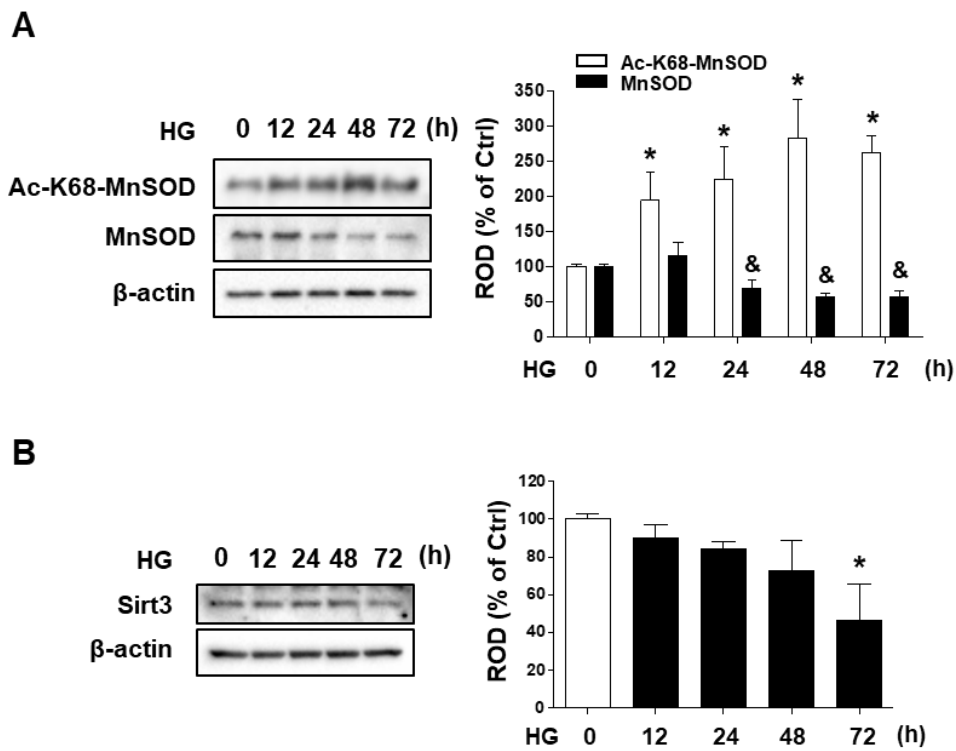
A
HG 0 12 24 48 72 (h)
Ac-K68-MnSOD
MnSOD
β-actin
Ac-K68-MnSOD
MnSOD
ROD (% of Ctrl)
350
300
250
200
150
100
50
0
*
&
HG 0 12 24 48 72 (h)
B
HG 0 12 24 48 72 (h)
Sirt3
β-actin
ROD (% of Ctrl)
120
100
80
60
40
20
0
*
HG 0 12 24 48 72 (h)

Figure 45. Effect of high glucose on MnSOD activation and Sirt3 expression in hUCB-MSCs. (A) Cells were incubated with high glucose for various times (0-72 h) where Ac-K68-MnSOD and MnSOD were detected by western blot. β-actin was used as a loading control. Ac-K68-MnSOD and MnSOD were quantified with ImageJ software. Data are presented as mean ± SEM. n=3. $*p < 0.05$ versus 0 h of Ac-K68-MnSOD and $\&p < 0.05$ versus 0 h of MnSOD. (B) Cells were incubated with high glucose for various times (0-72 h) and Sirt3 was detected by western blot. β-actin was used as a loading control. Sirt3 was quantified with ImageJ software. Data are presented as mean ± SEM. n=3. $*p < 0.05$ versus 0 h of Sirt3.

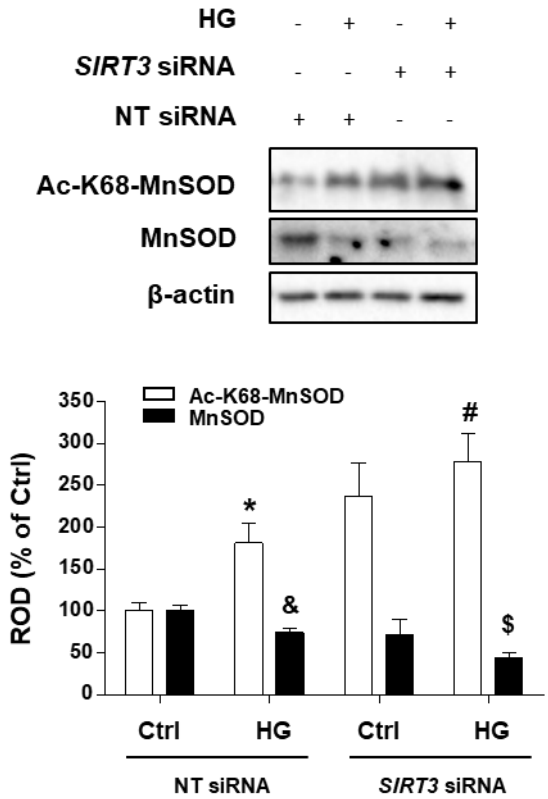

Figure 46. Effect of high glucose on MnSOD activation through Sirt3 signaling in hUCB-MSCs. Cells were transfected with *SIRT3* siRNA or NT siRNA for 24 h prior to high glucose treatment for 72 h where Ac-K68-MnSOD and MnSOD were detected by western blot. β-actin was used as a loading control. Ac-K68-MnSOD and MnSOD were quantified with ImageJ software. Data are presented as mean ± SEM. n=3. $*p < 0.05$ versus ctrl of Ac-K68-MnSOD with NT siRNA, $\#p < 0.05$ versus high glucose of Ac-K68-MnSOD with NT siRNA, $\&p < 0.05$ versus ctrl of MnSOD with NT siRNA, and $\$p < 0.05$ versus high glucose of MnSOD with NT siRNA.

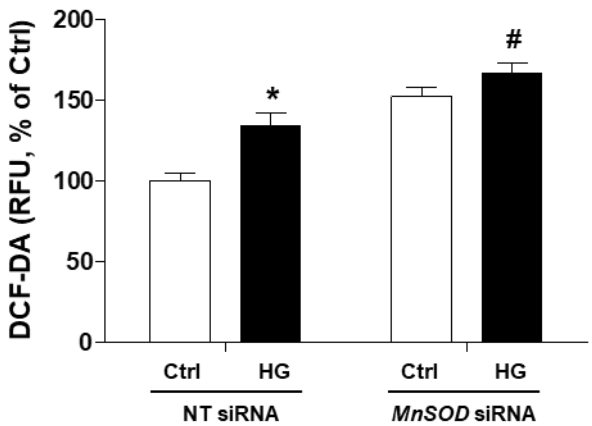

Figure 47. Effect of high glucose on ROS production through MnSOD signaling in hUCB-MSCs. Cells were transplanted with *MnSOD* siRNA or NT siRNA for 24 h prior to high glucose treatment for 72 h where DCF-DA was detected by luminometer. Data are presented as mean ± SEM. n=5. $*p < 0.05$ versus ctrl with NT siRNA and $\#p < 0.05$ versus high glucose with NT siRNA.

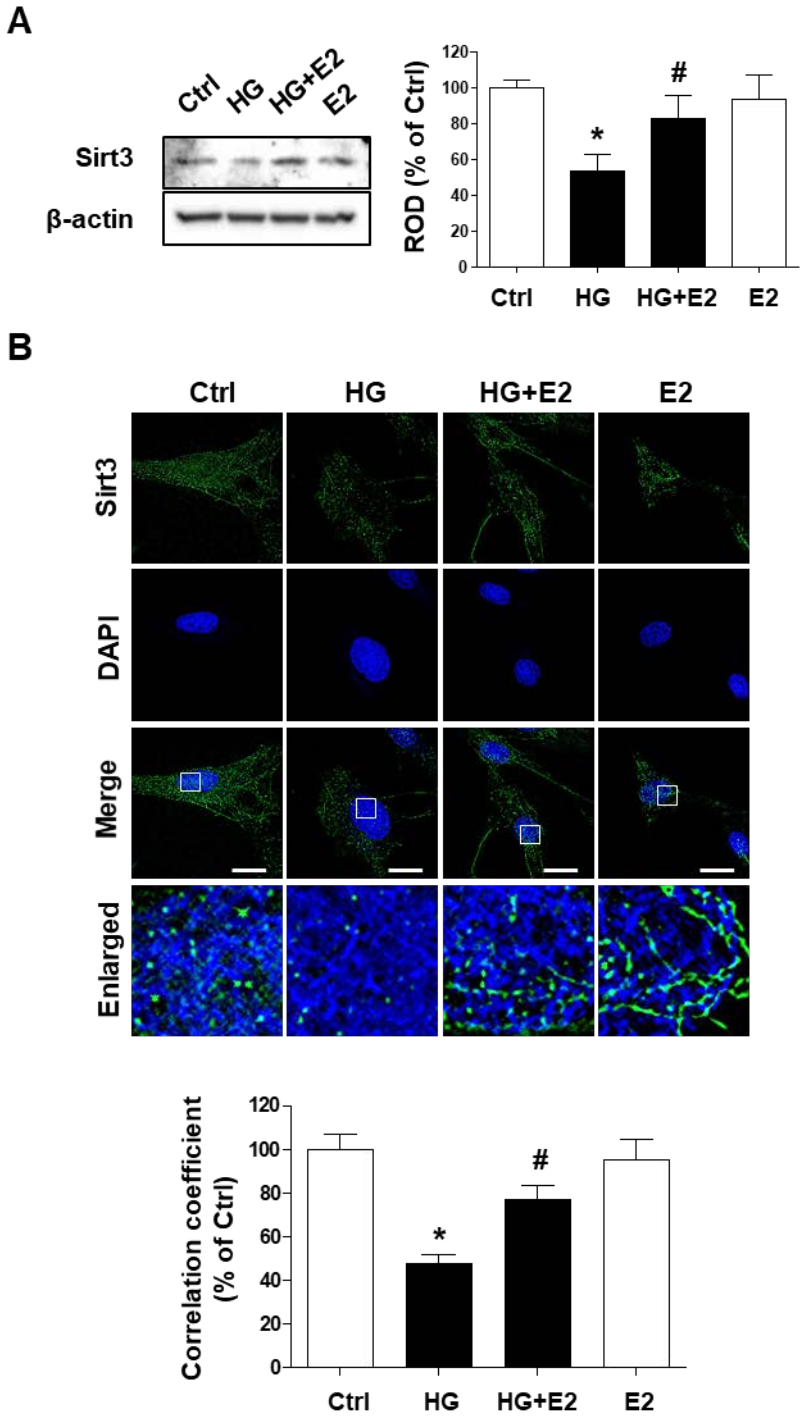
A
Ctrl
HG
HG+E2
E2
Sirt3
β-actin
ROD (% of Ctrl)
120
100
80
60
40
20
0
*
#
Ctrl
HG
HG+E2
E2
B
Ctrl
HG
HG+E2
E2
Sirt3
DAPI
Merge
Enlarged
Correlation coefficient (% of Ctrl)
120
100
80
60
40
20
0
*
#
Ctrl
HG
HG+E2
E2

Figure 48. Effect of E2 on high glucose-induced Sirt3 repression in hUCB-MSCs. (A) Cells were treated with E2 for 6 h prior to high glucose treatment for 72 h where Sirt3 was detected by western blot. β-actin was used as a loading control. Sirt3 was quantified with ImageJ software. Data are presented as mean ± SEM. n=3. $*p < 0.05$ versus ctrl and $\#p < 0.05$ versus high glucose alone. (F) Cells were treated with E2 for 6 h prior to high glucose treatment for 72 h where the expression of Sirt3 was detected by immunofluorescence staining and visualized by SRRF imaging system. Scale bar was set as 20 μm (Magnification x 1,000). Data are presented as mean ± SEM. n=3. Representative gross images of Sirt3 was quantified with Fiji software. $*p < 0.05$ versus ctrl and $\#p < 0.05$ versus high glucose alone.

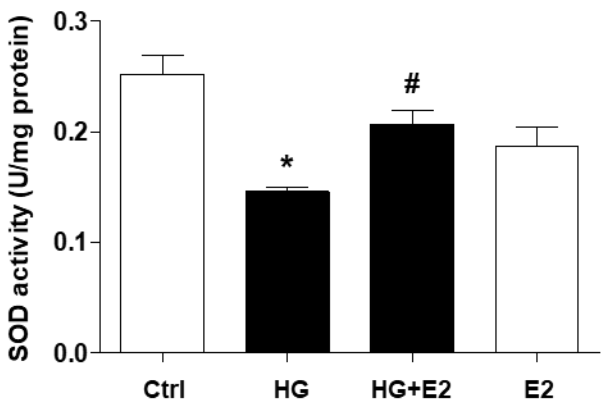

Figure 49. Effect of E2 on SOD activity under high glucose conditions in hUCB-MSCs. Cells were treated with E2 for 6 h prior to high glucose treatment for 72 h where SOD activity assay was carried out. Absorbance at 450 nm was measured with a multiplate reader. Data are presented as mean ± SEM. n=5. $*p < 0.05$ versus ctrl and $\#p < 0.05$ versus high glucose alone.

3.6. Role of E2 on the mouse skin wound healing effect via ERα signaling in OVX diabetic mice

I have found that E2 has protective effects on the mtROS-induced autophagic cell death in hUCB-MSCs under high glucose conditions. Thus, I examined the functional role of E2 by which E2 treatment may affect wound healing on the *in vivo* OVX diabetic mouse model. To confirm the effect of ERα on hUCB-MSCs in OVX diabetic mice, I transfected *ERα* siRNA into hUCB-MSCs before injecting it into the mouse wound sites. In my results, the wound closure effect in the OVX + STZ + E2 group did not show a significant difference from the OVX + STZ group on day 9 ($p > 0.05$). Interestingly, the wound healing effect in OVX + STZ + NT siRNA + hUCB-MSC + E2 was significantly higher than in the OVX + STZ + NT siRNA + hUCB-MSC group 9 days after wounding. In addition, the wound healing effect was significantly reduced in OVX + STZ + *ERα* siRNA + hUCB-MSC + E2 compared to the OVX + STZ + NT siRNA + hUCB-MSC + E2 group. The OVX + STZ group had a similar wound size as other groups on day 6, but the wound size was observed to be the largest 9 days after wounding (Figure 50A and 50B). Histological examination of wound tissues on

day 10 showed that the wound site was almost filled with granulation tissues for OVX + STZ + NT siRNA + hUCB-MSC + E2 compared to the wounds of OVX + STZ + *ERα* siRNA + hUCB-MSC + E2 group (Figure 51). To track transplanted hUCB-MSC *in vivo* on day 10, wound tissues were stained with anti-human nuclear antigen (HNA) antibodies. Immunohistochemistry revealed many HNA-positive cells in the OVX + STZ + NT siRNA + hMSC + E2 group, while no HNA-positive cells were found in the Sham / OVX / OVX+STZ / OVX + STZ + E2 group (Figure 52). Blood vessels that developed many branches were observed in all hUCB-MSC transplantation groups compared to the no hUCB-MSC transplantation groups. In particular, developed blood vessels were observed in the OVX + STZ + NT siRNA + hUCB-MSC + E2 group compared to other hUCB-MSC transplantation groups. Blood vessels that reduced branches were observed in OVX + STZ + *ERα* siRNA + hUCB-MSC + E2 groups compared to OVX + STZ + NT siRNA + hUCB-MSC + E2 groups (Figure 53). Overall, these data indicate that transplantation of hUCB-MSCs with E2 injection into OVX diabetic mice results in faster wound healing than E2 injection only or hUCB-MSC transplantation only.

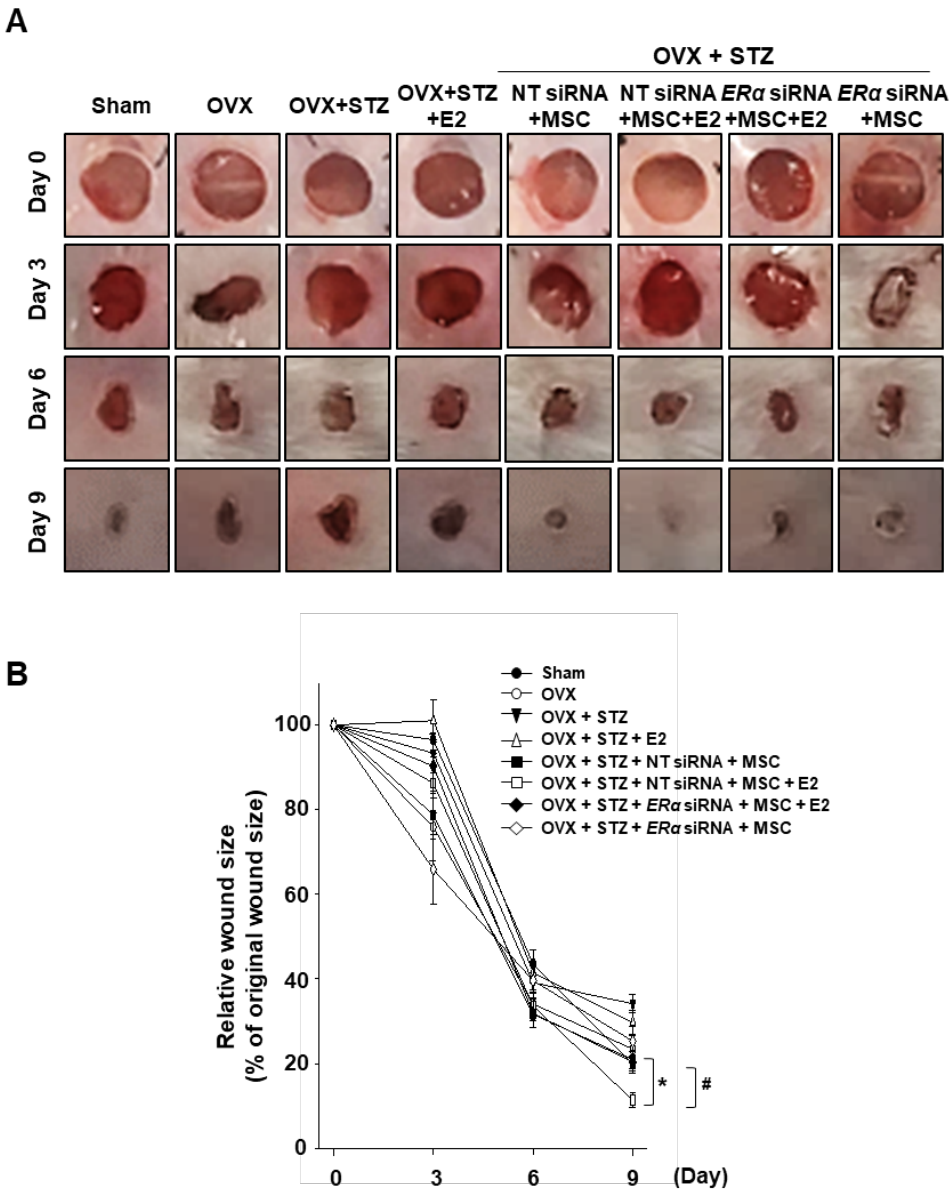
A
OVX + STZ
Sham
OVX
OVX+STZ
OVX+STZ +E2
NT siRNA +MSC
NT siRNA +MSC+E2
ERα siRNA +MSC+E2
ERα siRNA +MSC
Day 0
Day 3
Day 6
Day 9
B
Sham
OVX
OVX + STZ
OVX + STZ + E2
OVX + STZ + NT siRNA + MSC
OVX + STZ + NT siRNA + MSC + E2
OVX + STZ + ERα siRNA + MSC + E2
OVX + STZ + ERα siRNA + MSC
Relative wound size (% of original wound size)
100
80
60
40
20
0
0
3
6
9
(Day)
*
#

Figure 50. Effect of ERα-silenced hUCB-MSC transplantation with E2 injection in OVX diabetic mouse model. (A) OVX diabetic mice were randomly divided into six groups (n=6 each group): OVX + STZ, OVX + STZ + E2, OVX + STZ + NT siRNA + hUCB-MSC (MSC), OVX + STZ + NT siRNA + MSC + E2, OVX + STZ + *ERα* siRNA + MSC + E2, and OVX + STZ + *ERα* siRNA + MSC. Representative gross images of wounds on days 0, 3, 6, and 9 are shown. (B) Percentage of wound sizes on days 0, 3, 6, and 9 are shown. Wound sizes were measured with ImageJ software. Data are presented as mean ± SEM. n=6 each group. $*p < 0.05$ versus OVX + STZ + *ERα* siRNA + MSC + E2 group and $\#p < 0.05$ versus OVX + STZ + NT siRNA + MSC group.

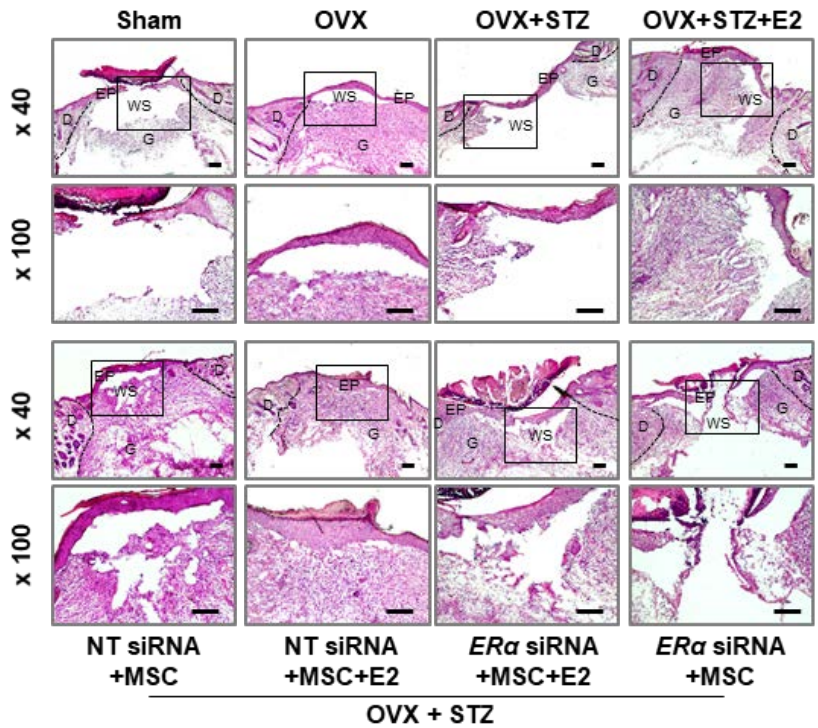

Figure 51. Effect of ERα-silenced hUCB-MSC transplantation in OVX diabetic mouse model. Wound tissues were stained by H&E staining and photographed under brightfield microscopy. Scale bars were set as 200 μm or 100 μm.

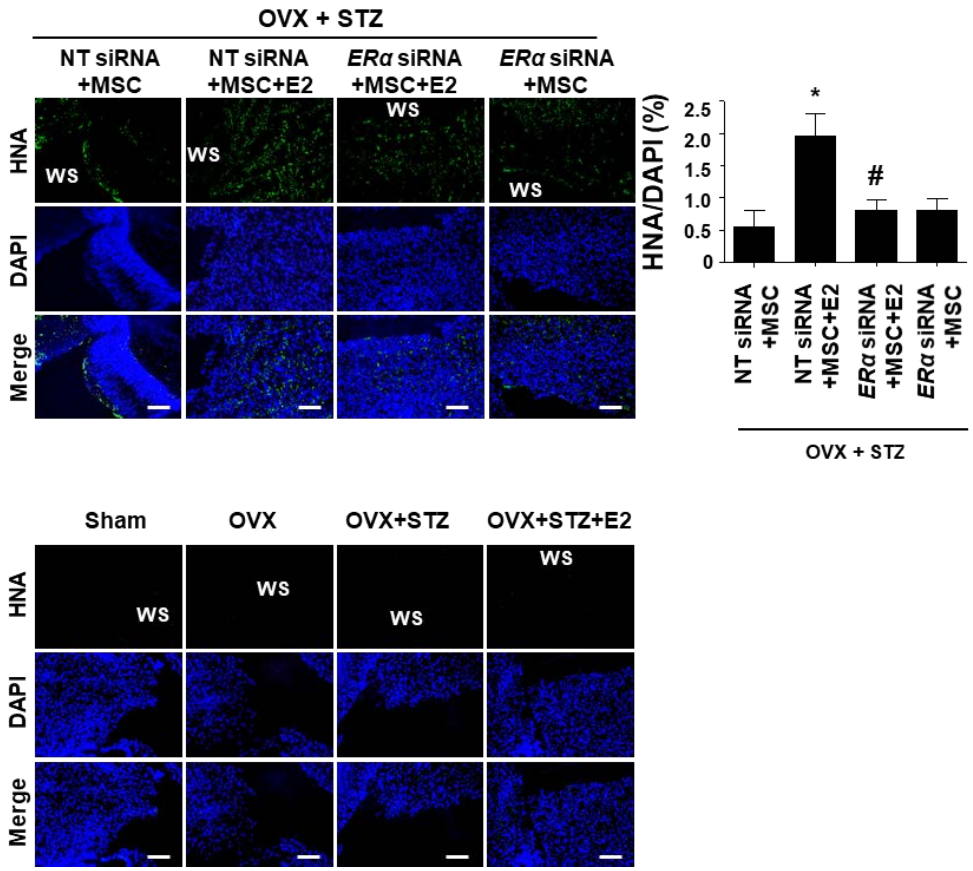

Figure 52. Effect of ERα-silenced hUCB-MSC transplantation on HNA expression in OVX diabetic mouse model. Wound tissues were immunostained with HNA (green) and DAPI (blue), before being visualized by fluorescence microscopy. Scale bar was set as 100 μm (Magnification x 100). The percentage of HNA-positive cells in total cells were analyzed with Fiji software (upper right panel). n=3.

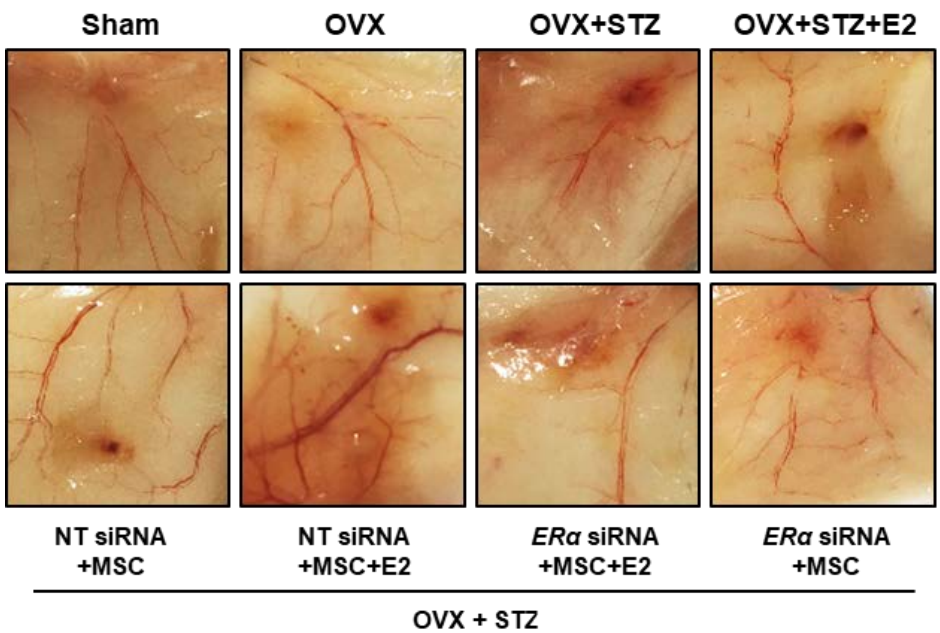

Figure 53. Effect of ER α -silenced hUCB-MSC transplantation with E2 injection on blood vessel formation in OVX diabetic mouse model. Representative gross images of blood vessels in wound site are shown.

4. DISCUSSION

In the present study, I showed that E2 (10 nM) has a protective effect on high glucose (25 mM)-induced mtROS generation and autophagic cell death through ERα-dependent signaling including nuclear translocation of Nrf2 and subsequent Sirt3-induced MnSOD activation in hUCB-MSCs (Figure 54). Moreover, this study demonstrated that the therapeutic efficacy of hUCB-MSCs in mouse cutaneous wound healing model with E2 deficiency and diabetes was enhanced by E2 treatment (40 μg/kg/day). Since high glucose regulates the intracellular signaling cascade of ROS through a variety of intracellular events and induces excessive ROS generation, the exposure to high glucose eventually leads to cell toxicity including cell death in various types of cells (Yu et al., 2011; Zhao et al., 2015) as well as a therapeutic efficacy reduction of cells (Raffaele et al., 2016). In bone marrow-derived MSC, high glucose exposure regulates ROS-induced senescence, which is associated with enhanced autophagy and leads to shutting down the apoptotic process (Chang et al., 2015). However, my data indicate that high glucose causes mitochondrial dysfunction through

excessive ROS production, consequently leading to autophagic cell death. According to the previous reports, exposure to high glucose affects cell death by autophagy dysfunction (Wang et al., 2015) and high glucose is known to regulate autophagy through mitochondrial damage by increasing oxidative stress (Park and Park, 2013). For this reason, reducing the mtROS levels can restore mitochondrial damage and autophagy dysfunction, which may prevent oxidative stress-induced diabetes-associated diseases.

E2 can be considered an important antioxidant for cytoprotection to reduce the excessive ROS generation by high glucose. Thus, in the present study, I demonstrated that treatment of E2 attenuates mtROS production and facilitates cell survival under high glucose exposure. Earlier studies showed that E2 enhances mitochondrial efficiency and suppresses mtROS through increased MnSOD by reduced superoxide production (Razmara et al., 2007; Stirone et al., 2005). In addition, E2 induces in mitochondrial protection through ROS reduction, decreasing mitochondrial membrane potential and ATP depletion in an ER-dependent manner under ischemic states in which oxygen and glucose transfer were insufficient (Guo et al., 2012). However, under high glucose conditions, my data reveal that

a potential role of E2 through translocation of ERα upregulates antioxidant enzymes that directly target high glucose-mediated ROS generation, finally decreasing autophagic cell death. Many reports have demonstrated that hyperglycemia leads to decreased ERα in diabetic animals (Cushman et al., 2009; Kim et al., 2006). Furthermore, ERα expression was downregulated by glucolipotoxicity in old rats and can alter their resistance to diabetic injuries since ERα enhances the survival rate (Kilic et al., 2014). Thus, I confirmed that E2 could inhibit the generation of mtROS and autophagic cell death by high glucose exposure in an ERα-dependent manner.

Since E2 binds with ERα to inhibit Nrf2-mediated transcription in breast cancer cells, it has been suggested that the function of ERα should be minimized for Nrf2 activation (Ansell et al., 2005; Yao et al., 2010). However, in my results, Nrf2 translocation into the nucleus was inhibited by *ERα* siRNA transfection under high glucose conditions. Nrf2 is a crucial transcription factor that protects against oxidants and increases cell survival in many tissues. In addition, Nrf2 plays an important role in maintaining cellular redox homeostasis by regulating the ROS production by

NADPH oxidase. Nuclear Nrf2 binds to the antioxidant-related elements and expresses antioxidant genes such as MnSOD and catalase, thus cellular protection by ROS suppression. Many studies have shown that Keap1 binds to Nrf2 and degrades through the proteasomal degradation process in unstressed conditions or basal conditions while Nrf2 is activated and translocated to the nucleus by oxidative stress (Kobayashi et al., 2006; Zhang, 2006). However, in my results, nuclear Nrf2 is decreased by high glucose while the levels of Keap1 are elevated in a time-dependent manner. This seems to be a deficit in the function of Nrf2 when exposed long-term to high glucose, which may contribute to oxidative stress-mediated diabetic complications. Indeed, Nrf2 expression is reduced in the late-stage diabetic/insulin resistance model (Miao et al., 2012; Tan et al., 2011). Together, these results suggest that ERα plays a key role in enhancing nuclear Nrf2 under high glucose conditions.

Moreover, my data reveal that ERα silencing decreased Sirt3 expression more than cells with high glucose treatment. Sirtuin is an NAD^+-dependent deacetylase involved in energy metabolism, DNA repair, and stress response. Sirt3 activates antioxidant

enzymes, such as MnSOD, through deacetylation. Therefore, the most persuasive interpretation of my results is that E2 leads to the activation of MnSOD by inducing functional Sirt3. Indeed, ERα silencing attenuated the SOD activation under high glucose conditions, suggesting a molecular cross-talk blocking Sirt3. In the current study, the main issue is how E2 enhancing Sirt3 expression through genomic signaling may attenuate the ROS production in hUCB-MSCs. Recent studies demonstrated that Sirt3 reduced high glucose-induced cytotoxicity and cell senescence (Zhang et al., 2013; Liu et al., 2015). Therefore, I demonstrated that high glucose attenuates Sirt3 expression and induces MnSOD acetylation. Although there are various ways to reduce high glucose-induced mtROS, I found that Sirt3 and MnSOD-induced mtROS reduction through E2-induced ERα signaling under high glucose conditions. Thus, I suggest that E2 treatment enhances Sirt3 and MnSOD expressions under high glucose conditions and increases in Sirt3 and MnSOD may reduce autophagic cell death for cellular protection. Although the exact mechanism of E2-dependent ERα signaling is unknown in mitochondrial dysfunction and cell protection, I have proven that Nrf2 and Sirt3 have the effects to regulate MnSOD-

induced mtROS reduction under high glucose conditions, suggesting that E2 plays an important role in enhancing the hUCB-MSC protection through ERα signaling pathways.

In this study, I observed that E2 treatment with hUCB-MSC transplantation facilitates tissue repair and vascular regeneration *in vivo*. Although I anticipated that E2 treatment by itself has the ability to improve wound healing, wound closure rates were not significantly different between the OVX + STZ + E2 group and the OVX + STZ group. According to epidemiological data, the degree and duration of hyperglycemia is related to microvascular complications of diabetes (Ohkubo et al., 1995; Valeri et al., 2004). In addition, the therapeutic effect of E2 has very narrow index when exposed to chronic or long-term diabetes (Mauvais-Jarvis et al., 2017). Thus, it is possible that the hyperglycemic conditions may be considered to decrease the therapeutic effect of E2 in OVX diabetic mice. My results also indicated that the wounds are almost closed and filled with granulation tissues by E2-treated hUCB-MSC transplantation in OVX diabetic mice model. Thus, it is possible that hUCB-MSC transplantation with E2 treatment may be more effective for wound healing than hormone therapies with E2 or

hUCB-MSC transplantation. My data observed that *ERα* siRNA-transfected hUCB-MSC transplantation is not affected by the E2 treatment in OVX diabetic mice. Therefore, my observations suggest that hUCB-MSC transplantation efficiency facilitates when circulating E2 is processed while ERα silencing reduces hUCB-MSC transplantation efficiency and delays skin wound healing in OVX diabetic mice, suggesting a more predominate role for ERα in enhancing the stem cell transplantation efficacy.

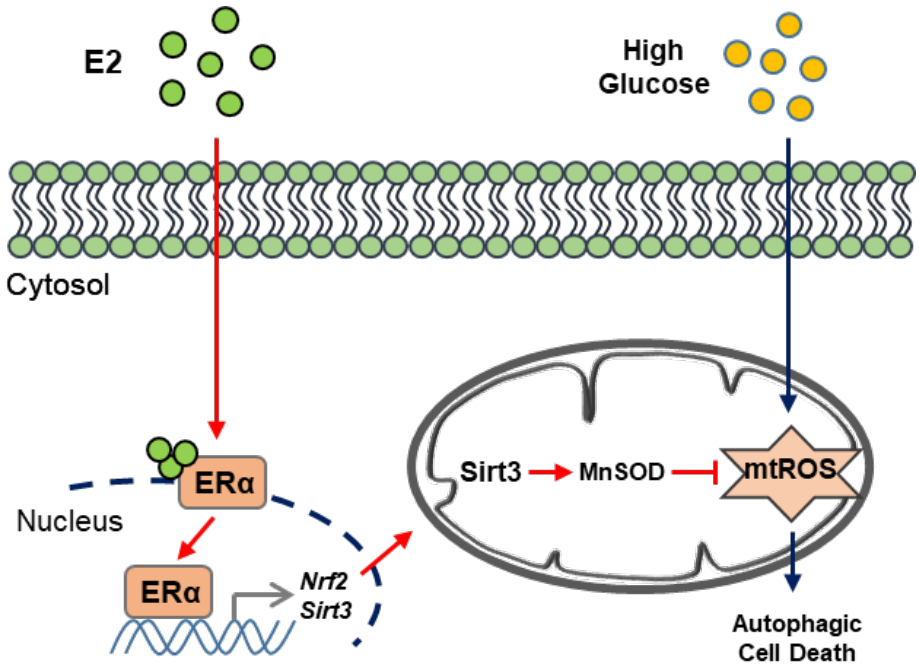

Figure 54. The schematic model for mechanism in the protective effect of E2 on high glucose-induced mtROS through ERα-dependent Nrf2 and Sirt3 upregulation in hUCB-MSCs. Hypothetical model for E2-induced ERα signaling under high glucose conditions in hUCB-MSCs. Red arrows represent E2-induced ERα signaling pathways shown. Blue arrows represent high glucose-induced autophagic cell death signaling pathways shown. Abbreviations: E2, 17β-estradiol; ERα, estrogen receptor alpha; Nrf2, nuclear factor (erythroid-derived 2)-like 2; Sirt3, Sirtuin 3; MnSOD, manganese superoxide dismutase; mtROS, mitochondrial reactive oxygen species.

CHAPTER IV.

GENERAL CONCLUSION

My study demonstrated that high glucose-induced E-cadherin repression increases migration through the expressions of EZH2 and Snail. High glucose specifically induces the recruitment of PRC2 to the E-cadherin promoter, where high glucose triggers ROS production to promote either the activation of JNK-mediated cleaved Notch or PI3K/Akt signaling pathways. Moreover, high glucose pretreatment improved the migratory ability of the transplanted hUCB-MSCs to the wound site, which facilitates tissue regeneration. Therefore, I strongly suggest that pre-activation by high glucose promotes the therapeutic capability of hUCB-MSCs for clinical skin wound healing models.

Next, the observations presented here indicate that E2 is an attractive candidate with the potential to maintain mtROS homeostasis through ERα-induced Nrf2 and Sirt3 signaling under high glucose conditions. In addition, E2-induced mtROS reduction affects cytoprotection by decreasing autophagic cell death in hUCB-MSCs. Consistent with *in vitro* results, transplantation of hUCB-MSC with E2 treatment increases skin wound healing and angiogenesis, thus therapeutic efficiency ultimately can be increased. Therefore, I propose E2 in stem cell therapy to prevent and treat diabetes-related diseases in postmenopausal patients in order for new therapeutic options in the future.

In conclusion, this study demonstrated that 1) high glucose-

induced ROS production activates E-cadherin repression through the interplay between Snail and EZH2, which leads to hUCB-MSC migration, 2) E2 has a protective effect on high glucose-induced mtROS generation via ERα-dependent MnSOD activation via Nrf2 and Sirt3 upregulation.

REFERENCES

Ansell PJ, Lo SC, Newton LG, Espinosa-Nicholas C, Zhang DD, Liu JH, Hannink M, Lubahn DB. (2005). Repression of cancer protective genes by 17β-estradiol: ligand-dependent interaction between human Nrf2 and estrogen receptor α. *Mol Cell Endocrinol.* 243(1-2):27-34.

Balaji S, Keswani SG, Crombleholme TM. (2012). The role of mesenchymal stem cells in the regenrative wound healing phenotype. *Adv Wound Care (New Rochelle).* 1(4);159-165.

Barry FP, Murphy JM. (2004). Mesenchymal stem cells: clinical applications and biological characterization. *Int J Biochem Cell Biol.* 36(4): 568-584.

Bednarek-Tupikowska G, Bohdanowicz-Pawlak A, Bidzinska B, Milewicz A, Antonowicz-Juchniewicz J, Andrzejak R. (2001). Serum lipid peroxide levels and erythrocyte glutathione peroxidase and superoxide dismutase activity in premenopausal and postmenopausal women. *Gynecol Endocrinol.* 15(4):298-303.

Bednarek-Tupikowska G, Tupikowska K, Bidzinska B, Bohdanowicz-Pawlak A, Antonowicz-Juchniewicz J, Kosowska B, Milewicz A. (2004). Serum lipid peroxides and total antioxidant

status in postmenopausal women on hormone replacement therapy. *Gynecol Endocrinol*. 19(2):57-63.

Bellanti F, Matteo M, Rollo T, Rosario FD, Greco P, Vendemiale G, Serviddio G. (2013). Sex hormones modulate circulating antioxidant enzymes: impact of estrogen therapy. *Redox Biol.* 1:340-346.

Boller K, Vestweber D, Kemler R. (1985). Cell-adhesion molecule muvomolurin is localized in the intermediate junctions of adult intestinal epithelial cells. *J Cell Biol*. 100(1):327-332.

Borras C, Gambini J, Lopez-Grueso R, Pallardo FV, Vina J. (2010). Direct antioxidant and protective effect of estradiol on isolated mitochondria. *Biochim Biophys Acta*. 1802(1):205-244.

Brand JS, van der Schouw YT, Onland-Moret NC, Sharp SJ, Ong KK, Khaw KT, Ardanaz E, Amiano P, Boeing H, Chirlaque MD, Clavel-Chapelon F, Crowe FL, de Lauzon-Guillanin B, Duell EJ, Fagherazzi G, Franks PW, Grioni S, Groop LC, Kaaks R, Key TJ, Nilsson PM, Overvad K, Palli D, Panico S, Quiros JR, Rolandsson O, Sacerdote C, Sanchez MJ, Slimani N, Teucher B, Tjonneland A, Tumino R, van der A DL, Feskens EJ, Langenberg C, Forouhi NG, Riboli E, Wareham NJ; InterAct Consortium. (2013). Age at menopause, reproductive life span, and type 2 diabetes risk: results from the EPIC-InterAct study. *Diabetes Care*. 36(4): 1012-1019.

Bryzgalova G, Gao H, Ahren B, Zierath JR, Galuska D, Steiler TL, Dahlman-Wright K, Nilsson S, Gusstafsson JA, Efendic S, Khan A. (2006). Evidence that oestrogen receptor-α plays an important role in the regulation of glucose homeostasis in mice: insulin sensitivity in the liver. *Diabetologia.* 49(3):588-597.

Cagnacci A, Soldani R, Carriero PL, Paoletti AM, Fioretti P, Melis GB. (1992). Effects of low doses of transdermal 17 beta-estradiol on carbohydrate metabolism in postmenopausal women. *J Clin Endocrinol Metab*. 74(6):1396-1400.

Cai D, Chen SC, Prasad M, He L, Wang X, Choesmel-Cadamura V, Sawyer JK, Danuser G, Montell DJ. (2014). Mechanical feedback through E-cadherin promotes direction sensing during collective cell migration. *Cell.* 157(5):1146-1159.

Cersosimo MG and Benarroch EE. (2015). Estrogen actions in the nervous system. *Neurology*. 82(3): 263-273.

Chang HK, Kim PH, Cho HM, Yum SY, Choi YJ, Son Y, Lee D, Kang I, Kang KS, Jang G, Cho JY. (2016). Inducible HGF-secreting human umbilical cord blood-derived MSCs produced via TALEN-mediated genome editing promoted angiogenesis. *Mol Ther*. 24(9):1644-1654.

Chang TC, Hsu MF, Wu KK. (2015). High glucose induces bone marrow-derived mesenchymal stem cell senescence by upregulating autophagy. *PLoS One.* 10(5):e0126537.

Chang YS, Choi SJ, Ahn SY, Sung DK, Sung SI, Yoo HS, Oh WI, Park WS. (2013). Timing of umbilical cord blood derived mesenchymal stem cells transplantation determines therapeutic efficacy in the neonatal hyperoxic lung injury. *PLoS One*. 8(1):e52419.

Chen D, Wu Z, Luo LJ, Huang X, Qian WQ, Wang H, Li SH, Liu J. (2015). E-cadherin maintains the activity of neural stem cells and inhibits the migration. *Int J Clin Exp Pathol*. 8(11):14247-14251.

Chen JS, Wong VW, Gurtner GC. (2012). Therapeutic potential of bone marrow-derived mesenchymal stem cells for cutaneous wound healing. *Front Immunol.* 10(3):192.

Chen Y, McMillan-Ward E, Kong J, Israels SJ, Gibson SB. (2008). Oxidative stress induces autophagic cell death independent of apoptosis in transformed and cancer cells. *Cell Death Differ.* 15(1):171-182.

Chess PR, O'Reilly MA, Sachs F, Finkelstein JN. (2005). Reactive oxidant and p42/44 MAP kinase signaling is necessary for mechanical strain-induced proliferation in pulmonary epithelial cells. *J Appl Physiol*. 99(3):1226-1232.

Christofori G, Semb H. (1999). The role of the cell-adhesion molecule E-cadherin as a tumour-suppressor gene. *Trends Biochem Sci.* 24(2):73-86.

Cramer C, Freisinger E, Jones RK, Slakey DP, Dupin CL, Newsome ER, Alt EU, Izadpanah R. (2010). Persistent high glucose concentrations alter the regenerative potential of mesenchymal stem cells. *Stem Cells Dev.* 19(12):1875-1884.

Crespo CJ, Smit E, Snelling A, Sempos CT, Andersen RE, Nhanes, III. (2002). Hormone replacement therapy and its relationship to lipid and glucose metabolism in diabetic and nondiabetic postmenopausal women: results from the Third National Health and Nutrition Examination Survey (NHANES III). *Diabetes Care.* 25(10):1675-1680.

Cushman T, Kim N, Hoyt R, Traish AM. (2009). Estradiol restores diabetes-induced reductions in sex steroid receptor expression and distribution in the vagina of db/db mouse model. *J Steroid Biochem Mol Biol.* 114(3-5):186-194.

Dandona P. (2017). Minimizing glycemic fluctuations in patients with type 2 diabetes: approaches and importance. *Diabetes Technol Ther.* 19(9):498-506.

Davidson MH et al., (2000). Effects of continuous estrogen and estrogen-progestin relacement regimens on cardiovascular risk

markers in postmenopausal women. *Arch Intern Med*. 160(21): 3315-3325.

De Becker A, Riet IV. (2016). Homing and migration of mesenchymal stem cells: how to improve the efficacy of cell therapy? *World J Stem Cells*. 8(3):73-87.

Dhanasekaran M, Indumathi S, Rajkumar JS, Sudarsanam D. (2013). Effect of high glucose on extensive culturing of mesenchymal stem cells derived from subcutaneous fat, omentum fat and bone marrow. *Cell Biochem Funct.* 31(1):20-29.

Di Croce L, Kristian H. (2013). Transcriptional regulation by polycomb group proteins. *Nat Struct Mol Biol.* 20(10):1147-1155.

Drees, F., S. Pokutta, S. Yamada, W. J. Nelson and W. I. Weis (2005). α-Catenin is a molecular switch that binds E-cadherin-β-catenin and regulates actin-filament assembly. *Cell.* 123(5): 903-915.

Essick EE, Sam F. (2010). Oxidative stress and autophagy in cardiac disease, neurological disorders, aging and cancer. *Oxid Med Cell Longev.* 3(3):168-177.

Farnoodian M, Halbach C, Slinger C, Pattnaik BR, Sorenson CM, Sheibanin N. (2016). High glucose promotes the migration of retinal

pigment epithelial cells through increased oxidative stress and PEDF expression. *Am J Physiol Cell Physiol*. 311(3):C418-436.

Folmes CD, Nelson TJ, Martinez-Fernandez A, Arrell DK, Lindor JZ, Dzeja PP, Ikeda Y, Perez-Terzic C, Terzic A, (2011). Somatic oxidative bioenergetics transditions into pluripotency-dependent glycolysis to facilitate nuclear reprogramming. *Cell Metab.* 14:264-271.

Giordano S, Darley-Usmar V, Zhang J. (2013). Autophagy as an essential cellular antioxidant pathway in neurodegenrative disease. *Redox Biol*. 25(2):82-90.

Gonzalez ME, Moore HM, Li X, Toy KA, Huang W, Sabel MS, Kidwell KM, Kleer CG. (2014). EZH2 expands breast stem cells through activation of NOTCH1 signaling. *Proc Natl Acad Sci U S A*. 111(8):3098-3103.

Goodman Y, Bruce AJ, Cheng B, Mattson MP. (1996). Estrogen attenuate and corticosterone exacerbates excitotoxicity, oxidative injury, and amyloidβ-peptide toxicity in hippocampal neurons. *J Neurochem*. 66(5):1836-1844.

Granero-Molto F, Weis JA, Miga MI, Landis B, Myers TJ, O' Rear L, Longobardi L, Jansen ED, Mortlock DP, Spagnoli A. (2009). Regenerative effects of transplanted mesenchymal stem cells in fracture healing. *Stem Cells.* 27(8):1887-1898.

Gu H, Yu J, Dong D, Zhou Q, Wang JY, Fang S, Yang P. (2016). High glucose-repressed CITED2 Expression through miR-200b triggers the unfolded protein response and endoplasmic reticulum stress. *Diabetes*. 65(1):149-163.

Gumbiner BM. (2005). Regulation of cadherin-mediated adhesion in morphogenesis. *Nat Rev Mol Cell Biol.* 6(8):622-634.

Guo J, Duckles SP, Weiss JH, Li X, Krause DN. (2012). 17β-Estradiol prevents cell death and mitochondrial dysfunction by an estrogen receptor-dependent mechanism in astrocytes after oxygen-glucose deprivation/reperfusion. *Free Radic Biol Med.* 52(11-12):2151-2160.

Guo J, Xia N, Yang L, Zhou S, Zhang Q, Qiao Y, Liu Z. (2014). GSK-3β and viatamin D receptor are involved in β-catenin and snail signaling in high glucose-induced epithelial-mesenchymal transition of mouse podocytes. *Cell Physiol Biochem*. 33(4):1087-1096.

Guppy M, Greiner E, Brand K. (1993). The role of the Crabtree effect and an endogenous fuel in the energy metabolism of resting and proliferating thymocytes. *Eur J Biochem*. 15;212(1):95-99.

Ha H, Lee HB. (2000). Reactive oxygen species as glucose signaling molecules in mesangial cells cultured under high glucose. *Kidney Int Suppl*. 77:S19-25.

Hall G, Phillips TJ. (2005). Estrogen and skin: the effects of estrogen, menopause, and hormone replacement therapy on the skin. *J Am Acad Dermatol*. 53(4):555-568.

Han SJ, Rodriguez ML, Al-Rekabi Z, Sniadecki NJ. (2016). Spatial and temporal corrdination of traction forces in one-dimensional cell migration. *Cell Adh Migr*. 10(5):529-539.

He X, Ma Q. (2012). Disruption of Nrf2 synergizes with high glucose to cause heightened myocardial oxidative stress and severe cardiomyopathy in diabetic mice. *J Diabetes Metab.* Suppl 7:002.

Herranz N, Pasini D, Diaz VM, Franci C, Gutierrez A, Dave N, Escriva M, Hernandez-Munoz I, Di Croce L, Helin K, Garcia de Herreros A, Peiro S. (2008). Polycomb complex 2 is required for E-cacdherin repression by the Snail1 transcription factor. *Mol Cell Biol.* 28(15):4772-4781.

Hinz B. (2007). Formation and function of the myofibroblast during tissue repair. *J Invest Dermatol*. 127(3):526-537.

Honda A, Hirose M, Ogura A. (2009). Basic FGF and Activin/Nodal but not LIF signaling sustain undifferentiated status of rabbit embryonic stem cells. *Exp Cell Res*. 15(12):2033-2042.

Horwitz EM, Prockop DJ, Fitzpatrick LA, Koo WW, Gordon PL, Neel M, Sussman M, Orchard P, Marx JC, Pyeritz RE, Brenner MK.

(1999). Transplantability and therapeutic effects of bone marrow-derived mesenchymal cells in children with osteogenesis imperfecta. *Nat Med.* 5(3):309-313.

Huang Q, Sheibanin N. (2008). High glucose promotes retinal endothelial cell migration through activation of Src, PI3K/Akt1/eNOS, and ERKs. *Am J Physiol Cell Physiol.* 295(6):1647-1657.

Ito K, Suda T. (2014). Metabolic requirements for the maintenance of self-renewing stem cells. *Nat Rev Mol Cell Biol.* 15(4):243-256.

Jackson WM, Nesti LJ, Tuan RS. (2012). Concise review: clinical translation of wound healing therapies based on mesenchymal stem cells. *Stem Cells Transl Med.* 1(1):44-50.

Jing E, Emanuelli B, Hirschey MD, Boucher J, Lee KY, Lombard D, Verdin EM, Kahn CR. (2011). Sirtuin-3 (Sirt3) regulates skeletal muscle metabolism and insulin signaling via altered mitochondrial oxidation and reactive oxygen species production. *Proc Natl Acad Sci U S A.* 108(35):14608-14613.

Jung YH, Lee SJ, Oh SY, Lee HJ, Ryu JM, Han HJ. (2015). Oleic acid enhances the motility of umbilical cord blood derived mesenchymal stem cells through EphB2-dependent F-actin formation. *Biochim Biophys Acta.* 1853(8):1905-1917.

Kanji S, Das H. (2017). Advances of stem cell therapeutics in cutaneous wound healing and regeneration. *Mediators Inflamm*. 2017:5217967.

Kilic G, Alvarez-Mercado AI, Zarrouki B, Opland D, Liew CW, Alonso LC, Myers MG Jr, Jonas JC, Poitout V, Kulkarni RN, Mauvais-Jarvis F. (2014). The islet estrogen receptor-α is induced by hyperglycemia and protects against oxidative stress-induced insulin-deficient diabetes. *PLoS One.* 9(2):e87941.

Kim NN, Stankovic M, Cushman TT, Goldstein I, Munarriz R, Traish AM. (2006). Streptozotocin-induced diabetes in the rat is associated with changes in vaginal hemodynamics, morphology and biochemical markers. *BMC Physiol.* 6:4.

Kim SK, Park HJ, Hong HS, Baik EJ, Jung MW, Mook-Jung I. (2006). ERK1/2 is an endogenous negative regulator of the γ-secretase activity. *FASEB J.* 20(1):157-159.

Kim YH, Heo JS, Han HJ. (2006). High glucose increase cell cycle regulatory proteins level of mouse embryonic stem cells via PI3-K/Akt and MAPKs signal pathways. *J Cell Physiol.* 209(1):94-102.

Kirfel G, Rigort A, Borm B, Herzog V. (2004). Cell migration: mechanisms of rear detachment and the formation of migration tracks. *Eur J Cell Biol.* 83 (11-12):717-724.

Kobayashi A, Kang MI, Watai Y, Tong KI, Shibata T, Uchida K, Yamamoto M. (2006). Oxidative and electrophilic stresses activate Nrf2 through inhibition of ubiquitination activity of Keap1. *Mol Cell Biol.* 26(1):221-229.

Kwon YW, Heo SC, Jeong GO, Yoon JW, Mo WM, Lee MJ, Jang IH, Kwon SM, Lee JS, Kim JH. (2013). Tumor necrosis factor-α-activated mesenchymal stem cells promote endothelial progenitor cell homing and angiogenesis. *Biochim Biophys Acta.* 1832(12): 2136-2144.

Le Belle JE, Orozco NM, Paucar AA, Saxe JP, Mottahedeh J, Pyle AD, Wu H, Kornblum HI. (2011). Proliferative neural stem cells have high endogenous ROS levels that regulate self-renewal and neurogenesis in a PI3K/Akt-dependant manner. *Cell Stem Cell.* 8(1):59-71.

Lee DE, Ayoub N, Agrawal DK. (2016). Mesenchymal stem cells and cutaneous wound healing: novel methods to increase cell delivery and therapeutic efficacy. *Stem Cell Res Ther.* 7:37.

Lee SJ, Jung YH, Oh SY, Yong MS, Ryu JM, Han HJ. (2014). Netrin-1 induces MMP-12-dependent E-cadherin degradation via the diatinct activation of PKCα and FAK/Fyn in promoting mesenchymal stem cell motility. *Stem Cells Dev.* 23(16):1870-1882.

Lee SS, Lee SJ, Lee SH, Lee SH, Ryu JM, Leim HS, Kim JS, Song EJ, Jung YH, Lee HJ, Kim CH, Han HJ. (2016). Netrin-1-induced stem cell bioactivity contributes to the regeneration of injured tissues via the lipid raft-dependent integrin $\alpha 6\beta 4$ signaling pathway. *Sci Rep*. 6:37526.

Lee YJ, Han HJ. (2010). Troglitazone ameliorates high glucose-induced EMT and dysfunction of SGLTs through PI3K/Akt, GSK-3β, Snail1, and β-catenin in renal proximal tubule cells. *Am J Physiol Renal Physiol.* 298(5):F1263-1275.

Lee YS, Kang YS, Lee JS, Nicolova S, Kim JA. (2004). Involvement of NADPH oxidase-mediated generation of reactive oxygen species in the apototic cell death by capsaicin in HepG2 human hepatoma cells. *Free Radic Res*. 38(4):405-12.

Le May C, Chu K, Hu M, Ortega CS, Simpson ER, Korach KS, Tsai MJ, Mauvais-Jarvis F. (2006). Estrogens protect pancreatic β-cells from apoptosis and prevent insulin-deficient diabetes mellitus in mice. *Proc Natl Acad Sci U S A.* 103(24):9232-9237.

Liu G, Cao M, Xu Y, Li Y. (2015). SIRT3 protects endothelial cells from high glucose-induced cytotoxicity. *Int J Clin Exp Pathol.* 8(1):353-360.

Li JH, Zhang N, Wang JA. (2008). Improved anti-apoptotic and anti-remodeling potency of bone marrow mesenchymal stem cells

by anoxic pre-conditioning in diabetic cardiomyopathy. *J Endocrinol Invest.* 31(2):103-110.

Li L, He Y, Zhao M, Jiang J. (2013). Collective cell migration: implications for wound healing and cancer invasion. *Burns Trauma.* 1(1):21-26.

Li N, Alam J, Venkatesan MI, Eiguren-Fernandez A, Schmitz D, Di Stefano E, Slaughter N, Killeen E, Wang X, Huang A, Miguel AH, Cho A, Sioutas C, Nel AE. (2004). Nrf2 is a key transcription factor that regulates antioxidant defense in macrophages and epithelial cells: protecting against the proinflammatory and oxidizing effects of diesel exhaust chemicals. *J Immunol.* 173(5):3467-3481.

Li YM, Schilling T, Benisch P, Zeck S, Meissner-Weigl J, Schneider D, Limbert C, Seufert J, Kassem M, Schutze N, Jakob F, Ebert R. (2007). Effects of high glucose on mesenchymal stem cell proliferation and differentiation. *Biochem Biophys Res Commun.* 363(1):209-215.

Lin Y, Dong C, Zhou BP. (2014). Epigenetic regulation of EMT: the Snail story. *Curr Pharm Des.* 20(11):1698-1705.

Liu G, Cao M, Xu Y, Li Y. (2015). SIRT3 protects endothelial cells from high glucose-induced cytotoxicity. *Int J Clin Exp Pathol.* 8(1):353-360.

Lunyak VV, Rosenfeld MG. (2008). Epigenetic regulation of stem cell fate. *Hum Mol Genet.* 17(R1):R28-36.

Madonna R, Gorbe A, Ferdinandy P, De Caterina R. (2013). Glucose metabolism, hyperosmotic stress, and reprogramming of somatic cells. *Mol Biotechnol.* 55(2):169-178.

Marambaud P, Shioi J, Serban G, Georgakopoulos A, Sarner S, Nagy V, Baki L, Wen P, Efthimiopoulos S, Shao Z, Wisniewski T, Robakis NK. (2002). A presenilin-1/γ-secretase cleavage releases the E-cadherin intracellular domain and regulates disassembly of adherens junctions. *EMBO J.* 21(8):1948-1956.

Margolis KL, Bonds DE, Rodabough RJ, Tinker L, Phillips LS, Allen C, Bassford T, Burke G, Torrens J, Howard BV, Women's Health Initiative Investigators. (2004). Effect of oestrogen plus progestin on the incidence of diabetes in postmenopausal women: results from the Women's Health Initative Hormone Trial. *Diabetologia*. 47(7):1175-1187.

Matough FA, Budin SB, Hamid ZA, Alwahaibi N, Mohamed J. (2012). The role of oxidative stress and antioxidants in diabetic complications. *Sultan Qaboos Univ Med J.* 12(1):5-18.

Mauvais-Jarvis F, Clegg DJ, Hevener AL. (2013). The role of estrogens in control of energy balance and glucose homeostasis. *Endocr Rev*. 34(3)309-338.

Mauvais-Jarvis F, Manson JE, Stevenson JC, Fonseca VA. (2017). Menopausal hormone therapy and type 2 diabetes prevention: evidence, mechanisms, and clinical implications. *Endocr Rev.* 38(3):173-188.

McClelland Descalzo DL, Satoorian TS, Walker LM, Sparks NR, Pulyanina PY, Zur Nieden NI. (2016). Glucose-induced oxidative stress reduces proliferation in embryonic stem cells via FOXO3A/β-Caternin-dependent transcription of p21 (cip1). *Stem Cell Reports.* 7(1):55-68.

Miao X, Bai Y, Sun W, Cui W, Xin Y, Wang Y, Tan Y, Miao L, Fu Y, Su G, Cai L. (2012). Sulforaphane prevention of diabetes-induced aortic damage was associated with the up-regulation of Nrf2 and its down-stream antioxidants. *Nutr Metab (Lond).* 9(1):84.

Monnier L, Colette C. (2008). Glycemic variability: should we and can we prevent it?. *Diabetes Care.* Suppl 2:S150-154.

Munshi A, Kurland JF, Nishikawa T, Tanaka T, Hobbs ML, Tucker SL, Ismail S, Stevens C, Meyn RE. (2005). Histone deacetylase inhibitors radiosensitize human melanoma cells by suppressing DNA repair activity. *Clin Cancer Res*. 11(13):4912-4922.

Murphy E. (2011). Estrogen signaling and cardiovascular disease. *Circ Res*. 109(6): 687-696.

Murphy MP. (2009). How mitochondria produce reactive oxygen species. *Biochem J*. 417(1):1-13.

Naziroglu M, Simsek M, Simsek H, Aydilek N, Ozcan Z, Atilgan R. (2004). The effects of hormone replacement therapy combined with vitamins C and E on antioxidants levels and lipid profiles in postmenopausal women with Type 2 diabetes. *Clin Chim Acta.* 344(1-2):63-71.

Nieto MA. (2002). The snail superfamily of zinc-finger transcription factors. *Nat Rev Mol Cell Biol*. 3(3):155-166.

Niewiadomska P, Godt D, Tepass U. (1999). DE-Cadherin is required for intercellular motility during Drosophila oogenesis. *J Cell Biol*. 144(3):533-547.

Ochocki JD, Simon MC. (2013). Nutrient-sensing pathways and metabolic regulation in stem cells. *J Cell Biol.* 203(1):23-33.

Oh SY, Lee SJ, Jung YH, Lee HJ, Han HJ. (2015). Arachidonic acid promotes skin wound healing through induction of human MSC migration by MT3-MMP-mediated fibronectin degradation. *Cell Death Dis*. 7(6):e1750.

Ohkubo Y, Kishikawa H, Araki E, Miyata T, Isami S, Motoyoshi S, Kojima Y, Furuyoshi N, Shichiri M. (1995). Intensive insulin therapy prevents the progression of diabetic microvascular complications in Japanese patients with non-insulin-dependent diabetes mellitus: a randomized prospective 6-year study. *Diabetes Res Clin Pract.* 28(2):103-117.

Palecek SP, Huttenlocher A, Horwitz AF, Lauffenburger DA. (1998). Physical and biochemical regulation of integrin release during rear detachment of migrating cells. *J Cell Sci.* 111(Pt 7):929-40.

Panchatcharam M, Miriyala S, Yang F, Leitges M, Chrzanowska-Wodnicka M, Quilliam LA, Anaya P, Morris AJ, Amyth SS. (2010). Enhanced proliferation and migration of vascular smooth muscle cells in response to vascular injury under hyperglycemic conditions is controlled by β3 integrin signaling. *Int J Biochem Cell Biol.* 42(6):965-974.

Park CJ, Zhao Z, Glidewell-Kenney C, Lazic M, Chambon P, Krust A, Weiss J, Clegg DJ, Dunaif A, Jameson JL, Levine JE. (2011). Genetic rescue of nonclassical ERα signaling normalizes energy balance in obese ERα-null mutant mice. *J Clin Invest.* 121(2):604-612.

Park EY, Park JB. (2013). High glucose-induced oxidative stress promotes autophagy through mitochondrial damage in rat notochordal cells. *Int Orthop.* 37(12):2507-2514.

Peinado H, Ballestar E, Esteller M, Cano A. (2004). Snail mediates E-cadherin repression by the recruitment of the Sin3A/histone deacetylase 1 (HDAC1)/HDAC2 complex. *Mol Cell Biol.* 24(1):306-319.

Peppicelli S, Bianchini F, Toti A, Laurenzana A, Fibbi G, Galorini L. (2015). Extracellular acidity strengthens mesenchymal stem cells to promote melanoma progression. *Cell Cycle.* 14(19):3088-3100.

Pittenger MF, Mackay AM, Beck SC, Jaiswal RK, Douglas R, Mosca JD, Moorman MA, Simonetti DW, Craig S, Marshak DR. (1999). Multilineage potential of adult human mesenchymal stem cells. *Science.* 284(5411):143-147.

Qiu X, Brown K, Hirschey MD, Verdin E, Chen D. (2010). Calorie restriction reduces oxidative stress by SIRT3-mediated SOD2 activation. *Cell Metab.* 12(6):662-667.

Raffaele M, Li Volti G, Barbagallo IA, Vanella L. (2016). Therapeutic efficacy of stem cells transplantation in diabetes: role of Heme Oxygenase. *Front Cell Dev Biol.* 4:80.

Razmara A, Duckles SP, Krause DN, Procaccio V. (2007). Estrogen suppresses brain mitochondrial oxidative stress in female and male rats. *Brain Res.* 1176:71-81.

Rosa MD, Distefano G, Gagliano C, Rusciano D, Malaguarnera L. (2016). Autophagy in diabetic retinopathy. *Curr Neuropharmacol.* 14(8):810-825.

Rosova I, Dao M, Capoccia B, Link D, Nolta JA. (2008). Hypoxia preconditioning results in increased motility and improved therapeutic potential of human mesenchymal stem cells. *Stem Cells.* 26(8):2173-2182.

Ryu JM, Han HJ. (2015). Autotaxin-LPA axis regulates hMSC migration by adherent junction disruption and cytoskeletal rearrangement via LPAR1/3-dependent PKC/GSK3β/β-catenin and PKC/Rho GTPase pathway. *Stem Cells.* 33(3):819-832.

Saki N, Jalalifar MA, Soleimani M, Hajizamani S, Rahim F. (2013). Adverse effect of high glucose concentration on stem cell therapy. *Int J Hematol Oncol Stem Cell Res.* 7(3):34-40.

Sauer H, Wartenberg M, Hescheler J. (2001). Reactive oxygen species as intracellular messengers during cell growth and differentiation. *Cell Physiol Biochem.* 11(4):173-186.

Scherz-Shouval R, Shvets E, Fass E, Shorer H, Gil L, Elazar Z. (2007). Reactive oxygen species are essential for autophagy and specifically regulate the activity of Atg4. *EMBO J.* 26(7):1749-1760.

Schroder K. (2014). NADPH oxidases in redox regulation of cell adhesion and migration. *Antioxid Redox Signal.* 20(13):2043-2058.

Sen S, Domingues CC, Rouphael C, Chou C, Kim C, Yadava N. (2015). Genetic modification of human mesenchymal stem cells helps to redce adiposity and improve glucose tolerance in an obese diabetic mouse model. *Stem Cell Res Ther.* 9(6):242.

Shirayoshi Y, Okada TS, Takeichi M. (1983). The calcium-dependent cell-cell adhesion system regulates inner cell mass formation and cell surface polarization in early mouse development. *Cell.* 35(3 Pt 2):631-638.

Shen C, Chen Y, Liu H, Zhang K, Zhang T, Lin A, Jing N. (2008). Hydrogen peroxide promotes Aβ-dependent activation of γ-secretase. *J Biol Chem.* 283(25):17721-17730.

Siebert N, Xu W, Grambow E, Zechner D, Vollmar B. (2011). Erythropoietin improves skin wound healing and activates the TGF-β signaling pathway. *Lab Invest.* 91(12):1753-1765.

Simon JA, Kingston RE. (2013). Occupying chromatin: polycomb mechanisms for getting to genomic targets, stopping transcriptional traffic, and staying put. *Mol Cell*. 49(5):808-824.

Simsek T, Kocabas F, Zheng J, DeBerardinis RJ, Mahmoud AI, Olson EN, Schneider JW, Zhang CC, Sadek HA. (2010). The distinct metabolic profile of hematopoietic stem cells reflects their location in a hypoxic niche. *Cell Stem Cell.* 7(3):380-390.

Smith AG. (2001). Embryo-derived stem cells: of mice and men. *Annu Rev Cell Dev Biol.* 17:435-462.

Sohni A, Verfaillie CM. (2013). Mesenchymal stem cells migration homing and tracking. *Stem Cells Int.* 2013:130763.

Song X, Xie T. (2002). DE-cadherin-mediated cell adhesion is essential for maintaining somatic stem cells in the Drosophila ovary. *Proc Natl Acad Sci U S A*. 99(23):14813-14818.

Song X, Zhu CH, Doan C, Xie T. (2002). Germline stem cells anchored by adherens junctions in the Drosophila ovary niches. *Science*. 296(5574):1855-1857.

Stirone C, Duckles SP, Krause DN, Procaccio V. (2005). Estrogen increases mitochondrial efficiency and reduces oxidative stress in cerebral blood vessels. *Mol Pharmacol.* 68(4):959-965.

Sun BK, Siprashvili Z, Khavari PA. (2014). Advances in skin grafting and treatment of cutaneous wounds. *Science*. 346(6212):941-945.

Suzuki N. Svensson K, Eriksson UJ. (1996). High glucose concentration inhibits migration of rat cranial neural crest cells *in vitro*. *Diabetologia*. 39(4):401-411.

Takatani-Nakase T, Matsui C, Maeda S, Kawahara S, Takahashi K. (2014). High glucose level promotes migration behavior of breast cancer cells through zinc and its transporters. *PLoS One*. 9(2):e90136.

Takeichi M. (1991). Cadherin cell adhesion receptors as a morphogenetic regulator. *Science*. 251(5000):1451-1455.

Tan Y, Ichikawa T, Li J, Si Q, Yang H, Chen X, Goldblatt CS, Meyer CJ, Li X, Cai L, Cui T. (2011). Diabetic downregulation of Nrf2 activity via ERK contributes to oxidative stress-induced insulin resistance in cardiac cells *in vitro* and *in vivo*. *Diabetes.* 60(2):625-633.

Tao R, Coleman MC, Pennington JD, Ozden O, Park SH, Jiang H, Kim HS, Flynn CR, Hill S, Hayes McDonald W, Olivier AK, Spitz DR, and Gius D. (2010). Sirt3-mediated deacetylation of evolutionarily conserved lysine 122 regulates MnSOD activity in response to stress. *Mol Cell*. 40:893-904.

Theveneau E, Mayor R. (2012). Cadherins in collective cell migration of mesenchymal cells. *Curr Opin Cell Biol.* 24(5):677-684.

Thomson JA, Itskovitz-Eldor J, Shapiro SS, Waknitz MA, Swiergiel JJ, Marshall VS, Jones JM. (1998). Embryonic stem cell lines derived from human blastocysts. *Science.* 282(5391):1145-1147.

Tong ZT, Cai MY, Wang XG, Kong LL, Mai SJ, Liu YH, Zhang HB, Liao YJ, Zheng F, Zhu W, Liu TH, Bian XW, Guan XY, Lin MC, Zeng MS, Zeng YX, Kung HF, Xie D. (2012). EZH2 supports nasopharyngeal carcinoma cell aggressiveness by forming a co-repressor complex with HDAC1/HDAC2 and Snail to inhibit E-cadherin. *Oncogene.* 31(5):583-594.

Valeri C, Pozzilli P, Leslie D. (2004). Glucose control in diabetes. *Diabetes Metab Res Rev.* 20 Suppl 2:S1-8.

Vina J, Sastre J, Pallardo F, Borras C. (2003). Mitochondrial theory of aging: importance to explain why females live longer than males. *Antioxid Redox Signal.* 5(5):549-556.

Vincent AM, Russell JW, Low P, Feldman EL. (2004). Oxidative stress in the pathogenesis of diabetic neuropathy. *Endocr Rev.* 25(4):612-628.

Vogelmann R, Nguyen-Tat MD, Giehl K, Adler G, Wedlich D, Menke A. (2005). TGFβ-induced downregulation of E-cadherin-based cell-cell adhesion depends on PI3-kinase and PTEN. *J Cell Sci.* 118(Pt20):4901-4912.

Volarevic V, Arsenijevic N, Lukic ML, Stojkovic M. (2011). Concise review: Mesenchymal stem cell treatment of the complications of diabetes mellitus. *Stem Cells.* 29(1):5-10.

Volpe CMO, Villar-Delfino PH, Dos Anjos PMF, Nogueira-Machado JA. (2018). Cellular death, reactive oxygen species (ROS) and diabetic complications. *Cell Death Dis.* 9(2):119.

von Burstin J, Eser S, Paul MC, Seidler B, Brandl M, Messer M, von Werder A, Schmidt A, Mages J, Pagel P, Schnieke A, Schmid RM, Schneider G, Saur D. (2009). E-cadherin regulates metastasis of pancreatic cancer in vivo and is suppressed by a SNAIL/HDAC1/HDAC2 repressor complex. *Gastroenterology.* 137(1):361-371.

Wang C. Yue Y, Shao B, Qiu Z, Mu J, Tang J, Han X, Xiang T, Ren G. (2017). Dickkopf-related protein 2 is epigenetically inactivated and suppresses colorectal cancer growth and tumor metastasis by antagonizing Wnt/β-catenin signaling. *Cell Physiol Biochem.* 41(5):1709-1724.

Wang H, Fang R, Wang XF, Zhang F, Chen DY, Zhou B, Wang HS, Cai SH, Du J. (2013). Stabilization of Snail through AKT/GSK-3β signaling pathway is required for TNF-α-induced epithelial-mesenchymal transition in prostate cance PC3 cells. *Eur J Pharmacol*. 714(1-3):48-55.

Wang K, Zhang T, Dong Q, Nice EC, Huang C, Wei Y. (2013). Redox homeostasis: the linchpin in stem cell self-renewal and differentiation. *Cell Death Dis*. 4(3):e537.

Wang X, Ge J, Tredget EE, Wu Y. (2013). The mouse excisional wound splinting model, including applications for stem cell transplantation. *Nat Protoc.* 8(2):302-309.

Wang XY, Li S, Wang G, Ma ZL, Chuai M, Cao L, Yang X. (2015). High glucose environment inhibits cranial neural crest survival by activating excessive autophagy in the chick embryo. *Sci Rep.* 5:18321.

Webb DJ, Parsons JT, Horwitz AF. (2002). Adhesion assembly, disassembly and turnover in migrating cells–over and over and over again. *Nat Cell Biol*. 4(4):E97-100.

Weissman IL, Anderson DJ, Gage F. (2001). Stem and progenitor cells: origins, phenotypes, lineage commitments, and transdifferentiations. *Annu Rev Cell Dev Biol*. 17:387-403.

Weitzmann MN, Pacifici R. (2006). Estrogen deficiency and bone loss: an inflammatory tale. *J Clin Invest*. 116(5):1186-1194.

Wend K, Wend P, Krum SA. (2012). Tissue-specific effects of loss of estrogen during menopause and aging. *Front Endocrinol (Lausanne)*. 3:19.

Wu et al. (2007). Mesenchymal stem cells enhance wound healing through differentiation and angiogenesis. *Stem Cells.* 25:2648-2659.

Yao Y, Brodie AM, Davidson NE, Kensler TW, Zhou Q. (2010). Inhibition of estrogen signaling activates the NRF2 pathway in breast cancer. *Breast Cancer Res Treat.* 124(2):585-591.

Yi P, Bhagat S, Hilf R, Bambara RA, Muyan M. (2002). Differences in the abilities of estrogen receptors to integrate activation functions are critical for subtype-specific transcriptional responses. *Mol Endocrinol.* 16(8):1810-182.

Ying QL, Nichols J, Chambers I, Smith A. (2003). BMP induction of Id proteins suppresses differentiation and sustains embryonic stem cell self-renewal in collaboration with STAT3. *Cell.* 115(3):281-292.

Yoh K, Hirayama A, Ishizaki K, Yamada A, Takeuchi M, Yamagishi S, Morito N, Nakano T, Ojima M, Shimohata H, Itoh K, Takahashi S,

Yamamoto M. (2008). Hyperglycemia induces oxidative and nitrosative stress and increases renal functional impairment in Nrf2-deficient mice. *Genes Cells.* 13(11):1159-1170.

Yu T, Jhun BS, Yoon Y. (2011). High-glucose stimulation increases reactive oxygen species production through the calcium and mitogen-activated protein kinase-mediated activation of mitochondrial fission. *Antioxid Redox Signal.* 14(3):425-437

Zhang B, Cui S, Bai X, Zhuo L, Sun X, Hong Q, Fu B, Wang J, Chen X, Cai G. (2013). SIRT3 overexpression antagonizes high glucose accelerated cellular senescence in human diploid fibroblasts via the SIRT3-FOXO1 signaling pathway. *Age (Dordr).* 35(6):2237-2253

Zhang B, Liu N, Shi H, Wu H, Gao Y, He H, Gu B, Liu H. (2016). High glucose microenvironments inhibit the proliferation and migration of bone mesenchymal stem cells by activating GSK3β. *J Bone Miner Metab*. 34(2):140-50.

Zhang DD. (2006). Mechanistic studies of the Nrf2-Keap1 signaling pathway. *Drug Metab Rev.* 38(4):769-789.

Zhang J, Khvorostov I, Hong JS, Oktay Y, Vergnes L, Nuebel E, Wahjudi, PN, Setoguchi K, Wang G, Do A, Jung HJ, McCaffery JM, Kurland IJ, Reue K, Lee WN, Koehler CM, Teitell MA. (2011). UCP2 regulates energy metabolism and differentiation potential of human pluripotent stem cells. *EMBO J.* 30:4860-4873.

Zhang L, Marsboom G, Glick D, Zhang Y, Toth PT, Jones N, Malik AB, Rehman J. (2014). Bioenergetic shifts during transitions between stem cell states. *Pulm Circ.* 4(3):387-394.

Zhang L, Pang S, Deng B, Qian L, Chen J, Zou J, Zheng J, Yang L, Zhang C, Chen X, Liu Z, Le Y. (2012). High glucose induces renal mesangial cell proliferation and fibronectin expression through JNK/NF-κB/NADPH oxidase/ROS pathway, which is inhibited by resveratrol. *Int J Biochem Cell Biol.* 44(4):629-638.

Zhao K, Hao H, Liu J, Tong C, Cheng Y, Xie Z, Zang L, Mu Y, Han W. (2015). Bone marrow-derived mesenchymal stem cells ameliorate chronic high glucose-induced β-cell injury through modulation of autophagy. *Cell Death Dis.* 6:e1885.

Zhu X, Li Y, Zhou R, Wang N, Kang S. (2018). Knockdown of E-cadherin expression of endometrial epithelial cells may activate Wnt/β-catenin pathway in vitro. *Arch Gynecol Obstet.* 297(1):117-123.

국 문 초 록

고포도당 처리 인간 제대혈 유래 중간엽 줄기세포의 E-cadherin 발현 변화와 피부 상처 치유 효능

서울대학교 대학원

농생명공학부

오 지 영

지도교수 이 창 규

포도당은 영양소 대사 조절을 위한 필수 요소이며 줄기세포의 항상성 조절 및 운명 결정과 행동에 중요한 역할을 한다. 그러나 포도당의 농도가 높으면 고혈당 합병증의 주요 원인으로 알려져 있는 활성산소종을 과잉 생성하게 된다. 이전 연구자들은 산화 스트레스, 특히 활성산소종 함량이 줄기세포의 이주능에 영향을 미친다고 보고했다. 줄기세포의 운명 결정은 분화능, 증식능, 이주능에 관여하는 유전자에 의해 조절된다. 17β-Estradiol (E2)은 에너지 항상성 및 포도당 신진대사의 중요한 조절 인자이므로 고포도당에 의해 발생되는 대사 장애의 예방 및 치료에 적합한 표적으로 고려될 수 있다. 그러나 고포도당이 줄기세포 기능에 어떤 역할을 하는지 정확한 분자생물학적 기전은 알려져 있지 않으며, E2가 고포도당에 의해 유도되는 활성산소종을 어떻게 조절할 수 있는지 알려져 있지 않다. 따라서 본 연구는 1) 고포도당이 줄기세포 이주능에 미치는 영향과 줄기 세포 행동을 조절하는 기전과 2) 고포도당이 유도하는 산화 스트레스에 E2가 미치는 영향을 조사하여 궁극적으로 줄기세포 치료 효율을 향상시키는 방법을 제시하기 위하여 수행되었으며, 결과는 아래와 같다.

1. 고포도당 처리 (D-글루코오스)에 의해 줄기세포의 이주능을 증가시켰다. 또한 고포도당 처리는 세포 부착 단백질로 잘 알려진 E-cadherin 발현을 감소시켰고, cleaved Notch, Snail, EZH2의 발현을 증가시켰다. 고포도당 환경은 Snail과 EZH2 경로 활성을 통하여 E-cadherin의 발현을 억제시켰는데, 이는 Snail과 EZH2는 각각의 경로 활성을 통해 촉진되었다. 또한 고포도당은 세포 내의 활성산소종을 증가시켰으며, 이는 JNK나 PI3K/Akt 신호 전달을 활성화 시켰다.

고포도당에 의해 유도된 JNK의 활성은 γ-secretase를 활성화시켜 Notch 단백질이 잘리도록 유도하였으며, 잘려진 Notch는 핵으로 전이되었다. 핵에서 Snail은 고포도당에 의해 PRC2와 결합하고, E-cadherin의 프로모터 내 E-box와 결합하여 E-cadherin의 발현을 감소시켰다. 마우스 상처 치유 모델에서 고포도당의 전처리는 줄기세포의 상처 치유 효과와 이식의 생착률을 증가시켰으며, 이러한 효과는 Snail과 EZH2의 발현이 억제된 줄기세포에 고포도당 전처리에 의해 억제되었다. 따라서 고포도당에 의해 증가하는 활성산소종은 Snail과 EZH2의 증가를 통해 E-cadherin을 억제함으로써 줄기세포의 이주능을 촉진시켰다.

2. 고포도당 처리는 줄기세포내 미토콘드리아 활성산소종을 증가시켰으며, 자가 탐식 관련 단백질인 Beclin1의 발현과 LC3-II/LC3-I의 비율을 증가시켰고, 세포 생존력을 감소시켰다. 대조적으로, E2 처리는 고포도당에 의해 유도된 미토콘드리아 활성산소종을 현저히 감소시켰고, 이어서 세포 생존 능력을 회복시켰다. 또한 고포도당 상태에서 E2의 처리는 에스트로겐 수용체 알파를 핵으로 전이시켜 Nrf2 발현을 촉진시켰다. 핵 내의 Nrf2 증가는 Sirt3의 발현을 유도하고 MnSOD의 탈아세틸화를 통한 활성을 촉진시켰다. 그러나 고포도당은 Nrf2의 핵 전이를 하향 조절함으로써 미토콘드리아 활성산소종을 증가시켰고, 이는 Sirt3를 감소시켜 MnSOD의 아세틸화를 촉진시켰다. 난소 절제 당뇨병 마우스 모델에서, E2를 주입한 마우스의 피부 상처에 줄기세포를 이식하였더니 피부 상처의 세포 생착률 및 치료 효과를 향상시켰다. 그러나 에스트로겐 수용체 알파의 발현이 억제된

줄기세포를 이식 받은 마우스는 세포의 생착률 및 상처 치유 효과가 감소되었다. 또한 난소 절제 당뇨병 마우스에 E2를 주입한 후 줄기세포를 이식한 마우스는 에스트로겐 수용체 알파의 발현을 억제한 줄기세포를 주입한 마우스에 비해 혈관신생효과가 뛰어났다. 따라서 세포 내 E2에 의해 유도된 에스트로겐 수용체 알파에 의한 Nrf2 및 Sirt3의 증가 및 MnSOD 활성화에 의해 고포도당이 유도한 미토콘드리아 활성산소종으로부터 보호되었다.

결론적으로 1) 고포도당은 Snail과 EZH2의 신호전달 경로를 통한 E-cadherin을 억제 함으로써 인간 제대혈 유래 중간엽 줄기세포의 이주능을 향상시켰다. 2) E2는 에스트로겐 수용체 알파를 통해 MnSOD를 활성화 시킴으로써 고포도당이 유도한 미토콘드리아 활성산소종을 감소시켜 인간 제대혈 유래 중간엽 줄기세포의 생존 능력을 회복시켰다. 이러한 연구 결과를 바탕으로 고포도당에 의해 유도되는 산화 스트레스를 조절 기전을 확립한다면 줄기세포 치료제의 기능과 치료효과를 개선시킬 수 있을 것이다.

주요어: 고포도당, 활성산소종, E-cadherin, 17β-Estradiol, Sirtuin-3, Manganese superoxide dismutase

학번: 2010-21245